UNIVERSITY OF SOUTHAMPTON

An Automated Instrument for Measurement of Total Alkalinity in Seawater

David Robert Owsianka

Thesis for the degree of Doctor of Philosophy

FACULTY OF NATURAL AND ENVIRONMENTAL SCIENCES

Ocean and Earth Sciences

24 April 2014

UNIVERSITY OF SOUTHAMPTON

ABSTRACT

FACULTY OF NATURAL AND ENVIRONMENTAL SCIENCES

Ocean and Earth Sciences

Doctor of Philosophy

An Automated Instrument for Measurement of Total Alkalinity in Seawater

by David Robert Owsianka

Understanding the effects of increased CO_2 uptake on the marine environment is a high priority for scientific study, as this leads to acidification. Precise means of measuring the degree of acidification, and doing so regularly over long time periods is a key requirement in separating natural from man-made variation. This project examines new technologies for development of an instrument to measure one of the four main carbonate system variables, total alkalinity (TA), which is determined by acid/base titration. A red green and blue photodiode (RGB-PD) is examined as a novel photodetector for spectrophotometric measurements. This offers ≈ 400 times reduction in size (footprint) and cost compared to a conventional charge coupled device (CCD) spectrophotometer. Using bromocresol green (BCG) indicator, spectrophotometric pH measurements with the RGB-PD give a precision of <0.007 pH, and agree to within ≈0.01 pH units between pH 3.0 and 5.0 with measurements made using a conventional spectrophotometer. pH measurements are made by performing simultaneous photometry on two absorption bands in the BCG visible spectrum. The RGB-PD is also examined for TA determination. A fully automated prototype instrument utilising microfluidic technology achieved a precision of between ±8 - 19 μmol kg^{-1}. The precision is close to that reported for in situ prototypes (±4 μmol kg^{-1}, Sami-alk) and the required precision for ocean acidification measurements (±1 μmol kg^{-1}). This represents the first demonstration of TA titration using microfluidic technology, and the first use of an RGB-PD for high precision multi-wavelength spectrophotometry for chemical analysis. These are significant steps towards development of small, cheap, and rugged automated instruments for TA measurement. These contributions advance the realisation of extensive, long-term measurements in challenging environments.

Contents

List of Figures

List of Tables

Authors Declaration

I, David Robert Owsianka declare that this thesis, entitled **An Automated Instrument for Measurement of Total Alkalinity in Seawater,** and the work presented in it are my own and generated by me as the result of my own original research.

I confirm that:

1. This work was done wholly or mainly while in candidature for a research degree at this University;
2. Where any part of this thesis has previously been submitted for a degree or any other qualification at this University or any other institution, this has been clearly stated;
3. Where I have consulted the published work of others, this is always clearly attributed;
4. Where I have quoted from the work of others, the source is always given. With the exception of such quotations, this thesis is entirely my own work;
5. I have acknowledged all main sources of help;
6. Where the thesis is based on work done by myself jointly with others, I have made clear exactly what was done by others and what I have contributed myself;
7. Either none of this work has been published before submission, or parts of this work have been published as:

"**RGB photodiodes as detectors for spectrophotometry: Examination with a colorimetric pH assay**". Manuscript submitted to Optics Express

Signed:

Date:

Acknowledgements

This work was funded through a studentship provided by the by the school of Ocean and Earth Sciences, Faculty of Natural and Environmental Sciences, University of Southampton. The NERC Oceans 2025 programme (themes 5 and 8) provided additional funding and support.

Todd Bishop (ams AG), Jerry Koontz (ams AG), and Alan Liddle (Pacer) provided permission to use photodiode data, and were helpful with technical support.

Prof Michael DeGrandpre (UMT) kindly supplied a worked example of the TMT method. I would also like to thank Prof Andrew Dickson (Scripps Institution) for his advice and encouragement regarding error analysis of total alkalinity measurements.

Mr Andy Harris and Dr Iain Ogilvie provided invaluable engineering assistance in the early stages of the project. Catherine Burd saved me the toils of purchasing and equipment maintenance.

Thanks to the staff and students of the Centre for Marine Microsystems for their support throughout this project, and to the NOCS postgraduate community for many pleasant hours of discussion and distraction.

Dr Victoire Rerolle generously allowed adaptation of her microfluidic designs as the basis for the instrument developed, and provided practical assistance in innumerable ways. I am further indebted to both Victoire and Dr Alex Beaton for taking time to help winnow these chapters to legibility with their proof reading.

I wish to thank Dr Edward Waugh for his friendship, perseverance and encouragement, which brought me back to productivity from the inertia and despair of bereavement. Ed imparted technological and programming assistance throughout the project. The influence of his organisational zeal will be an enduring legacy.

Finally, my thanks to my supervisory panel, Dr Matthew Mowlem, Dr Douglas Connelly and Prof Eric Achterberg, for the opportunity to work on this project, and for their belief, patience, and encouragement throughout.

Chapter 1

Introduction

1.1 "The Other CO_2 Problem"

Increasing atmospheric CO_2 is a major environmental concern for the near future. Atmospheric CO_2 levels have risen by around 40% since the industrial revolution, from 280 ppmv (parts per million volume) to 400 ppmv [1, 2]. Earth system models have estimated that this will increase to over 2000 ppmv by the year 2300 in a "business-as-usual" scenario [3]. Should all anthropogenic CO_2 emissions be stopped during the next century, it has been predicted that the climate could still take around 1000 years to settle, and yet not recover to preindustrial CO_2 concentrations [4].

A large proportion of CO_2, estimated as being up to 48% of anthropogenic release [5], is taken up by the ocean where it perturbs the carbonate system and lowers pH [6]. This ocean acidification has been recognised as a major consequence of climate change in addition to global warming [6, 7]. Ocean acidification has significant potential to affect marine organisms through decrease in $CaCO_3$ saturation states, particularly calcifiers such as corals, pteropods, coccolithophores and foraminifera [7]. The stressing or removal of phytoplankton species would undermine marine food webs, these accounting for a majority of primary production in the world's oceans, however the specifics of how these organisms could be affected are not well understood. The cocolithophore *Emiliania huxleyi* was absent from a seasonally under-saturated $CaCO_3$ environment (Baltic Sea), but present in a year-round supersaturated environment of similar salinity (Black Sea). This indicates that coccolithophores could suffer under acidic conditions where seasonal $CaCO_3$ under-saturation will become more prevalent [8]. Conversely it has been shown from historical data and high-CO_2 laboratory experiments that increased

calcification occurs in some coccolithophore species [9]. Some species of echinoderm have demonstrated increased calcification and metabolism under acidified ocean regimes, but at the cost of muscle wastage [10]. This highlights that the degree of calcification may not be the most useful indicator for the effect of ocean acidification on calcifying organisms. It has been suggested that the incoherence of the response of organisms to ocean acidification, even within the same species, shows that better behaved mesocosm studies may be more useful in examining the effects of ocean acidification than those of species in isolation [11]. While these studies have demonstrated the potential damage which could be caused by ocean acidification, the current ability to monitor changes in the oceanic carbonate system cannot deliver the time and space resolution required to distinguish long term changes over natural short-term variation [12].

1.2 Definitions of uncertainty, and handling of errors

The theme of measurement quality and the evaluation of analytical system performance are crucial concepts that arise throughout this thesis, appearing in every chapter. It makes sense therefore to define these first.

1.2.1 Uncertainty

The definition of uncertainty used throughout this thesis is taken from the EURACHEM/CITAC guide *Quantifying Uncertainty in Analytical Measurement* is "*a parameter associated with the result of a measurement that characterises the values that could reasonably be attributed to the measureand*" [13]. An analytical measurement is usually derived from the results several other measurements. Preparing an aqueous solution with known concentration of NaCl for example requires measurement of the amount of NaCl and H_2O , and the relative molecular mass of NaCl. There will be an uncertainty associated with each of these. When expressed as a standard deviation (see Equation (1.1) below) this is known as the standard uncertainty. The cumulative effect of these on the uncertainty of NaCl concentration can be expressed as the **combined standard uncertainty**, expressed here as $U_c([NaCl])$. This is a measure of the bound over which the true value of [NaCl] will exist for a given level of confidence. More detail of how combined standard uncertainty is calculated is given in Chapter 3.

1.2.2 Error

When making a measurement, there may be a difference between the measured value and the true value. Error is defined as the difference between the measured and the true value. The crucial difference between error and uncertainty is that error is a single value, whereas uncertainty is a range or interval. A single measurement can have a very small error, but may be associated with a relatively large uncertainty.

Systematic errors are consistent in magnitude and sign for repeats of the measurement. An example would be temperature measurement with a thermometer that consistently measures 1 °C above the true temperature. The measured temperatures will always be 1 °C above the true temperature. Making more measurements does not reduce systematic error.

Random errors change in magnitude and sometimes also in sign for repeats of the measurement. An example would be repeated measurement of the mass of a coin by an unstable balance. The measured masses will be a spread of values about the true mass of the coin. Making more measurements can reduce the random error associated with a measurement.

Noise is used within this thesis to describe random fluctuations in an electronic signal being measured. To record an electronic signal many individual measurements are made over a period of time, and each measurement will have a random error associated with it. The signal to noise ratio is used to express the magnitude of the measured signal relative to the magnitude of the noise.

1.2.3 Accuracy and Precision

Precision is the spread of measured values about the mean. It arises from random errors, and is obtained by taking repeat measurements. The standard deviation (σ) is used to express precision, and has the same units as the measured quantity (equation (1.1)) [14].

$$\sigma = \sqrt{\frac{\sum_{i=1}^{n} (x_i - \bar{x})^2}{n}} \tag{1.1}$$

Precision is expressed throughout this thesis as 1 standard deviation (or σ), either as an absolute value or as a percentage of the measured value (percent relative standard

deviation, %RSD). Where graphs use error bounds, these will demonstrate ± 1σ of the measured data.

Accuracy is the difference between the true value and measured value. It can be determined for a chemical analyser by measuring a known concentration standard, or by comparing results with a separate trusted instrument.

1.2.4 Discrepancy

Discrepancy describes disagreement between two independent measurements of the same quantity. Consider the example of measurement of surface seawater using two identical thermometers. The first measures 6.8 °C, the second 7.4 °C. There is a discrepancy of 0.6 °C between the two measurements. This is similar to the concept of accuracy, however in this case the true value of seawater temperature is not known.

1.3 Carbonate Chemistry

1.3.1 Chemical Equilibrium– The Seawater Carbonate System

Carbon dioxide uptake acidifies the ocean through a series of reactions with water. This first forms carbonic acid, H_2CO_3, which can dissociate to bicarbonate (HCO_3^-), and carbonate (CO_3^{2-}), producing a proton with each step (Figure 1-1). The concentration of H_2CO_3 is low in comparison to other dissolved carbonate species, and so is often incorporated into a single effective concentration for dissolved carbon dioxide, $[CO_{2(aq)}]$ [15]. Square bracket notation will denote stoichiometric concentrations of chemical species throughout this thesis.

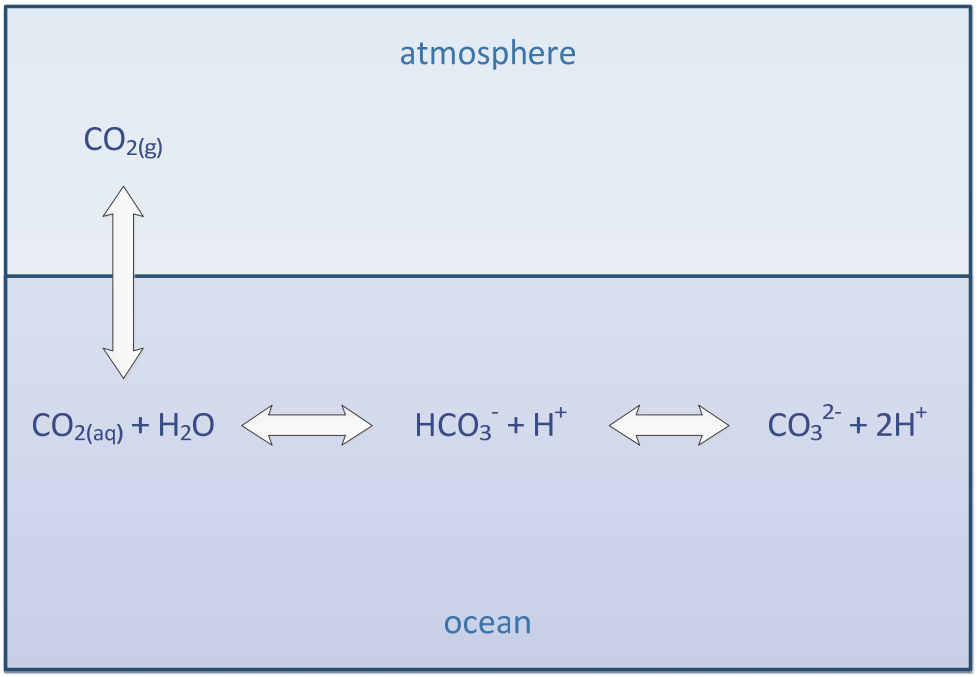

Figure 1-1 - The seawater carbonate system

Though there may be net input or removal of carbon from the system by interactions with atmosphere and organisms, or by precipitation and dissolution of particulate matter, these species equilibrate. Knowledge of the individual equilibrium constants allows calculation of the instantaneous individual species concentrations shown in Figure 1-1 according to equation (1.2)-(1.4).

$$[CO_2]_{aq} = K_0 \cdot fCO_2 \qquad (1.2)$$

Where K_O is Henrys constant [16], and fCO_2 is the fugacity of carbon dioxide (see Section 1.3.2).

$$K_1 = \frac{[HCO_3^-][H^+]}{[CO_2]} \qquad (1.3)$$

$$K_2 = \frac{[CO_3^-][H^+]}{[HCO_3^-]} \qquad (1.4)$$

Where K_1 and K_2 in equations (1.3) and (1.4) are the first and second equilibration constants for the dissociation of carbonic acid [17].

1.3.2 The Big 4: Carbonate System Parameters

Determination of the equilibrium position of the seawater carbonate chemistry would be relatively simple were there robust methods for the direct measurement of its principle species, CO_2, HCO_3^-, CO_3^{2-}, and H^+. This is not the case, and so four more easily measureable parameters are used. These are:

pCO2 – The partial pressure of CO_2. Also reported is fCO_2, the fugacity of CO_2. Fugacity is analogous to the definition of the activity of a solute ion given in Section 1.4.2, in this case representing the chemical potential of a real as opposed to an ideal gas. Fugacity approaches the value of partial pressure when partial pressure approaches zero. Where an accuracy of less than 0.7% is required, pCO_2 and fCO_2 can be taken as equal [16], though a more exact relationship exists, given by equation (1.5) below [15].

$$\mathrm{fCO_2} = \mathrm{pCO_2} \cdot \exp\left(\mathrm{p}\frac{\mathrm{B} + 2\delta}{\mathrm{RT}}\right) \tag{1.5}$$

Pressure p is given in pascals, the gas constant R in $JK^{-1}mol^{-1}$, the first virial coefficient of CO_2, B, and cross virial coefficient δ are expressed as variables dependent upon temperature T (K) as shown in equations (1.6) and (1.7) [15]. The relationship between pCO_2 and fCO_2 is therefore only temperature and pressure dependant.

$$\mathrm{B} = (-1636.75 + 12.048\mathrm{T} - 3.27957 \cdot 10^{-2}\mathrm{T}^2 + 3.16528 \cdot 10^{-5}\mathrm{T}^3) \cdot 10^{-6} \tag{1.6}$$

$$\delta = (57.7 - 0.118\mathrm{T}) \cdot 10^{-6} \tag{1.7}$$

pH – originally defined as the negative log of the concentration of hydrogen ions in a pH is more properly defined in terms of hydrogen ion activity (equation (1.8)) [18]. There are a number of different pH scales used in seawater analysis, and pH is subject to several definitions which are detailed further in Section 1.4.2.

$$\mathrm{pH} = -\log_{10}\{\mathrm{H}^+\} \tag{1.8}$$

Dissolved Inorganic Carbon (DIC) – a summation of the concentrations of all dissolved inorganic carbon species, equation (1.9).

$$\mathrm{DIC} = [\mathrm{HCO_3^-}] + [\mathrm{CO_3^{2-}}] + [\mathrm{CO_2}]_{(aq)} \qquad (1.9)$$

Total Alkalinity (TA) – defined by Dickson (1981) as "*the number of moles of hydrogen ion equivalent to the excess of proton acceptors (bases formed from weak acids with a dissociation constant $K \leq 10^{-4.5}$, at 25C and zero ionic strength) over proton donors (acids with $K > 10^{-4.5}$) in one kilogram of sample*" [19]. The individual species that contribute to TA, and characteristics of their behaviour in the marine environment are examined more closely in Section 1.4.1.

Along with measurements of the in situ temperature and salinity, a knowledge of any two of these parameters can be used to calculate the entire carbonate system for a seawater sample [15]. However it has been shown that some pairings of carbonate parameters give favourable precisions in the determined parameters while others do not, the poorest precisions in calculated parameters are determined from pairings of pH and fCO_2, or TA and DIC. These are summarised in Table 1-1 [15, 20, 21].

Input	ΔpH	ΔTA (μmol kg^{-1})	ΔDIC (μmol kg^{-1})	ΔfCO_2 (μ*atm*)
pH, TA	-	-	±3.8	±2.1
pH, DIC	-	±2.7	-	±1.8
pH, fCO_2	-	±18	±15	-
DIC, fCO_2	±0.0023	±3.0	-	-
TA, fCO_2	±0.0021	-	±3.4	-
TA, DIC	±0.0062	-	-	±5.8

Accuracies assumed: DIC: ±2 μmol kg^{-1}, TA: ±4 μmol kg^{-1}, pH: ±0.002, fCO_2: 2 μatm

Table 1-1 – Uncertainties in determined carbonate system parameters from pairings of measurements. Taken from Zeebe and Wolf-Gladrow [15]

The uncertainties presented in Table 1-1 are obtained by uncertainty analysis based on known errors associated with these parameters. The worst combinations arise from determinations of TA and DIC from pH and fCO_2, and vice versa. Conversely with current technology, if pH and DIC measurements are used to determine fCO2 and TA the resultant uncertainty is approximately equal to that observed for direct measurement of these parameters. For all other combinations, determination of a carbonate parameter from other measurements has a larger uncertainty associated with it than if it were measured directly. fCO_2 measurements with precision in excess of 0.9 μatm have been performed at sea [22], and sensor technology is relatively well developed with commercial systems currently available [12], Instruments for in situ DIC measurement are in development, and reasonable precision (around 4 μmol kg^{-1}) was achieved in a

dockside deployment [23]. Systems for pH measurement are relatively well developed, as discussed further in Section 2.3 [12, 24]. As such, the most readily available instruments for carbonate measurements (pH and fCO_2) measure parameters that combine most poorly for the determination of others according to Table 1-1. In most cases, if a specific measurement is required by a study it is far better to measure it than to determine it from other parameters [25].

Apparatus capable of measuring TA in relevant environments and meaningful timescales have been relatively underdeveloped in comparison to other carbonate measurements [12, 26]. The required precision of TA measurements has been placed at around 0.5 µmol kg^{-1} for a 2300 µmol kg^{-1} sample, the equivalent of 0.02 % relative standard deviation (%RSD) [27]. This has been achieved in laboratory environments [28], however such levels of precision are not widespread, and have not been achieved on board ship (see Section 2.3). Pragmatically a value of 0.1 %RSD or better is considered acceptable for modern automated TA determination [29]. Measuring alkalinity frequently (every few minutes) allows short time or distance scale events to be observed [30]. In the case of a mobile platform, measurement frequency dictates spatial resolution. For example, underway measurements taken on board a ship will be separated by ≈ 10 km for a sampling period of 20 minutes, while a profiling float operating at the same rate would have measurements separated by ≈ 120 m [31]. Additionally it is desirable to take measurements over long periods of time (weeks to months) and do so autonomously, as large seasonal variability in CO_2 parameters has been observed [32]. This can mask ocean acidification effects, and the ability to distinguish between these is important. This project aims to address these requirements through development of a low-cost automated TA measurement system that with further development would be capable of deployment on a variety of oceanographic measurement platforms. Section 1.6 gives more detail on specific aims and objectives.

Not shown in Figure 1-1 is the equilibrium with respect to calcium carbonate $CaCO_3$, both an important source and sink for dissolved inorganic carbon in seawater. $CaCO_3$ will spontaneously dissolve or precipitate depending on the carbonate saturation state (Ω), calculated according to Equation (1.10) [15, 33].

$$\Omega = \frac{[Ca^{2+}]_{SW}[CO_3^{2-}]_{SW}}{K_{sp}^*} \quad (1.10)$$

$[Ca^{2+}]_{SW}$ and $[CO_3^{2-}]_{SW}$ represent the concentrations of these species in seawater (in mol kg^{-1}), and K_{sp}^* is the stoichiometric solubility product for these two species (in $mol^2\ kg^{-2}$) for a given temperature, salinity, and pressure. Where $\Omega \leq 1$ the water mass is under-saturated with respect to $CaCO_3$, which will spontaneously dissolve. Alkalinity is intrinsically linked to carbonate saturation as precipitation and dissolution of $CaCO_3$ removes and adds two equivalents of alkalinity respectively, thus alkalinity is typically measured in studies wishing to calculate Ω [34, 35].

1.4 Alkalinity Theory

1.4.1 An Expression for Total Alkalinity

Dickson's 1981 definition of total alkalinity given in Section 1.3.2 can be represented in terms of the differences in concentrations of individual species classified as proton acceptors and proton donors according to equation (1.11);

$$\begin{aligned} TA = {} & [HCO_3^-] + 2[CO_3^{2-}] + [OH^-] + [HPO_4^{2-}] + 2[PO_4^{3-}] \\ & + [B(OH)_4^-] + [SiO(OH)_3^-] + [NH_3] + [HS^-] \\ & + [B] \ldots \\ & -[H^+] - [HSO_4^-] - [HF] - [H_3PO_4] - [HA] \ldots \end{aligned} \quad (1.11)$$

where [HA]… and [B]… represent minor concentrations of unidentified proton donors and acceptors respectively. A multiplier of two applied to the species CO_3^{2-} and PO_4^{3-} indicate that these are capable of accepting two protons.

The components of the expression consist of

- carbonate species (HCO_3^-, CO_3^{2-})
- hydrolysis products (OH^-)
- protons (H^+)
- species conservative with salinity, that is those whose concentrations remain proportional to salinity for a given water mass (borate, sulphate, fluoride)
- nutrients (silicate, ammonia, phosphate)
- unknown protolytes (HA..., B...)

The carbonate species contained within the alkalinity expression can be treated as an alkalinity term in their own right, known as the Carbonate Alkalinity (C_A, equation (1.12)), which is used in calculation of other carbonate parameters.

$$C_A = [HCO_3^-] + 2[CO_3^{2-}] \qquad (1.12)$$

In order to obtain a value for C_A it is necessary to subtract all non-carbonate species from TA, which may require simultaneous measurement of nutrients in high nutrient or eutrophicated waters, such as High Nutrient Low Chlorophyll (HNLC) regions or near riverine inputs, in addition to in-situ salinity (S). Practically S can be determined using a combined conductivity and temperature probe, or with a laboratory salinometer. Salinity measurements are necessary to determine contributions to TA from the species mentioned above. For determination of other carbonate parameters, in situ temperature (T) measurements are also required. In oligotrophic surface waters, nutrient concentrations are sufficiently low that TA behaves almost conservatively with salinity. This has been used to determine both TA and DIC in the North Atlantic from sea surface salinity (SSS) and fCO_2, with precisions of the order of 0.3 %RSD [36].

Dissolved Organic Matter (DOM) can contribute significantly to TA, and this has been quantified for fjordic waters containing a high concentration of DOM. Analysis of the Organic Alkalinity (OA) shows that these organic species contribute around 3 μmol kg^{-1} to TA in this case [37]. In the absence of simultaneous OA measurements when calculating carbonate system parameters from TA, an over-estimation of C_A will occur and affect determined values. Before explicit determination of OA was performed, unknown protolytic species in the expression for TA (1.11) were attributed to unidentified organic species within seawater [38]. Concentrations up to 20 μmol kg^{-1} for a

hypothetical species with a pKa around 6.00 (a proton acceptor in the definition of TA) was suggested as potentially being responsible.

1.4.2 pH Scales – NBS, Free Hydrogen, Total Hydrogen, Seawater

Since $[H^+]$ forms part of the definition of TA in equation (1.11) and pH measurement is central to alkalinity titrations, a short discussion regarding seawater pH is warranted. As stated in equation (1.8), a definition of pH is the negative log of hydrogen ion activity (rather than concentration) in solution. In reality, the hydrogen ion concentration in aqueous solution will be very low, with H^+ tending to be bound to water molecules forming a hydroxonium ion (equation (1.13)) [15].

$$H^+ + H_2O \rightleftharpoons H_3O^+ \qquad (1.13)$$

The concept of concentration in solution chemistry is incapable of describing the availability of species to undergo reactions, due to interactions with other species and the solution matrix itself. A high ionic strength medium such as seawater magnifies this effect, reducing the effective concentration of hydrogen ions. The activity of a solute represents its availability within a medium, denoted by curly brackets (1.14):

$$\{H^+\} = \gamma_{H+}[H^+] \qquad (1.14)$$

γ_{H+} is the activity coefficient specific to both the ion and the medium. Although equation (1.8) could be represented in terms of activity, this cannot be measured experimentally [15], and is instead estimated through the use of pH scales.

The NBS pH scale, devised by the International Union of Pure and Applied Chemistry (IUPAC), uses a series of standard pH buffers with assigned pH values close to the value of pH_a (antilog H^+ activity) which samples can be referenced against. As these have a low ionic strength compared to seawater, they do not represent the true activities of hydrogen ions in seawater, also a source of error when pH electrodes are used in measurement (see Section 2.2.3).

pH scales based on artificial seawater buffers overcome the problem of pH discrepancies caused by these differences in ionic strength.;

The free hydrogen scale pH_F, is simply defined as the concentration of free hydrogen available, $[H^+]_F$. In seawater, some H^+ remains bound to sulphate and fluoride ions, and so pH_F cannot be determined analytically [39, 40].

The total hydrogen scale pH_T, is based on buffered artificial seawater medium containing sulphate ions, defined according to equation (1.15). This takes into account the protonation effects of sulphate, and as such pH_T can be determined analytically [41].

$$pH_T = -\log_{10}([H^+]_F + [HSO_4^-]) = -\log_{10}[H^+]_T \quad (1.15)$$

pH_F can therefore be determined from pH_T, however in order to do so it is necessary to calculate $[HSO_4^-]$, requiring an accurate value of the dissociation constant K_S^* for the protonation equilibrium shown in (1.16), followed by calculation according to (1.17).

$$HSO_4^- \leftrightarrow H^+ + SO_4^{2-}; \quad K_S^* \quad (1.16)$$

$$[H^+]_F = [H^+]_T - [HSO_4^-] = [H^+]_T(1 + [SO_4^{2-}]/K_S^*)^{-1} \quad (1.17)$$

The seawater scale pH_{SWS} additionally takes into account the protonation of fluoride in seawater by including fluoride ions in the reference media (1.18) [15].

$$pH_{SWS} = -\log_{10}([H^+]_F + [HSO_4^-] + [HF]) \quad (1.18)$$

These pH scales solve many of the problems associated with the NBS system for carbonate system studies, however the NBS scale is still of practical use where a wide range of ionic strengths exists between samples [42]. In the context of most modern carbonate system measurements, the total hydrogen scale has been deemed sufficient as fluoride is generally much lower in concentration than sulphate [15, 26, 43].

1.4.3 Acid/Base Titration - The Equivalence Point and proton condition

Total alkalinity, in the absence of direct measurements for HCO_3^- and CO_3^{2-} is measured by titrating a seawater sample with acid and evaluating the titration data with some suitable mathematical method. Section 1.5 below discusses the theory behind titration, while a review of the techniques and instruments in Chapter 2 considers the best methods available for performing this.

1.5 Total Alkalinity Determination

Titration of seawater with acid is the most common method for total alkalinity determination. Following each acid addition, the pH is measured and a curve is produced, an example of which is shown as a solid black line in Figure 1-2. Each acid equivalent increases $[H^+]$ by one unit in equation (1.11), reducing TA by an equal amount. H^+ can then equilibrate by reaction with alkali species HCO_3^- and CO_3^{2-}, however this has no further affect upon TA as reaction of each alkali equivalent consumes an equal amount of H^+. For a simplified seawater system with carbonate-only alkalinity, the relationship between TA, the added acid equivalents *Acy*, and dissolved proton donating and accepting species is expressed according to (1.19).

$$\mathrm{TA} - \mathrm{Acy} = [\mathrm{HCO_3^-}] + 2[\mathrm{CO_3^{2-}}] + [\mathrm{OH^-}] - [\mathrm{H^+}] \qquad (1.19)$$

The titration curve shown in Figure 1-2 exhibits points of inflection at pH ≈ 7 and pH ≈ 4, caused by conversion of carbonate (CO_3^{2-}) and bicarbonate (HCO_3^-) upon reaction with the added acid (H^+), as the buffering action of each of these species is overcome. Concentrations of the principle dissolved species change during titration (Figure 1-2).

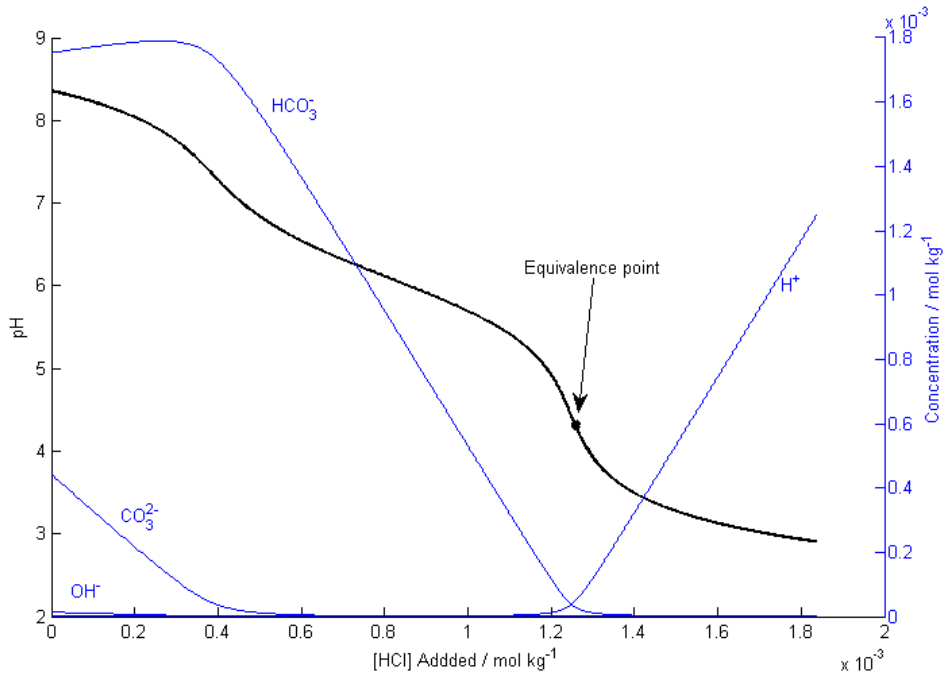

Figure 1-2 - Speciation during total alkalinity titration. The thick black line shows the titration pH curve, blue lines are concentrations of dissolved species. The concentrations of H^+ and HCO_3^- are approximately equal at the equivalence point, CO_3^{2-} and OH^- being relatively low here.

The second point of inflection in Figure 1-2 is referred to as the equivalence point, and the speciation here can be expressed according to equation (1.20), also known as the 'proton condition'. Effectively the TA of the solution reduces to zero, therefore both sides of equation (1.19) also equal zero, and added acid equivalents (Acy) equal TA. Determination of the amount of acid required to reach the equivalence point position is therefore effectively determination of TA.

$$[H^+] = [HCO_3^-] + 2[CO_3^{2-}] + [OH^-] \qquad (1.20)$$

Early approaches for TA determination focussed on numerical differentiation of the titration curve as the equivalence point would correspond to a peak in $\delta pH/\delta Acy$. This approach yielded poor estimation of TA however, as competing equilibria leads to peak asymmetry in the differential making evaluation difficult. In response, a general analysis method proposed by Gran in 1952 improved this [44]. The analytical excess of hydrogen is defined according to (1.21) where V_o is the volume of sample, V_a is the volume of acid

added, [acid] is the concentration of the acid titrant and V_{ep} is the volume of acid necessary to bring the equilibrium to the equivalence point.

$$V_0 + V_a = [\text{acid}] \cdot V_a - TA \cdot V_0 = (V_A - V_{ep})[\text{acid}] \qquad (1.21)$$

After the equivalence point, the excess of hydrogen $[H] \approx [H^+]$, so plotting $(V_o+V_a)[H^+]$ against V_a will produce a straight line with slope [acid] and intercept the x-axis at $V_a = V_{ep}$. An additional plot proportional to $-[H^+]$ against V_a is sometimes also created for error checking. Both lines should intercept the x-axis at V_{ep}, although in practice, they often do not and V_{ep} is instead said to lie at the intersection of the two straight lines. An example of a Gran evaluation is given in Figure 1-3.

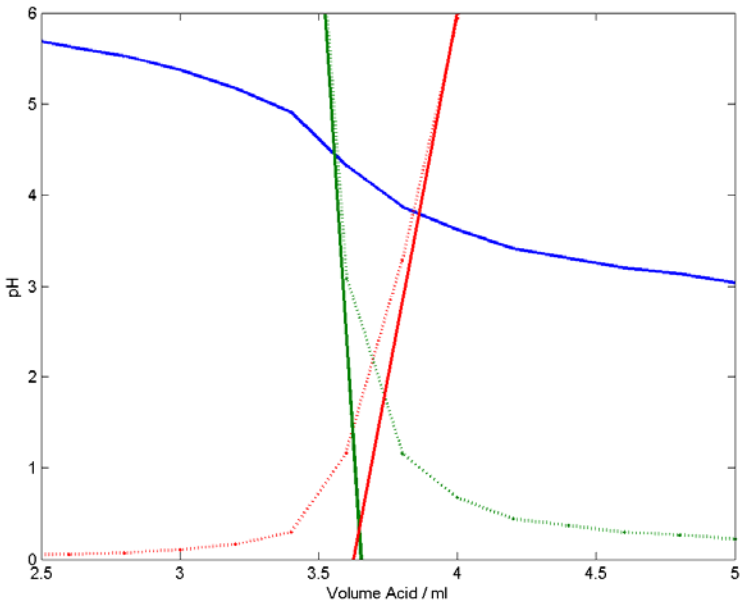

Figure 1-3 - A Gran plot for a seawater alkalinity titration, based on data taken from Dyrssen 1965 [45]. Solid blue line is the titration curve, dotted green and red the Gran functions and solid green and red are lines of best fit for the linear regions of these. Acid concentration is 0.1M, so determined alkalinity 2430 µmol L^{-1}

Though Gran's original method was applied to seawater analysis with little in the way of modification [45], it was prone to systematic error from competing acid/base equilibria. With more readily available computer technology able to perform complex calculations, an improved 'Modified Gran' was developed by Hansson and Jagner (1973) [46]. Following a traditional Gran evaluation, titration parameters were recalculated from the

determined equivalence point and optimised iteratively. Such is the precision and accuracy of the modified Gran approach that it is still in use today.

1.5.2 Non-linear least squares

The modified Gran approach can be thought of as a form of curve fitting, with system parameters iteratively tweaked to converge on the best estimate of TA. An alternative to the modified Gran proposed by Dickson (1981) uses a non-linear least squares technique to fit a chemical model to the titration data. Equation (1.19) is rearranged to equal zero, forming a basis for a 'residual' term for each titration point, equations (1.22) and (1.23).

$$0 = [HCO_3^-] + 2[CO_3^{2-}] + [OH^-] - [H^+] - TA + Acy \qquad (1.22)$$

$$r = [HCO_3^-] + 2[CO_3^{2-}] + [OH^-] - [H^+] - TA + Acy \qquad (1.23)$$

By squaring and summing the residual terms, experimental data inputted can have parameters varied in order to minimise this, giving the best fit of experimental parameters for the data collected. Figure 1-4 and Figure 1-5 show graphical examples of this.

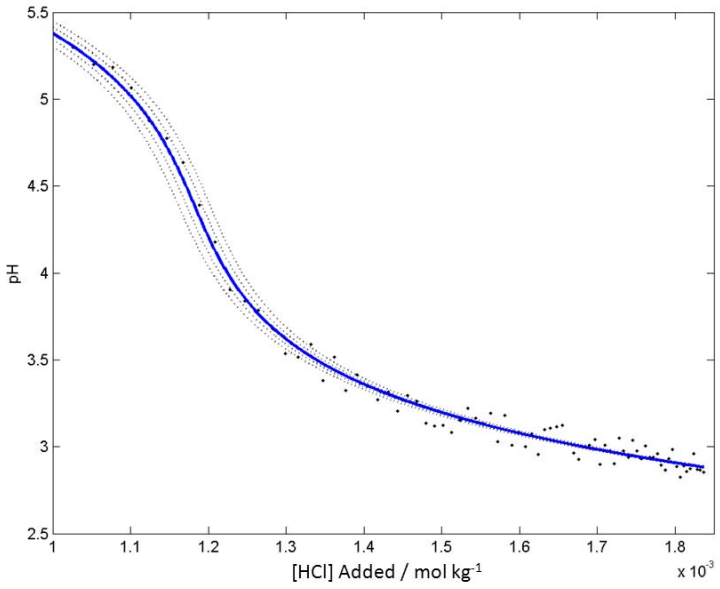

Figure 1-4 - Demonstration of a NLLS titration evaluation. Experimental data (black dots) can be fitted with various values of TA (grey dotted lines) to find the best fit (solid blue line).

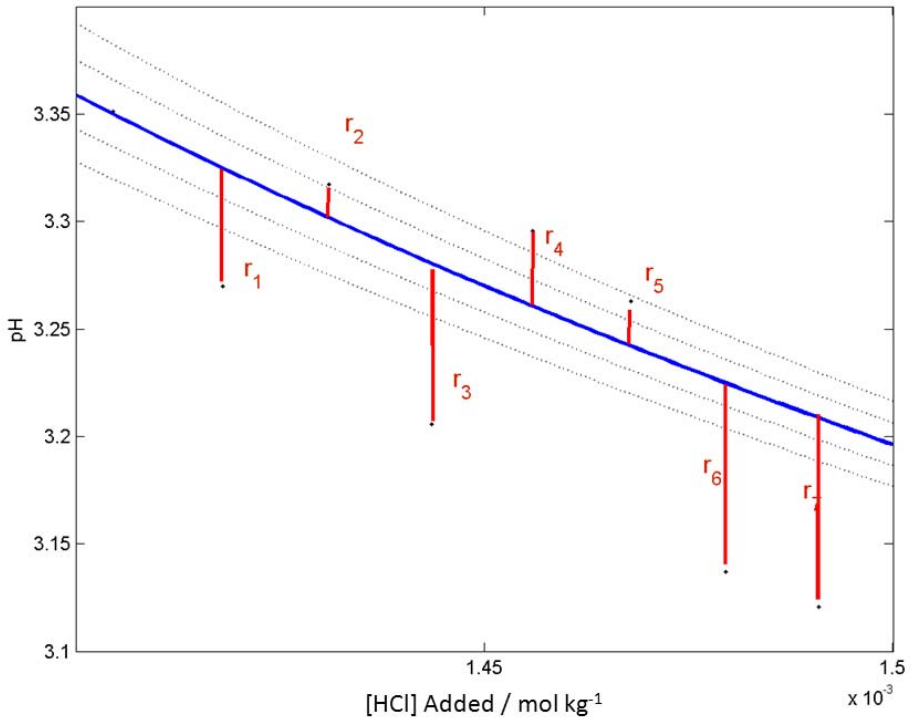

Figure 1-5 - NLLS routine performed by minimising the sum of residuals (r_{1-7}) generated as TA or other parameters are varied.

1.5.3 Open vs. Closed Cell Titration

The above examples of titration assume that no equilibration occurs between sample and atmosphere during titration. This allows assumption that DIC remains constant throughout the titration, and that CO_2 liberated by reaction of HCO_3^- and CO_3^{2-} with H^+ remains in equilibrium. The equivalence point position for a closed cell titration is partly dependent upon DIC, as increasing the concentration of CO_2 at the left hand side of the equilibrium in Figure 1-1 resists further conversion of HCO_3^- according to Le Chatelier's principle. Figure 1-6 highlights the DIC dependence of the equivalence point, and Section 2.2.1 examines the practical implications of maintaining constant DIC in open cell titration. Common to all the titrations discussed above is the need to record pH at regular intervals following titrant addition.

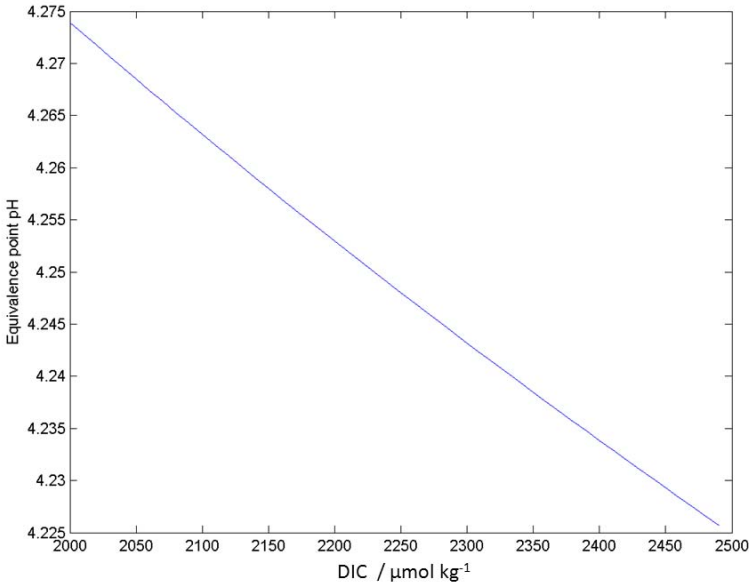

Figure 1-6 – Dissolved inorganic carbon (DIC) affects the pH at which the equivalence point occurs in a closed cell due to H_2CO_3 dissociation.

As an alternative, open cell titrations have been performed whereby CO_2 is driven off during titration [19, 47]. This removes the DIC dependence of the equivalence point, simplifies analysis and allows departure from the traditional multipoint analysis. In the excess acid method, a single aliquot of acid sufficient to push the equilibrium past the equivalence point is added and CO_2 driven off. pH measurement of the resulting solution allows estimation of the amount of acid consumed by alkali species, equivalent to the total alkalinity. This single step titration approach allows for much simpler and potentially faster analysis, but is less practical for in situ deployment due to the CO_2 purge. The excess acid method and open cell working are discussed further in Section 2.3.1.

1.6 Aims and Objectives

The overall aim of this project is to improve automated seawater TA determination. It is hypothesised that TA determination can benefit from further research and development of methods and instrumentation, and that recent technological advances will facilitate this. These have the potential to deliver smaller, cheaper, more robust instruments, which can improve the quality of measurements and be employed to make measurements which have hitherto been prohibitively risky, complex, or expensive. In

order to test this hypothesis, more detailed aims and objectives are identified and given as bullet points below, grouped according to the chapters of this thesis in which they will be addressed.

1.6.1 Chapter 2

- Examine available literature relevant to total alkalinity measurement.
- From the available literature identify key innovations and successes in TA measurement, including the current state of the art in both laboratory based and automated TA measurement.
- Identify which methods of TA analysis are most suitable for further development to deliver automated systems
- Identify key areas in which improvements need to be made to better address the needs of research scientists to examine the state of oceanic CO_2 uptake and ocean acidification.
- Identify whether analytical methods can be improved upon, and routes to achieve this.
- Aim to utilise techniques and components that can be further developed beyond the scope of this project. Try to ensure that there is potential for widespread uptake of the instrument by researchers. Identify what characteristics of the instrument may influence this.
- From this research, produce a list of target specifications for a new automated TA analysis system.

1.6.2 Chapter 3

- Given that a spectrophotometric technique is to be employed, identify the most suitable component for spectrophotometric measurement of TA. Examine the literature to determine which components have been successfully employed in chemical analysers. Identify from manufacturers whether a new type of detector can be employed.
- As an interim to automated TA determination, use the component to determine the quality of pH measurement that can be made.
- Examine whether this optical detection system will be suitable for TA determination by the method chosen in Chapter 2.
- Predict the performance characteristics of, and uncertainty associated with, the potential automated TA analysis device. Compare this with previous work by others.

1.6.3 Chapter 4

- Design and build an instrument capable of performing total alkalinity titration with specifications matching those identified at the end of chapter 2.
- Implement a microfluidic design in the building of the instrument.
- Optimise the operation of the instrument
- Analyse a series of simplified total alkalinity standards covering the range of oceanic pH values, within a simplified seawater matrix
- Analyse real seawater samples that may include a certified reference material (CRM).
- Determine the performance of the instrument and identify how well the performance satisfies the target specification in chapter 2. Identify shortcomings and determine methods for improvement.

Chapter 5 will summarise key findings and critically examine how well the above aims and objectives have been met. Necessary future work and opportunities for further development with be identified and examined for their feasibility.

Chapter 2

Literature Review

2.1 Total Alkalinity Measurements

Total Alkalinity (TA) measurements are based on the titration of weakly basic seawater with an acid. Modern approaches cover a variety of methods within this general experimental envelope, chosen for historical, operational and pragmatic reasons. It is possible to classify these according to the following:

- the reaction vessel (open vs. closed cell)
- titrant dosing (gravimetric vs. volumetric vs. measurement free)
- pH measurement method (potentiometric vs. spectrophotometric)

Each has its merits and shortcomings, detailed in Section 2.2. Additionally several standard techniques exist for the processing of titration data in order to determine TA. Detailed standard operating procedures exist for laboratory based alkalinity determination, establishing routine best practice worldwide [48]. Elements of TA titration apparatus have been automated and are commercially available, however much of the burden of sample collection and processing is still carried out by skilled technicians [49, 50]. Low sample throughputs of less than 5 samples per hour are typical, which coupled with requirements for frequent sampling and replicates leads to queuing. The resulting need to preserve samples is typically achieved by poisoning with small amounts of mercuric chloride, a potentially harmful and environmentally damaging substance [48]. Manual sample collection from research vessels is costly and time consuming leading to a chronic under-sampling of the ocean, and short term variability in species concentration easily overlooked [30]. Studies of surface-ocean carbonate parameters also show significant spatial variability (20 μmol kg^{-1} in DIC) over

distances of 10 km in the North Atlantic [51], which would require a demanding sampling regime to resolve by underway measurement. Additionally vertical profiles show TA varying by around 60 μmol kg^{-1} within the top 500 m of the Pacific Ocean [52]. Satisfying the need for automated TA determination has been the focus of much research since the 1970s; however the potentiometric pH measurements used to follow the titration are well known for being prone to drift. Seiter and DeGrandpre examined this drift in 6 pH probes, and observed in the worst case a deviation in pH of 0.040 ± 0.017 over a period of 56 days compared to spectrophotometric pH measurement. The use of redundant measurements combined with statistical analysis showed that this could be improved 3 fold (pH accuracy ± 0.012) for seawater pH measurement, however this has not been incorporated into an instrument for TA measurement as of yet. As such, the endurance of automated potentiometric instruments has been limited. Watanabe et al. were able to make stable measurements in the laboratory over 1-2 days (±0.15%, ±3 μmol kg^{-1}) without regular recalibration for drift, although alkalinity standards were regularly introduced as a means of correcting for drift [53]. Martz et al. have demonstrated new apparatus based on spectrophotometry with a respective accuracy and precision of ±0.2% and 0.1% (4 μmol kg^{-1} and 2 μmol kg^{-1}) with the potential for uninterrupted deployments of over a month [29]. Watanabe's (Section 2.3) and Martz's (Section 2.4.3) techniques are reviewed in more detail later in this report. The deployment of autonomous systems at sea has been limited to short-term underway measurement with skilled operators on hand to monitor the instrument, enduring at least 5 days in the open ocean [54], and 6 days in coastal waters [30]. Deployment aboard truly remote platforms such as moorings or AUVs have not been reported.

By contrast, systems and technology for pH measurement are better developed for automated deployment in a variety of environments, yet share many similarities with alkalinity systems [24, 55]. The added complexities of the use of a titrant reagent, its quantification, and multiple measurements (see Section 1.5) for a single sample in conjunction with more complex flushing requirements between samples invariably makes TA systems more difficult to operate.

Automated TA titration instruments will require several common components irrespective of the specific methodology chosen. These are:

- a means of handling liquids (sample and titrant)
- a way of quantifying the relative proportions of sample to titrant
- a method of mixing titrant and sample
- a means of following pH during titration
- some form of temperature control and/or measurement

The above requirements are discussed in more detail in Section 2.2 below.

2.2 Components of a Titration System

2.2.1 The Titration Vessel

Conventional multipoint batch titrations are based around either an open or closed cell titration vessel [48]. Mixing within these has typically been achieved with magnetic stirrers, and all standard procedures require thermostatic temperature control via air or water baths in order to prevent variation in equilibrium constants during titration. A temperature error of 0.8 °C will cause a change in pK_1 of around 0.01, which propagates to a TA error of ~15 μmol kg^{-1} [29].

Open cell titrations purge CO_2 liberated during titration from the sample mixture, which permits the assumption that the DIC at titration points close to the equivalence point is equal to zero (Section 1.5.3). The titration vessel is usually a jacketed beaker, and purging of CO_2 is achieved by bubbling an inert gas such as nitrogen through the sample [48].

Closed cell titrations assume that upon commencement of the titration that no gas exchange with the external environment occurs as CO_2 is generated. DIC can therefore be assumed to remain constant throughout the analysis. As such, the titration vessel needs to be gas tight with no headspace of air within the vessel, else gas exchange will lead to variation in DIC as the reaction progresses and affect the determination. A variable volume titration cell, typically achieved through the use of a movable syringe plunger within a suitable housing attached to the cell, is required to accommodate incremental titrant additions [48]. In some configurations the sample is displaced with each acid addition and sent to waste [29]. Whilst building a variable volume flow cell

that will remain gastight is challenging, the lack of a nitrogen purge makes this type of system more attractive for use in situ.

Whilst delivering similar levels of precision (σ = 1 – 3 μmol kg^{-1}) the open and closed cell techniques differ in apparatus requirements, striking a compromise between the simplicity of operation and suitability to the operating environment. For open water studies, both methods suit alkalinity ranges between 2000 to 2500 μmol kg^{-1}. For alkalinities above and below this range, standard operating procedures recommend the use of closed and open cell methods respectively [48].

2.2.2 Sample Quantification and Titrant Additions

Gravimetric additions are achieved by quantification based on mass, and is achieved using a high precision balance where repeated measurements to within ± 0.05 mg are achievable. It should be noted that this performance can be affected by air buoyance and vibrations when measuring a sample within a container. Mass based measurements place all determined units in the preferred mol kg^{-1} standard negating conversion [56], however the inability to operate balances aboard ship precludes the use of gravimetric determination at sea.

Volumetric additions are commonly employed via the use of a dosimetric piston burette or piston pump. These are commercially available (Metrohm, SI Analytics) [57, 58] and deliver suitable accuracy (reproducible to 0.001 cm^3) for quality alkalinity measurements [48]. When working with lower sample volumes e.g. pore waters [59], the delivery of low volume titrant increments becomes a challenge. Burette dispensing equipment itself requires calibration, achieved by accurately weighing a series of dispensed volumes. As with gravimetric titrant additions, this cannot be performed at sea.

Measurement free methods have been demonstrated in some experimental systems, but not widely adopted for routine use (see Section 2.3) [12]. These systems use either: flow-rate as a means of determining the sample to titrant ratio [60], peak width vs. time approaches [61], or spectrophotometry of the titrant in the final solution (see Sections 2.3 & 2.4) [29]. Although these can be considered “gravimetric and volumetric free”, the burden of precision is shifted to some other part of the system, requiring high precision pumps, regular standard calibrations or sophisticated spectrophotometric apparatus.

2.2.3 pH Monitoring

During total alkalinity determination following each titrant addition it is necessary to monitor pH changes by some means (Section 1.5).

Potentiometry has been traditionally used as the means of following alkalinity titrations, and remains the standard choice for bench top determinations today [48]. Measurements are made using a standard hydrogen electrode (Figure 2-1) and pH is calculated according to the rearrangement of the Nernst equation (2.1).

$$\mathrm{pH} = \frac{\mathrm{E}^0 - \mathrm{E}}{2.303\mathrm{RT/F}} \qquad (2.1)$$

E^o is the standard electrode potential (V, equivalent to J C^{-1}) , E is the emf measured across the electrode (J C^{-1}), R is the universal gas constant (J K^{-1} mol^{-1}), T is the temperature (K) and F is the Faraday constant (C mol^{-1}). When the hydrogen electrode is immersed in a solution containing hydrogen ions, these induce a chemical potential between the sample and neutral buffer solution inside the electrode. This in turn raises an electrical potential across the internal and reference electrodes, measurable as a voltage by the pH meter. For accurate measurement calibration is necessary, typically achieved by a 2-point measurement for two pH buffers bracketing the range of pHs being measured. With equation (2.1) being of the form y = mx+c, this allows for adjustment of slope and y-intercept for the particular electrode. A liquid junction (component 4 in Figure 2-1) completes the 'circuit' of the standard. Should the ionic strength of the reference electrolyte and sample differ, a conflicting chemical potential is set up across the liquid junction, known as the 'liquid junction potential'. For this reason, the reference cell electrolyte must match the ionic strength of the water sample being measured, or corrections made for this. pH electrodes take around 2-5 minutes to stabilise between samples of different compositions under ideal conditions, so limiting the measurement frequency.

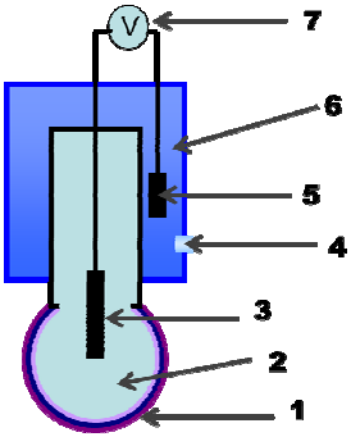

Figure 2-1 - Standard pH electrode

1) H+ sensitive glass bulb, 2) internal neutral buffer solution, 3) internal electrode, 4) reference/liquid junction 5) reference electrode, 6) reference electrolyte, 7) pH meter

Systems based on potentiometry are prone to drift and the noisy environment aboard ship is commonly blamed for loss of precision [29]. The voltages measured by the pH meter are small (a few 10s of millivolts) leading to a low signal to noise ratio. Drift has also been attributed to swelling and clogging of the liquid junction over time [62]. The drift between electrodes of the same design can therefore differ, as subtle differences in the operating environment or manufacturing tolerances means these effects may not be equal in all cases. In addition, differences in the solution chemistry of internal, reference, and sample media give rise to changes in the liquid junction potential [63, 64]. Incidentally, this is one of the reasons why the NBS buffer system is unsuitable for seawater pH measurement [15]. The requirement for recalibration to maintain precision complicates remote deployment, although strategies involving the use of redundant sensors in the form of multiple pH electrodes has shown that calibration-free potentiometric measurements are possible [62].

Spectrophotometric pH measurement involves the use of an indicator, which exhibits changes in its absorbance spectrum dependant on pH. This technique has been extensively used for oceanic pH [22, 63, 65-72] and alkalinity measurements [28, 29, 54, 73-75]. As indicators have a limited pH range over which useful measurements can be made, the selection of indicator is dictated by the pH range of interest in the titration, typically ranging from pH = 3.0 to 4.5 (see Section 1.5).

The relative merits of spectrophotometric vs. potentiometric methods have been examined for both pH [76] and alkalinity [77] determination in seawater. Anderson and Wedborg found in favour of potentiometric methods for alkalinity determination following an extensive study of both techniques with both Gran-type and curve fitting evaluation methods, whereas Byrne and co-workers reported similar imprecision for both approaches. The former study acknowledges that the apparently poorer precision seen in the spectrophotometric method could be caused by not accounting for the acid/base effects of the indicator. Sulfonephthaleins have been used successfully for in situ spectrophotometric pH measurements, though not yet for in situ alkalinity [55].

2.2.4 Titrant Composition

The majority of acidimetric alkalinity titrations use strong, monoprotic acids such as HCl as titrants. The drop in alkalinity upon each addition in this case equals the equivalents of added acid, due to full dissociation of the titrant in solution. It is standard practice to balance the ionic strength of the titrant to that of the sample being measured (0.7 μmol kg^{-1}), that is usually achieved by addition of NaCl. This keeps activity coefficients in the sample approximately constant throughout the titration [29, 48, 73].

The quality of titration results is directly linked to accuracy in titrant concentration (Section 1.5). High purity acids and careful titrant standardisation are recommended, with several strategies available to perform this by an alternate titration [19, 26, 54]. The standardisation procedure involves titrating the strong acid used for TA determination with an accurately prepared basic solution. It is sufficient for the titration data in this instance to be analysed by the unmodified Gran procedure (Section 1.5) [26]. Ionic strength is often balanced through salt additions to acid and base, though this introduces a potential source of impurities, a potential weaknesses in this approach. However, agreement in determined titrant acidity between methods of less than 0.05 % is possible [19].

2.2.5 Evaluation of Titration Data

Section 1.5 examines methods for evaluation of titration data to determine total alkalinity. Source code is available to perform the iterative NLLS procedure using a FORTRAN program [48], and has also been achieved through the use of Excel spread sheets with VBA scripting to handle filtering [29].

2.3 Performance of Existing Systems

Fully automatic total alkalinity systems have not shared the widespread application to seawater geochemical measurement seen in pH systems both aboard ship and in situ [55, 70, 78, 79]. Technology Readiness Levels (TRL - Table 2-1) provide a convenient means of quantifying the difference in the maturity of technology for pH and TA measurement capable of deployment in situ (Table 2-2), and have been previously used in the appraisal of marine sensor technologies [80, 81]. This disparity highlighted by the TRLs has been attributed to complexity in the design of TA systems, and the requirement for exceptional analytical performance [12].

TRL 1	Basic principles observed and reported.
TRL 2	Technology concept and/or application formulated.
TRL 3	Analytical and experimental critical function and/or characteristic proof-of-concept.
TRL 4	Technology basic validation in a laboratory environment.
TRL 5	Technology basic validation in a relevant environment.
TRL 6	Technology model or prototype demonstration in a relevant environment.
TRL 7	Technology prototype demonstration in an operational environment.
TRL 8	Actual Technology completed and qualified through test and demonstration.
TRL 9	Actual Technology qualified through successful mission operations.

Table 2-1 – Technology Readiness Levels (TRL), used in defence to gauge the maturity of technology used in mission scenarios[82]

System (pH or TA)	TRL	Reference
Semi-Autonomous Moored Instrument (SAMI™ pH)	8/9	[55]
Spectrophotometric Elemental Analysis System (SEAS pH)	8	[83]
Microfluidic pH	8/9	[71]
TMT (TA, spec) SAMI-Alk (development)	4 5-6	[29] [84]
GD (CA, spec)	5	[85]
EPM (TA, pot)	4	[53]
E.A. (TA, spec)	5	[74]

TMT Tracer Monitored Titration, **TA** Total Alkalinity, **GD** Gas Diffusion, **EPM** End Point Monitoring, **E.A.** Excess Acid, **spec** spectrophotometric, **pot** potentiometric

Table 2-2 – Comparison of the TRLs for automated pH and total alkalinity (TA) or carbonate alkalinity (CA) measurements designed for use in remote environments

The performance of TA measurements has not significantly improved since 1970, (Figure 2-2, Table 2-3) however the current level of precision achievable (± 0.6 μmol kg^{-1}) at sea is acceptable for ocean acidification studies [86]. Additionally highly precise laboratory based techniques have been developed (up to 0.012 %RSD / 0.3 μmol kg^{-1} in the case of Yao and Byrne 1998), though not employed at these precisions at sea [19, 28]. This method used the excess acid method, and continually monitoring pH with a sulfonepthalein indicator and linear array spectrometer. This way the titration could be terminated at a pH just below the equivalence point and thus the excess acid term was minimised. This, combined with accurate gravimetric titrant determination (0.001 g accuracy in around 130 g of sample) allowed for extremely precise analyses. As suggested in Section 1.3.2, an alternative to direct alkalinity measurements is to determine them from other carbonate parameters. Simultaneous flow through analysis of other carbonate parameters (DIC, fCO_2, and pH) aboard ship has been achieved and permitted reasonable calculation of total alkalinity values [22], with differences from discrete AT measurements performed using established methods consistent throughout the deployment at around 3.0 μmol kg^{-1}. Standard deviations better than 6 μmol kg^{-1} were achieved for seawater samples in this case [87, 88].

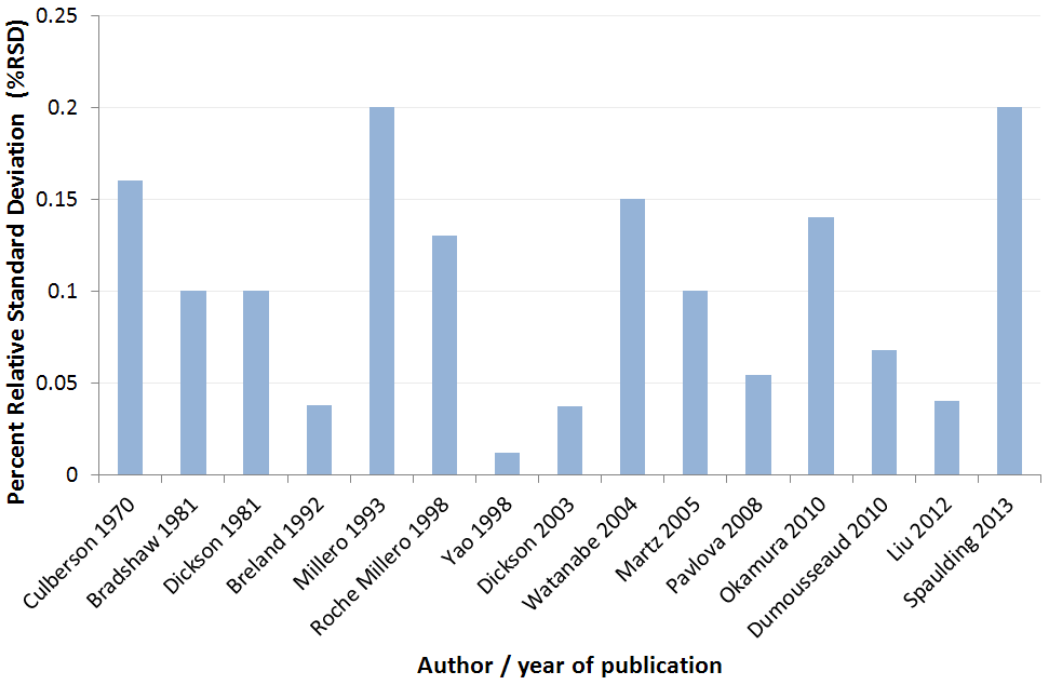

Figure 2-2 - Performance of precision TA methods since 1970, inspired by a figure taken from Martz 2005 [26], recalculated, and extended to include modern measurements. Only methods with a precision of 0.3 %RSD or better are considered. It should be noted that %RSD will vary depending on the TA of the sample analysed. Most fall short of the 0.02 %RSD suggested in Section 1.3.2 (reference [27]). Details of the methods are included in Table 2-3

The inability to utilise gravimetric methods at sea precludes direct automation of some of the highest precision (lowest %RSD) alkalinity techniques [28], and hence almost all attempts at automation rely on volumetric analysis. It is however possible to convert any gravimetric method to volumetry, so this should not preclude use of an otherwise promising technique. Quantitative sample and titrant dosing has been achieved through the use of calibrated volumetric pipettes and piston titrators [48], though these components are designed for semi-automated titration of larger sample quantities (1-100 ml, in 10,000 stepped increments) [58].

Method	Titrant Evaluation	Sample	%RSD	Reference	Author	Year
Pot. / E.A.	Vol	SW	0.16	[47]	Culberson	1970
Pot. / M.G.	Vol	SW	0.10	[89]	Bradshaw	1981
Pot. / NLLS	Grav	SW	0.10	[90]	Dickson	1981
CO_2 Equilib	n/a – Gas	SW	0.038	[91]	Breland	1992
Pot. / NLLS	Vol	SW	0.20	[87]	Millero	1993
Spec. / E.A.	Vol	SW	0.13	[54]	Roche	1998
Spec. / E.A.	Grav	CRM	0.012	[28]	Yao	1998
Pot. / NLLS	Vol	SW	0.037	[19]	Dickson	2003
Pot. / E.A.	Flow	Std. CRM	0.15	[53]	Watanabe	2004
Spec./ TMT	TMT	Std. CRM	0.10	[26]	Martz	2005
Bruevich*	Vol	SW	0.054	[56]	Pavlova	2008
Spec./NLLS	Vol	SW	0.14	[73]	Okamura	2010
VINDTA	Vol	SW	0.068	[86]	Dumousseaud	2010
Spec. / E.A.	Vol	SW	≈ 0.04	[74]	Liu	2012
Spec./ TMT	TMT	unknown	0.2	[84]	Spaulding	2013

Table 2-3 - Data to support Figure 2-2. For methods Pot. = Potentiometric, Spec. = Spectrophotometric, E.A. = Excess Acid, NLLS = Non-linear Least-squares, TMT = Tracer Monitored Titration, VINDTA = see ref [49, 86], Bruevich* = Bruevich's method[92] M.G. = Modified Gran, Grav = gravimetric, Vol = volumetric, CO_2 equilib = CO_2 equilibration method SW = Seawater, CRM = certified reference material

Automation of laboratory analyses is often approached via flow-through systems, where sample and reagents are continuously flowed together. Flow injection analysis is one such approach, with mixing of sample and reagents occurring due to turbulence in the flow [93]. The potential of such techniques to overcome the problem of performing automated gravimetric or volumetric additions of sample and titrant has seen the exploration of a variety of alternatives. As previously mentioned these "gravimetric and volumetric free" titrations invariably shift the burden of dosing to some other component in the system. Methods of sequential injection analysis performed by Fletcher and Van Staden[61], and Mesquita and Rangel[60] were used for spectrophotometric TA determination, with both methods reporting reduction in the required sample and reagent volumes. Sequential injection analysis differs from flow injection analysis in that sample and reagents are introduced sequentially into the analyser via a multiport valve. Fletcher used two indicator systems to determine both CO_3^{2-} and HCO_3^- equivalence points, allowing calculation of both TA and these individual species. Mesquita combined alkalinity, magnesium, and calcium determination with the same instrument. Indicator and acid titrant were premixed in both methods, with detection using single wavelength spectrophotometry. Sample and titrant were introduced one after the other into a holding coil, and then flowed to the

detector. The signal from the spectrophotometer is monitored over time producing a peak due to the indicator. By calibrating with known alkalinity standards, the alkalinity of a sample can be obtained from the width or area of the peak obtained. These systems require a precision peristaltic pumps to obtain quality measurements, which are both bulky and expensive. The precisions achieved were < 1.5 %RSD (Fletcher, 3700 – 11800 μmol samples) and 5%RSD (Mesquita, 164 – 1640 μmol kg^{-1} samples), which fall short of the 0.1 %RSD required for ocean acidification studies. The TAs were also measured outside the range of values that are of interest for ocean acidification studies. A potentiometric flow-through system demonstrated by Watanabe et al. achieved measurements over 1-2 day periods without regular recalibration [53]. Again acid was quantified from mixing ratios, and hence the performance of this system relies on the accuracy of the relative flow-rates of sample and titrant used to determine TA. Although a single-step technique, no purging of CO_2 with inert gas was used, which is surprising given the precision achieved. Some instability was experienced following the initial setup of the experiment, possibly due to bubbles. Once equilibrated with seawater samples the system stabilised significantly. The system was calibrated by comparison to a trusted instrument, with sodium carbonate standards, and with a seawater Certified Reference Material (CRM) distributed by A. Dickson, (Scripps Institution of Oceanography). The CRM was deemed better than prepared carbonate standard solutions for this purpose. Increasing the frequency of calibrations was said to improve precision in TA determination by a factor of two.

The spectrophotometric Tracer Monitored Titration (TMT) method of Martz et al. can be considered a truly gravimetric and volumetric free method, and does not require high precision pumps in its operation [29]. Total indicator concentration during titration is measured optically (via absorption and application of the Beer-Lambert law, see Section 2.4) and the result used to determine the amount of titrant added from a premixed indicator/titrant stock. Indicators sensitive to pH that exist in protonated and unprotonated forms (e.g. bromocresol green (BCG)) can be used to simultaneously determine pH and the amount of titrant added [29]. Here the burden of quantification is shifted onto the optical measurement system. A reasonable precision of around 0.1 % relative standard deviation (%RSD) was observed, though this was only achieved with a highly precise custom optical setup, and improvement on this would be challenging. TMT has been designed from the outset to be suitable for long-term automated operation, and has been run for over 40 days with operator intervention only to switch

between samples. The performance required from the photometric components of the system precludes the use of conventional spectrophotometer (precision better than σ = 0.0005 absorbance units (Abs) for desired 0.1 %RSD in TA). This required a specialist optical system based on trifurcated optical fibres, band pass filters, and a custom high precision system for electronic measurements of photodiodes. This enables measurement (at different wavelengths) of the concentration of the indicator in both protonated and unprotonated forms (to give pH and titrant amount) and provides a third measurement at a different wavelength used as a reference. The latter enables correction for changes in blank sample background absorbance (e.g. due to turbidity) and variation in the light source used for spectrophotometry. Alkalinity is determined from these measurements by fitting a model to titration data, using the non-linear least squares (NLLS) method [90].

Whilst TMT claims to be a simplified titration method, the extensive use of custom precision engineered components and assemblies are a significant hurdle to a researcher wishing to adopt the method. It is not surprising then that the technique has not yet been more widely adopted by other groups. The originators of TMT have however demonstrated the diversity of the technique for dissolved oxygen and complexation assays [94, 95]. Graneli's high precision automated TA determination method also relied on specially modified apparatus, and has not yet seen widespread use [96]. One goal of this study is to pursue ways of making improvements in automated measurements that will make them more accessible to oceanographers.

It has been suggested that fouling of the optical cell thwarted recent attempts to deploy the technique in situ, highlighting a potential weakness of TMT [97]. Because of its use in quantifying the titrant, TMT's performance is more heavily dependent of the quality of photometry than traditional spectrophotometric titration techniques. Where spectrophotometry is used for pH measurement only, and acid quantified volumetrically or gravimetrically, errors associated with photometry have less effect over determined alkalinity. This is due to multipoint titration evaluating several pH points for a single TA determination. In spite of this an instrument capable of month long deployment with reasonable precision (0.2 % RSD) based on the TMT method has recently been described [84].

Systems for selective determination of seawater carbonate ion concentrations have been developed based on spectrophotometric measurements of Pb(II)-carbonate complexes at

234 and 250 nm, although a relatively poor precision of 2 %RSD was observed [98]. Martz et al. also performed a titration coupled with direct UV spectrophotometric observation of carbonate within the laboratory [99]. The precision of the technique is reasonable at 0.7 %, however the use of ultraviolet spectrophotometry required an unusual custom-built optical cell with sapphire windows to follow the titration. As alkalinity is often used as a means of determining CO_3^{2-} in marine waters, particularly for elucidation of carbonate saturation state, these could potentially find use in calcification studies, though total alkalinity could not be determined from this measurement alone.

A continuous flow gas diffusion technique for carbonate alkalinity has been employed for estuarine waters aboard a small boat [85]. Sample is continuously reacted with a pH 4.5 buffer solution and liberated CO_2 quantified through spectrophotometric pH measurement of a weakly buffered bromothymol blue indicator solution separated by a PTFE membrane. Separation of the photometric indicator from the sample stream in this manner removes a consumable reagent from the system. As the indicator solution is stationary with respect to flow, fluctuations in absorbance associated with a flowing sample are less likely to be encountered. Membranes are themselves prone to fouling by a variety of mechanisms which would cause long term drift in the determined alkalinity [100]. The 1.0% RSD precision achieved by this method is an order of magnitude higher than that achieved by potentiometric methods (≈ 0.1 %RSD) [29, 53]. The influence of atmospheric CO_2 variation on the equilibration cell was blamed for some interference and in the confines of an open Rigid Inflatable Boat, exhaust fumes could also potentially play a role in this. Methods of mitigating this were implemented following the study by using glass containers fitted with a CO_2 trap for reagent storage.

2.3.1 Single step additions – the excess acid method

As mentioned in 1.5.3, a technique employing single step acid addition has seen limited use alongside the more widely used multipoint titration techniques. In this method, a single acid addition to a known volume of sample sufficient to push equilibrium past the equivalence point. Total alkalinity is determined from the resulting pH of the sample and the amount of acid added. The technique was demonstrated to be capable of high precision measurements by Culberson and co-workers (1970), and used successfully at sea with a precision of 0.16 % [101]. Purging with CO_2 is necessary to achieve higher precision, otherwise the equivalence point position is dependent upon remaining DIC (Section 1.5.3). Culberson also worked volumetrically rather than gravimetrically, and

did not pay particular attention to minimising the excess acid term. Further adaptation for spectrophotometric analysis achieved an excellent precision of up to 0.02 %, though these later developments employed gravimetric analysis and so is limited to shore-based laboratory work [28, 75]. To achieve this at sea it would be necessary to dose titrant in small quantities while continually monitoring pH to minimise the excess acid term, and to quantify the resulting titrant amount to 0.001 g, 1.0 µL or better. The method has been adapted for automated high precision continuous flow systems, where the conceptual simplicity of a constant mixing ratio of sample to titrant is suitable due to a restricted range of sample alkalinities [53, 54]. Early reports show that this method can be successfully applied at sea [74]. Sarazin and co-workers demonstrated a specific adaptation for small sample volumes and simple operation for the measurement of pore water alkalinity. The precision achieved was lower than would be required for ocean acidification studies (0.28 – 0.56 %RSD) [59]. Although not explicitly reported, as the amounts of sample and titrant specified in the method are given in units of volume, it is assumed that these were measured with manual volumetric dispensing equipment such as air displacement pipettes. The acceptable limit for the dispensed volume precision of these is around 0.6%, and is of the order of error in the precision observed. This was most likely done for speed and convenience, as the authors did have a precision balance at their disposal for gravimetric measurement of sample and titrant, capable of improving the precision of quantification by an order of magnitude or more. Additionally purging CO_2 by shaking the acidified sample in a container with a headspace of air meant that DIC was not fully reduced to zero, and so the "purged" mixture would have in fact still contain inorganic carbon species in an unknown equilibrium. The method could therefore be improved upon with better liquid handling and CO_2 purging.

Techniques that depart from conventional acidimetric titration have been explored and offer some advantages. A method based on equilibration of a seawater sample with CO_2 was developed by Breland and Byrne, essentially perturbing pH by reaction of water within the sample with introduced CO_2 [91]. This achieved a precision of (0.038 %RSD) for a 2368 µmol kg^{-1} sample. The method is relatively simple and precision comparable to high performance titrations. Its use as an in situ method is limited to surface waters because of the use of gas, and a long equilibration time (40 minutes) is required for each sample, around 3 times longer than most other methods. A refinement of the method was accepted as a patent, whereby a liquid core waveguide served as both equilibration

and photometry cell [102]. The potential for in situ operation is possible if equilibration with CO_2 stored in a liquid or solid state.

2.3.2 Conclusions about existing systems

Despite a need for robust automated systems for total alkalinity measurements in seawater (Section 2.1), these are under developed. For automated operation, the open cell titration method requires a CO_2 gas purge which limits the scope of deployments. This is unsuitable in situ and operationally challenging aboard surface platforms. The excess acid method also relies on a CO_2 purge to achieve the desired precision so this method can also be considered unsuitable for the same reason. By contrast, closed cell methods are more difficult to engineer, but are more suitable for automation and deployment. Potentiometry is still commonly used for following pH during titrations, however spectrophotometry is increasingly used in automated pH systems and is more suitable for in situ and long term deployments. It has therefore been decided to pursue a spectrophotometric method in this work.

Developments in continuous flow systems have reduced reagent consumption and sample volumes but the precision of measurements has fallen short of the requirements of modern oceanographic CO_2 studies (better than 0.1% RSD). While several systems claim to have removed the need for volumetric or gravimetric sample and titrant dosing, a greater demand is placed on some other component in the system (such as the optical system in TMT) to maintain precision.

The Tracer Monitored Titration method offers the best combination of simplicity, suitability for automation, and feasibility for deployment remotely and in situ. The precision demonstrated (0.1 %RSD) is not the best obtained, even compared to at-sea measurements (0.068 %RSD by Dumousseaud et al., Table 2-3), but is sufficient for ocean acidification and CO_2 system studies. It has to date however only been reported in the literature in a laboratory environment at a proof-of-concept level and would benefit from further refinement and testing at sea, although an advanced prototype (SAMI-alk) has been described [84].

2.4 Spectrophotometric pH Determination for Total Alkalinity Titrations

2.4.1 Introduction

As described in Section 2.3.2 spectrophotometry offers the most robust approach for long term automated deployment under a variety of operational conditions. It is therefore sensible to consider the background of the method in more detail.

2.4.2 Method

While the use of potentiometric titration methods remain commonplace [48], sulfonephthalein indicators for seawater alkalinity determination offer advantages for in situ and remote deployment, and have received significant attention in automated systems. In both spectrophotometric pH measurement and alkalinity titration, sulfonephthalein indicators are the mainstay of spectrophotometric seawater analysis. Sulfonephthaleins are large organic molecules with molar masses between 350 and 700 g mol^{-1}, and in solution behave as polyprotic weak acids (general formula H_2I), which undergo dissociation according to (2.2);

$$H_2I \overset{Ka1}{\longleftrightarrow} HI^- + H^+ \overset{Ka2}{\longleftrightarrow} I^{2-} + 2H^+ \qquad (2.2)$$

In the context of seawater alkalinity determination, the indicators Bromocresol Green (BCG)[75] Bromocresol Purple (BCP)[28] and Bromophenol Blue (BPB)[73] are extensively used. The structure of bromocresol green is shown in Figure 2-3.

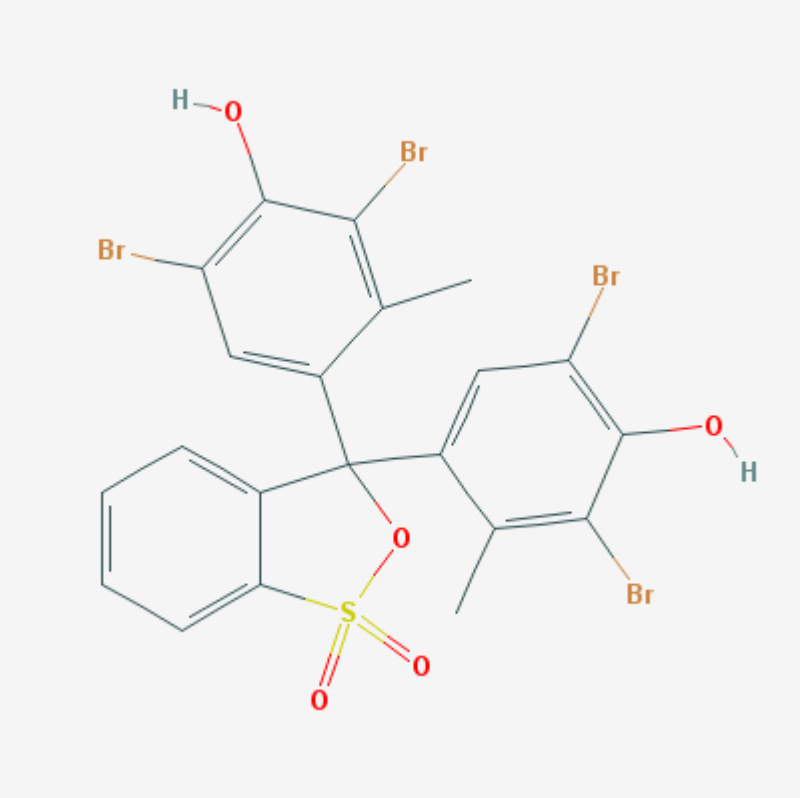

Figure 2-3 – Structure of bromocresol green (obtained from the Pubchem database, http://pubchem.ncbi.nlm.nih.gov)

All are available as sodium salts, which are reasonably soluble in water. For these, the first dissociation constant has a value significantly lower than the pH range of an alkalinity titration. As such, $[H_2I]$ is very small and the reaction scheme can be considered entirely in terms of HI^-, H^+, and I^{2-}, and the indicator treated as a simple monoprotic acid. The second dissociation constant Ka_2 is expressed as shown in (2.3).

$$Ka_2 = \frac{[I^{2-}][H^+]}{[HI^-]} \qquad (2.3)$$

pH can be related to Ka_2 (expressed as its negative log, pKa_2) through the Henderson-Hasselbalch equation (2.4).

$$pH = pKa_2 + \log\frac{[I^{2-}]}{[HI^-]} \qquad (2.4)$$

The acidic (HI^-) and basic (I^{2-}) forms of the indicator absorb light at different wavelengths. Derived from the Beer-Lambert law, the absorbance at a given wavelength λ is given by;

$$A_\lambda = l\left(\epsilon_{HI(\lambda)}[HI^-] + \epsilon_{I2(\lambda)}[I^{2-}] + B_\lambda + \text{error}\right) \quad (2.5)$$

Where ϵ_{HI} ϵ_{I_2} are the molar extinction coefficients for HI^- and I^{2-} respectively, ℓ is the path length of the absorption cell, B is the background absorption of the sample measured[1], and an error term is included for completeness [48]. The 'error' term in Equation (2.5) will include electrical noise in the light source and detector components of the spectrophotometer, mechanical disruption of the optical components and fluidic noise caused by any background absorbance in the flow-cell. Absorbance is measured experimentally from reference (I_o) and sample (I) light measurements.

$$A = -\log\frac{I}{I_o} \quad (2.6)$$

The molar extinction coefficients for the HI^- and I^{2-} species of BCG are shown in Figure 2-4 as a function of wavelength. By monitoring indicator absorbance at the peak wavelengths, the ratio $[I^{2-}]/[HI^-]$ of equation (2.4) is obtained using the following relationship (2.7) [64].

$$\frac{[I^{2-}]}{[HI^-]} = \frac{\left({}^{A_1}/_{A_2} - E_{HI}\right)}{\left(E_{I2} - {}^{A_1}/_{A_2}\right)E_2} \quad (2.7)$$

A_1/A_2 is the absorbance ratio of the two wavelengths λ_1 and λ_2 (444 nm and 615 nm according to Figure 2-4 and the values E_{HI}, E_{I2}, and E_2 are ratios calculated from the molar extinction coefficients of the acidic and basic forms of the indicator at the wavelengths of interest according to[64];

$$E_{HI} = {}^{\epsilon_{HI(\lambda1)}}/_{\epsilon_{HI(\lambda2)}}$$
$$E_{I2} = {}^{\epsilon_{I2(\lambda1)}}/_{\epsilon_{I2(\lambda2)}} \quad (2.8)$$
$$E_2 = {}^{\epsilon_{I2(\lambda2)}}/_{\epsilon_{HI(\lambda2)}}$$

[1] This is the absorption at the measurement wavelength not due to either form of the indicator (e.g. from turbidity). It is usually quantified by assuming a wavelength independence and determination of Absorbance at a wavelength where the absorption of the indicator is weak.

It should be noted that equation (2.7) and therefore also pH determination (equation (2.4)) are independent of both dye concentration and path length. pH itself is perturbed by dye concentration and can be corrected for [28].

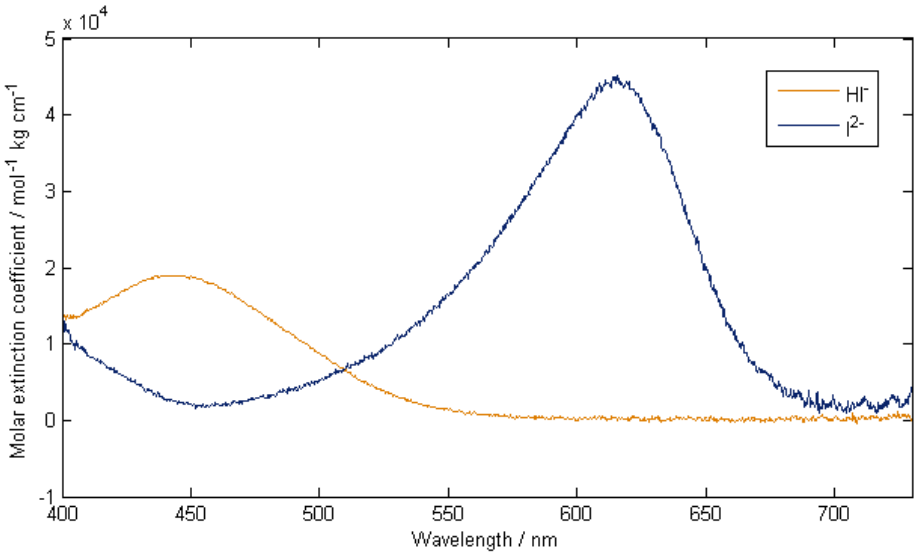

Figure 2-4 - Molar extinction coefficients of bromocresol green

The values E_{HI}, E_{I2}, E_2, and Ka_2 are empirically derived parameters and have been reported in the literature. They are however often determined for each new batch of indicator acquired as impurities in the sodium salts of indicators purchased cause variation [29, 64, 75]. pKa_2 values for BCG have for example been reported as 4.410 [64], 4.475 [26], and 4.435 [75]. The desire to utilise sulfonephthaleins in situ has led to investigation of the effects of pressure upon these parameters [103]. Although these studies have been limited to thymol blue for pH measurement, it has been shown that pressure changes have a small but significant effect: pKa_2 changing by less than 0.25 when pressure was increased to 827 bar, representative of full-ocean depth (around 8000 m). At depths of 1000 m, more relevant to a potential TA sensor deployment, the change in pK_2 was less than 0.03.

Investigations into the sources and substance of impurities in sulfonephthaleins have shown significant variation in the observed absorbance spectra between manufacturers and batches [26, 104]. Offsets in the measured pH of over 0.01 pH units have been observed, and although purification is possible using HPLC [104], this is not yet standard practice among indicator manufacturers. Additionally sulfonephthaleins photo-degrade when subjected to UV light. Husheer observed this during spectrophotometry of thymol blue, where over a period of 5 seconds the UV portion of the spectrophotometer's light

source caused a change in measured pH of 0.0005, with this decay remaining constant for around 5 minutes [105]. This would have a significant effect if photometry was performed over periods longer than a few seconds, or if the same solution was used for all measurements (e.g. Gray et al.) [85]. Steps should be taken therefore to ensure that no UV irradiation of sample occurs during spectrophotometry which can be achieved through filtering, or using light sources with no emission in the UV. Sulfonephthaleins should also be stored under dark conditions, where they have been shown to be stable for at least 2 months in an acidic titration mixture with dilute HCl [29].

2.4.3 Tracer monitored titrations

TMT is essentially a development of conventional spectrophotometric pH determination to include spectrophotometric determination of titrant amount. The latter is achieved via measurement of indicator concentration, which is premixed at a known concentration in the titrant.

Individual concentration terms for $[HI^-]$ and $[I^{2-}]$ can be expressed (using bromocresol green as the example) according to equations (2.9) and (2.10) [26].

$$\left[I^{2-}\right] = \frac{Abs_{615nm} - Abs_{444nm}\left(\frac{\varepsilon_{615nm}^{HI^-}}{\varepsilon_{444nm}^{HI^-}}\right)}{\varepsilon_{615nm}^{I^{2-}} - \varepsilon_{444nm}^{I^{2-}}\left(\frac{\varepsilon_{615nm}^{HI^-}}{\varepsilon_{444nm}^{HI^-}}\right)} \tag{2.9}$$

$$\left[HI^-\right] = \frac{Abs_{444nm} - Abs_{615nm}\left(\frac{\varepsilon_{444nm}^{I^{2-}}}{\varepsilon_{615nm}^{I^{2-}}}\right)}{\varepsilon_{444nm}^{HI^-} - \varepsilon_{444nm}^{I^{2-}}\left(\frac{\varepsilon_{615nm}^{HI^-}}{\varepsilon_{615nm}^{I^{2-}}}\right)} \tag{2.10}$$

The wavelengths 444nm and 615nm represent absorbance maxima for the HI^- and I^{2-} species of BCG, respectively. Concentrations are calculated from absorbance (Abs) and molar extinction coefficients (ϵ) at these wavelengths. $[I_{tot}]$, the total indicator concentration in the sample can then be calculated from the sum of these two terms, as $[H_2I]$ is negligible at the pH of interest.

$$[I_{tot}] = [HI^-] + [I^{2-}] \quad (2.11)$$

For a premixed titrant stock with known concentrations of indicator $[I_{stock}]$ and acid $[Acy_{stock}]$, the amount of titrant added can be determined by multiplying $[Acy_{stock}]$ by the dilution factor of the indicator, D;

$$D = \frac{[I_{tot}]}{[I_{stock}]} \quad (2.12)$$

In this case, titrant additions are determined in the concentration domain, and directly inputted as the value of Acy in equation (1.23) for TMT based TA determination.

2.4.4 Conclusions of the Spectrophotometric Method

Spectrophotometric methods are well established for Total Alkalinity and pH measurements of seawater. The indicators used in the highest impact recent research have all been of the sulfonephthalein class of compounds, with BCG, BCP and BPB. Despite values being reported for spectrophotometric properties and dissociation constants of the indicators, it is recommended that these are recorded for each new batch of indicator as manufacturers do not yet supply these at sufficient purity. Limited work into the sensitivity of sulfonephthaleins at high pressure suggests they are suitable for in situ deployment at up to 1 km [103]. They are stable when kept away from light, even when mixed with dilute acid, making them extremely useful for longer-term deployment. Spectrophotometric methods do not suffer from the drift and liquid junction problems associated with potentiometric methods, and are therefore more suited to automated methods. Tracer monitored titrations (TMTs) use spectrophotometry for acid quantification. While this places additional weight on the performance of the photometric measurement, it simplifies the acid delivery equipment requirements, and has been applied to a fully automated TA determination.

2.5 Conclusions Drawn from Reviewed Literature

The availability of instruments for automated total alkalinity measurement is limited, highlighting the need for further research in this area. Ocean acidification and other

carbonate system studies require time-series measurements to distinguish seasonal variation from long-term trends in ocean CO_2 concentrations. To achieve this by conventional sampling and analysis is impractical. Deploying instruments aboard moorings, ships of opportunity, and as underway systems on oceanographic cruises overcomes this obstacle. This requires robust, automated systems with the necessary endurance capability to operate in these challenging environments unattended for long periods (up to 1 year). Additionally in situ instruments are not currently available for total alkalinity studies. By contrast, systems with these capabilities are available for pH.

For oceanographic researchers to adopt any new developments on a significant scale, simplicity of operation and ready availability of any new technology are important factors to consider in design. Spectrophotometric techniques present a better approach for automated alkalinity determination than potentiometric techniques, as they suffer less from drift and salinity sensitivity, and can be deployed in situ. Research into spectrophotometric pH systems is extensive, and mature systems are available. By contrast, systems for total alkalinity measurement have only seen deployment in the laboratory and aboard ship. The TMT technique shows great potential for exploration, as the gravimetric and volumetric free method described allows a wide variety of fluid delivery methods, and the system can be scaled for large and small volume samples.

This project aims to address this shortfall by developing an instrument for high precision (better than 0.1 %RSD over a TA range of 2000 – 2500 μmol kg^{-1}) automated alkalinity measurements. Reducing the cost of instrumentation promotes the uptake of the technology and allows for measurements that are more extensive. This will be addressed by taking advantage of recent developments in sensor technology and optoelectronics. LEDs and photodiodes offer excellent reductions in cost and size over traditional spectrophotometers. Where possible only methods and technologies that could eventually be adapted for in situ measurement will be used. The developed instrument will take the form of an advanced prototype that pushes technological boundaries while attempting to preserve the quality of measurement. For TA, the precision should approach ±1 μmol kg^{-1} over the oceanic TA range.

Table 2-4 below summarised the target specifications for an automated TA instrument. The rationale behind this specification is that it will lead to an instrument that can be employed on board a research vessel as a continuously running underway instrument. The specifications reflect the fact that it is desirable that the instrument could be

adapted and improved for deployment beyond the ship, either in situ or on a mooring. This must be kept in mind during the design and building phase of the instrument, such that a decision is not taken which will preclude further deployment of a future generation of the device.

Specification	**Target performance**
Deployment environment	Capable of underway measurement onboard ship.
Size	60cm x 60cm x 60cm for a bench top instrument
Power consumption	3 kW* (assuming mains power available)
Endurance	Up to 1 month
pH Measurement method	Spectrophotometry
Precision of TA measurement	σ = 1 - 2 µmol kg^{-1} , or better than 0.1 %RSD over the range of oceanic TA
TA Measurement range	2000 – 2500 µmol kg^{-1}
Open / closed cell (reaction cell type)	Closed cell
Analysis time per sample	20 minutes
Amount of sample consumed per analysis	< 100 ml, allowing multiple measurements for 1 litre of collected sample.
Amount of titrant consumed per analysis	< 1 ml, allowing 1000 measurements for a 1 litre reservoir

Table 2-4 – Target specifications for a total alkalinity analyser.

*The system developed in this project is envisioned as being a bench-top laboratory system, where standard mains power will always be available, and incorporating a water bath. The power requirements for remote deployment beyond the laboratory would be more stringent, of the order of a few watts to tens of watts.

Chapter 3

A novel optical system for spectrophotometric pH and titration measurements

3.1 Introductory material

3.1.1 Introduction to experimental chapters

The previous chapters of this thesis have identified the scientific need for total alkalinity (TA) measurements, and the shortcomings of available instrumentation in terms of automation, portability, ruggedness, and cost. Conversely, the analytical quality of available laboratory methods is sufficient for meaningful analysis of the oceanic carbonate system. Developments in instrumentation for measuring total alkalinity therefore need to address these shortcomings without compromising performance. The ultimate goal is delivery of a low cost, precise, fully automated alkalinity analyser (Section 1.6). Also making long-term measurements aboard ship or i*n situ* is desirable. Reducing the cost associated with an instrument, particularly one which can be automated has several attractions. More individual instruments can be purchased for a given cost, allowing more extensive measurements to be made, and allows consideration of bolder deployments which carry risk of damage, or where the instrument would not be recovered. Reducing size allows for deployment on mobile platforms such as gliders, AUVs, and floats, or static platforms where space is at a premium. An example of this would be 'ferry box' type deployments aboard small ships. The aim of this project is to examine whether new technologies can help achieve this goal. The following chapters

will focus on developments in these key areas for the production of an instrument capable of extending scientific exploration of the carbonate system in oceanic environments.

Chapter 2 identified the spectrophotometric Tracer Monitored Titration (TMT) methodology as most promising for improvements in TA instrumentation. The analytical performance of this method depends heavily on the optical system. Chapter 3 therefore focusses on spectrophotometric technology, keeping in mind the key requirements of portability, ruggedness, and cost identified in the project aims and objectives (Section 1.6). Choosing the TMT method would require a specific high performance optical detection system, which in the original method consisted of a bespoke combination of photodiodes and bandpass filters. Red green and blue photodiodes (RGB-PDs) offer similar performance, but are cheap off-the-shelf components. The following chapters examine whether this device can perform TA measurements by the TMT method. The literature has few examples of RGB-PDs used for similar multi-wavelength photometry, and there is a lack of quality publications in this area. The measurement of pH with the photodiode was chosen to further demonstrate the potential of RGB-PDs for spectrophotometry, and to provide a basis for assessing their suitability for TA measurement by TMT. Part of the work described in this chapter forms a manuscript submitted to the journal Optics Express for publication.

Based on the theoretical work carried out in this chapter, the RGB-PD performs well as a replacement for spectrophotometers for pH measurement, and further examination for TA measurement by TMT is justified. The RGB-PD cannot make the diversity of measurements achievable with a spectrophotometer, and the unit examined does not possess the performance characteristics of the bespoke photometry system described for the TMT method. However, the extremely low cost and small form factor make the RGB-PD a pragmatic alternative, and the device is tested as a detector in a total alkalinity (TA) auto analyser in Chapter 4.

3.1.2 Introduction to spectrophotometry

UV-Visible spectrophotometry of aqueous solutions can determine the concentration of coloured dissolved species, mentioned for its role in total alkalinity determination in Section 2.4. Attenuation of a light source by the solution relative to a reference is used to determine absorbance ($\mathcal{A}$, equation (2.6)) through a path of length ℓ, allowing the concentration (c) of the dissolved species to be calculated according to the Beer-Lambert

law ($\mathcal{A} = \epsilon\ c\ \ell$), provided the molar extinction coefficient of the species (ϵ) is known [106]. Often the coloured species under investigation is the product of a chemical reaction, and evolves relative to the concentration of a colourless species following addition of a suitable reactant. The simplicity of these measurements, and the availability of assays for a wide variety of common, weakly coloured target species have contributed to the popularity of this approach [107].

In order to exclude non-absorbed background light and maintain linearity, photometry experiments require that optical components have a narrower spectral bandwidth than the absorbing species being studied. The Beer-Lambert law assumes the use of monochromatic light, which is not achievable in practical instruments. Instead the band-pass of incident light is restricted to the extent that deviation from the linear relationship between concentration and absorbance is within an acceptable limit. The Beer Lambert relationship is therefore approximated rather than adhered to [108, 109]. As a general rule the combination of light source and detector should possess a full width half maximum (FWHM) value of 1/10 or less that of the absorbing species being studied [110]. Larger ratios will hamper effective light attenuation by the absorbing species and limit the dynamic range of concentration measurements possible. The chromaphore concentrations encountered are often bracketed by the concentration range of standard solutions used to determine ϵ. If the standard concentrations chosen have linear absorbance responses, chromaphore measurement will adhere to Beer Lambert behaviour.

3.1.3 Available optical detection systems for spectrophotometry

The most readily available instrument for making the types of measurements outlined in 3.1.1 is a charge coupled device (CCD) spectrophotometer. These use a diffraction grating or prism to split broad-band light into its component wavelengths, and project the resulting spectrum over a CCD giving excellent optical specificity with band-pass of less than a nanometre [111]. While these devices are applied to a wide variety of photometry experiments, they are typically expensive ($500-$10,000 USD), fragile, and often bulky. Their ability to make simultaneous measurements at multiple wavelengths however has meant that they remain the go-to device for analyses such as colorimetric pH measurement (and therefore also TA measurement), where the absorbance of a pH indicator at two different wavelengths is measured [69].

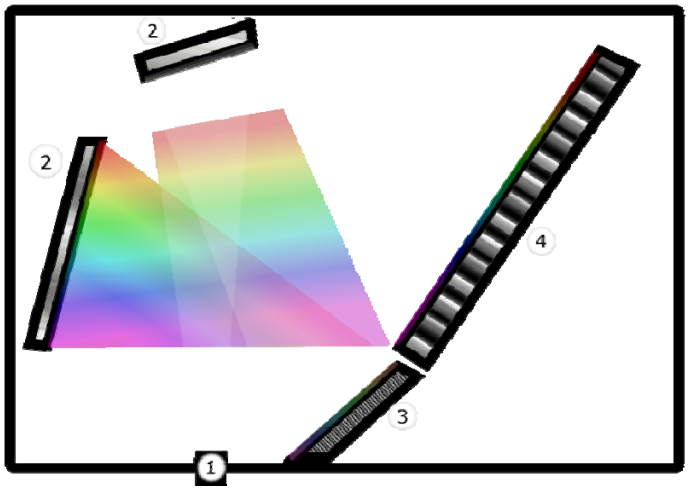

Figure 3-1 – Schematic of a charge coupled device (CCD) spectrophotometer, showing entrance slit (1), mirrors (2), diffraction grating (3) and CCD (4). The small size and high performance of these devices make them extremely versatile for light measurement.

The ability to make simultaneous light measurements across a spectrum of wavelengths is not required for the majority of assays, allowing simpler detection systems such as photodiodes to be used instead. Although photodiodes have broad spectral responses spanning several hundred nanometers of wavelength, Light Emitting Diodes (LEDs) have played a significant role in the development of absorbance-based analytical instruments, having sufficiently narrow bandwidth to be successfully employed as light sources [112, 113]. Where photodiodes have lacked the required sensitivity, photo-multiplier tubes (PMTs) and avalanche photodiodes are able to perform quality measurements with weaker light signals, though with increased cost [114]. LEDs themselves can be used as detectors, and a novel system using reverse-biased LEDs has demonstrated that a single carefully selected LED can function as both emission source and detector with good specificity for the target species [112, 115-120]. This type of detector, sometimes called a paired emitter-detector diode (PEDD) offers excellent performance when combined with a suitable amplifier circuit. In some cases two identical LEDs are sufficient, however in others a lower energy LED is used for the detector compared to the emitter. A system with this arrangement of two differently coloured LED has been demonstrated in the detection of total iron in groundwater samples [121].

Given the low cost and small size of photodiodes, where multiple wavelength analysis is needed efforts have been made to use these in place of spectrophotometers. Several approaches have been examined with success. The most straight forward uses a broad

spectral band-width detector by alternately switching between differently coloured LEDs, and this approach was successfully applied to acid-base titration [122, 123]. A progression of this technique has shown that multiple wavelengths can be simultaneously resolved with a single detector [124]. Several wavelengths of LEDs are driven with different square-wave frequencies, and FFT processing of the detector signal allows conversion from the time domain to frequency, from which the individual light intensities can be obtained. In this example light from the LEDs was passed through two separate channels, allowing reference measurements to be made simultaneously as is common in conventional bench-top spectrophotometers. More sophisticated electronics or computation is required for this approach. An alternative is performing monochromation (filtering broad band light to give a single, very narrow band) at the detector, and a dedicated system has been demonstrated combining several photodiodes with specific band-pass filters, albeit with increased cost and complexity of the optical system [29].

Within the context of TMT, the performance of typical CCD spectrophotometers falls below that required for quality TA measurements (see Section 2.3). The bench-top TMT instrument described by Martz and co-workers therefore made use of a high performance low-noise photodiode based system [26]. This combined several photodiodes with specific band-pass filters, allowing two absorbing wavelengths of bromocresol green (BCG) to be monitored, along with a background measurement at 750 nm. This extensive use of band-pass filters brings with it increased cost and complexity to the optical system. A digital camera sensor is essentially a 2D array of photosensitive elements able to distinguish red, green and blue light. A simple webcam was demonstrated as a detector for titration in undergraduate teaching experiments as a low cost alternative to a spectrophotometer. Only 1 channel was used to monitor titration however, and the sensitivity of the device was limited [125]. Although higher performance cameras are available, their price is comparable to a spectrophotometer and therefore makes little sense as a replacement.

RGB photodiodes (RGB-PDs) consist of an integrated package including an array of photosensitive elements that are doped or covered with filters. This allows discrimination of red green and blue wavelengths of light, essentially a one pixel digital camera. The potential for the RGB-PDs to function as spectrophotometric devices has been realized, and used for multicomponent analysis on an embedded device [126, 127].

Indeed colour sensors such as this have already been used to measure pH by examining the colour of indicator paper, essentially automating an analysis normally performed by hand and eye, and with similar sensitivity (1 pH unit) [128]. Though not demonstrated, their use in a titration device has been mentioned, and so the idea that they can perform in this role is not new [129]. At the time of writing, high precision, simultaneous multi-wavelength absorbance measurements made with RGB-PDs goes unreported, which is surprising considering their relatively low cost, and reduced size (Figure 3-2).

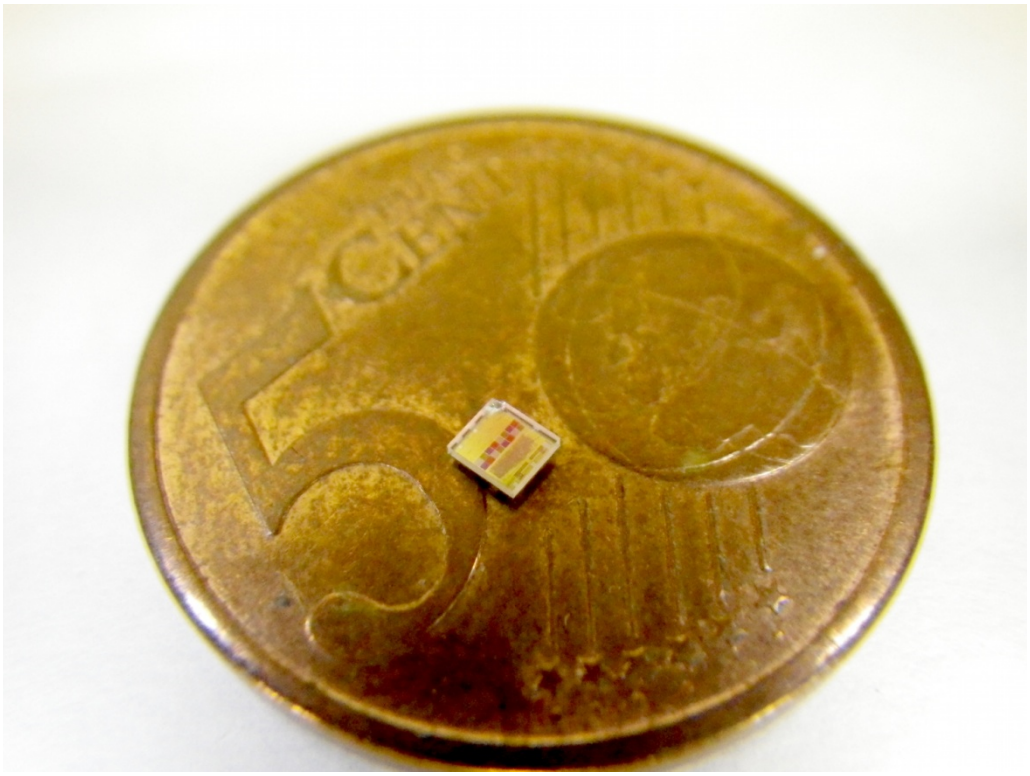

Figure 3-2 – TAOS TCS3414-CS photodiode, highlighting the small size of RGB-PDs. The photosensitive area is apparent as a series of coloured squares in a rectangular array in the centre of the component. The housing also contains circuitry for analogue to digital conversion and communication.

3.1.4 Spectrophotometric pH measurement

pH measurement is an example where multiple wavelength monitoring is required. At least two wavelengths are normally monitored, and several optical detection devices exist which are capable of this. The simplest optical detection system implemented for measurement of pH, and by extension total alkalinity (TA), is a charge coupled device (CCD) spectrophotometer. The excellent wavelength specificity and inclusion of a monochromation device allows use of a variety of light sources. The cost associated with

these systems is high however, with high specification devices costing approximately $10,000, although some low-end system are far cheaper at ≈ $500. Any experimental design of an optical detector for spectrophotometry has to be compared to a spectrophotometer (such as those supplied by Ocean Optics Inc., USA) as the "gold standard" measurement.

As mentioned, a quasi-monochromatic light source such as an LED allows a broadband detector such as a photodiode can replace the spectrophotometer. Multiple wavelength measurements with photodiodes need some way of preventing cross sensitivity when using two or more light sources. Whether this is achieved optically (filters), mechanically (two separate channels or a shutter), or electronically (FFT techniques or switching), an additional engineering requirement is encountered, invariably increasing cost and complexity.

An alternative is a ready-made filtered detector, such as a camera or RGB-PD. The optical band-pass of these filters cannot be easily varied, so the device needs to be chosen carefully, and it may be that an off the shelf component does not exist. High performance cameras are expensive, while RGB-PDs can be extremely cheap. Table 3-1 below summarises the available detection systems for spectrophotometric determination of pH.

The absorbance spectrum of bromocresol green (BCG) pH indicator has bands matching the spectral response of an RGB-PD (TCS3414CS, ams AG).

Given the objectives outlined above (improvement of cost, size, ruggedness, automation), and as pH measurement has no requirement for 2D resolution, the RGB-PD is well worth considering. There is novelty in the approach, as these devices are underrepresented in the literature. A commercially available RGB-PD device (TCS 3414CS, ams) has spectral specificity which matches the absorption bands of bromocresol green (BCG) pH indicator (Figure 3-3(a)), and pH measurement with this indicator is well reported in total alkalinity titration.

System	Cost	Pros	Cons
Charge coupled device Spectrophotometer such as Ocean Optics	$500 for a mini spectrometer, Up to $10000 for advanced models	Excellent wavelength specificity, versatility and commercially available	Delicate, often requires PC connectivity, may be too noisy. Expensive & bulky.
Photodiodes and filters (Martz 2006)	Photodiodes extremely cheap, but 6 filters were used ($250 each) so approx. $1500	Excellent noise performance, wavelength specificity, and once fabricated has relatively simple operation.	Specific to the system being used (cannot change from BCG to BCP for example), Expensive, must be fabricated
Photodiodes and LEDs with engineering solutions to cross sensitivity of the broadband detector. This includes switching, shuttering, or signal processing (e.g. FFT).	The light sources and detectors are cheap (<$10), electronic control systems vary from $10 – 1000, depending on the type of system used. In mass production this cost would likely be low.	Components are cheaper than the above 2 methods. Systems can be ruggedized and miniaturised.	Additional engineering requirements add complexity, and bring their own cost.
3 wavelength photodiode	Less than $10, sometimes large minimum order quantities	Extremely cheap, small, rugged, commercially available. Good noise performance	Spectral characteristics cannot be tailored, and may be unfit for some dyes, and unusable with others
Camera sensor	$10-20 for a 'webcam' $1000's for a sophisticated device	Can be relatively cheap, large sensing area available.	Spectral discrimination on RGB channels may be poor, not necessarily better than RGB-PD. Noise and resolution an issue

Table 3-1 - Comparison of optical systems suitable for spectrophotometric titration.

The remainder of this chapter is devoted to the examination of an RGB-PD as a detector for spectrophotometric pH measurements with BCG. Several models based on the optical properties of the RGB-PD are used to guide experimental design and predict performance. Uncertainty analysis is combined with this to determine the quality of measurements that can be made and explain experimental observations. These methods are introduced in Section (3.2). Section 3.4 experimentally evaluates the performance of this RGB-PD as a detector for pH measurement, compared with a commercial spectrophotometer. Section 3.5 then uses uncertainty analysis to examine the RGB-PD's suitability for TA determination using the tracer monitored titration (TMT) method.

3.2 Optical modelling

3.2.1 The purpose of optical models

Section 3.1 has identified the RGB-PD as a potential candidate detector for a spectrophotometric TA analyser based on the TMT technique. The remainder of this chapter will be spent examining whether the RGB-PD be successfully used in this way. This will largely be achieved through the use of optical models. The primary rationale for using this method within this project was to identify whether the experiments planned would work, without wasting time and resources in building and running experimental apparatus of unknown performance. Optical modelling allows determination of the theoretical performance of any combination of optoelectronic components (a light source and detector). This was used to select and verify other components of the optical detection system such as light sources. With light source and detector selected, the optical model is combined with uncertainty analysis to predict the quality of measurements that can be made. All modelling is performed within MATLAB.

3.2.2 The spectra used, and how they are obtained

The models used within this thesis are based only on the spectral properties of the optical components used, and the absorbing species that they are intended to measure. In this context, spectral properties means quantities which can be measured as intensity as a function of wavelength. In this study these are restricted to:

- The wavelength dependent emission of light sources. These are usually LEDs.
- The wavelength dependent light absorption properties of a coloured chemical species in solution. This is usually bromocresol green indicator. The quantity measured is the molar extinction coefficient (ϵ)
- The wavelength dependent response of a photodetector to light. This is usually the RGB-PD being examined.

These spectra are obtained through measurements with a spectrophotometer or are provided by suppliers of the components used. If for some reason these are unavailable, then estimates of their spectra can be generated mathematically. Gaussian functions are particularly useful for this purpose.

3.2.3 Molar extinction coefficients

For the purpose of modelling, molar extinction coefficients of indicators are measured as a function of wavelength, rather than at a single wavelength as is often performed in analytical chemistry. This is performed using a white (broad band) light source and spectrophotometer by measuring species absorbance at all wavelengths for several known concentrations. Indicators such as BCG exist as an equilibrium of two species depending on pH (Equation (2.2)). Therefore ϵ values are obtained for each species in isolation by performing the experiment at extremes of pH for several concentrations. The absorbance spectrum of the indicator at a given pH can be obtained by summing these spectra with appropriate scaling of each.

3.2.4 Modelling an absorbance measurement

The simplest case to consider for modelling is a single light source, absorbing species, and detector with identical spectra. First all spectra are normalised so that the maximum intensity is 1. For absorbance calculation according to Equation (2.6) a blank reference, or I_o measurement is required. This is simply obtained by multiplying light source and detector spectral functions together, numerically, then integrating the resulting peak. Obtaining the I measurement is slightly more complex. Equation (2.6) is rearranged in terms of I (Equation (3.1)).

$$I = I_0 10^{-A} \qquad (3.1)$$

The absorbance term (A) is then substituted with the right hand side of the Beer Lambert law ($A = \epsilon c l$). The desired concentration (c, mol kg^{-1}) of the absorbing species, wavelength dependent molar extinction coefficient (ϵ, mol^{-1} kg cm^{-1}), and path length (l, cm) values are then used, in addition to the earlier determined value of I_o to obtain I (equation (3.2)). This results in a value of I which is a function of wavelength. Integrating this function yields the detector measured value of I.

$$I = I_0 10^{-\epsilon c l} \qquad (3.2)$$

The absorbance measured by the detector can now be determined from the values of I and I_o obtained according to the original equation for absorbance (2.6).

Modelling the RGB-PD channels with multiple light sources is performed in exactly the same way. Appendix A 1.1 shows how this is performed for the RGB-PD for several pHs.

3.2.5 Use of optical models in this chapter

The technique of optical modelling is used for several specific tasks within this chapter. Section 3.4 examines the RGB-PD for pH measurement, both experimentally and theoretically. The model is used to predict the result of pH measurement using the RGB-PD, led light sources and BCG indicator (Section 3.4.5), and to assist in choosing the most appropriate LED light sources for the measurement. The modelled pH measurements provide a basis for comparison when experimental measurement of pH with the RGB-PD is performed. The model is then used for uncertainty analysis of systematic errors associated with RGB-PD measurement to help explain the observed results.

Optical modelling is then used to examine the performance of the RGB-PD for TA measurement by the TMT method. An alkalinity titration is modelled to obtain pH as a function of added acid. Each value of pH is converted to a photodiode measurement with the optical model. This is used for uncertainty analysis of random (Section 3.5.6) and systematic errors (section 3.5.5), which are treated separately. This is compared to results produced by the originator of the method to predict whether RGB-PD TA measurements by TMT are possible.

3.3 Uncertainty Analysis

3.3.1 The purpose of uncertainty analysis

Uncertainty analysis is combined with optical modelling within this thesis to predict the combined standard uncertainty (U_c) associated with measurements of pH and TA with the RGB-PD/LED optical system. At the design stage, uncertainty estimation allows performance of a proposed design to be checked. Uncertainty analysis can also be useful in explaining the results obtained.

These predictions require estimates or measurements of error associated with experimental measurements, and the parameters used in analysis. Two types of error are considered. Random errors arise from noise associated with temperature control and photometry. They are different for each measurement and are apparent in replicate measurements. Systematic errors are constant offsets from the true value of the

measurand, and will be the same for all the replicates (e.g. error in a determined equilibrium constant). Temperature is an example of a measurement that suffers from both random and systematic errors – temperature fluctuates in a thermostatic water bath, and the thermometer used to measure it may always give a reading that is 1.0 °C above the true temperature.

3.3.2 The limitation of uncertainty analysis

Calculation of combined standard uncertainty is limited to the data available for errors. These may be underestimated, which will carry through to the combined standard uncertainty. In addition some sources of error may not be accounted for. Though the approach is useful, the observed error associated with real measurements will be larger than uncertainty predicted by calculations.

3.3.3 Calculation of uncertainty within this thesis

The originator of the TMT method performed a substantial examination of the uncertainty associated with TA determination [26]. The approach used here is deliberately similar to allow for meaningful comparison between these two uncertainty analyses. Random and systematic errors are treated separately in this approach, systematic error associated with measurement parameters being examined by Kragten's method [130], random errors associated with temperature and photometric fluctuations (for TA measurement only) are examined by repeat runs of a numerical model (Section 3.5.6).

3.3.4 Systematic errors

Two identical approaches with different methodologies were considered for analysis of systematic error. The first is an algebraic method, which while useful for small-scale calculations, became troublesome to implement when a larger number of terms was included. The second is a numerical approach adapted for spread-sheet usage. In the first, uncertainty in a measured quantity (F), determined from n independent parameters (x_i) with associated errors (δx_i), is expressed according to equation (3.3) below. Uncertainty is then the sum of the partial differentials of F with respect to each parameter, squared and rooted to remove negative values [131].

$$Uc(F) = \sqrt{\sum_{i=1}^{n} \left(\frac{\partial F}{\partial x_i} \right)^2 (\delta x_i)^2} \quad (3.3)$$

Kragten described an equivalent numerical implementation specifically for calculation using spread sheets [130], and was used by Martz in the previous uncertainty analysis of the TMT procedure[26]. This uses *n* calculations of *F*, each time changing only the value of x_n *by* δx_n, and then subtracting the value of *F* with no error applied. Each calculation is performed in one column of the spread sheet, and the results squared, added, and rooted to give $U_c(F)$. While the spread sheet approach is convenient, determination of the combined standard uncertainty (U_c) at several pHs is required, and the repeated copying, pasting and minor adjustments required quickly become tiresome. Both approaches were therefore adapted for use in MATLAB. An example of the code used to determine the error in the concentration [BCG] in a titrant by both methods is given in Appendix A 1.9. The results are the same using both methods. Symbolic math is used which allows repeated substitution of different parameters into an expression without having to redefine it each time.

3.3.5 Random errors

Like the analysis of systematic error in TA determination described above, propagation of random errors can be achieved algebraically, however a purely numerical approach is the most convenient. Previous studies have used a similar approach [29, 90]. This is only performed for titration measurements by TMT, not for the pH measurements detailed in this section.

3.4 RGB-Photodiode for measurement of pH using bromocresol green indicator

3.4.1 Introduction to RGB-Photodiode spectrophotometry

The use of RGB-PDs in the role of a multi wavelength detector is poorly reported in the scientific literature, with much of the previous work being anecdotal at best. This section examines the suitability of RGB-PDs for high precision multi-wavelength photometry through measurement of pH with BCG. Measurement of pH with BCG in this study represents a convenient demonstration of the potential of RGB-PDs for multiple

wavelength photometry. This also serves as a test bed for their further employment in seawater TA determination. The work outlined in this section forms the basis of a manuscript submitted to the journal Optics Express.

3.4.2 Preparation of buffered indicator samples

All reagents were of analytical grade and purchased from Sigma Aldrich unless otherwise stated. A solution of BCG indicator ≈ 1 x 10^{-3} moles kg^{-1} was produced by dissolving the sodium salt in ultrapure water (Milli-Q, Millipore). This was further diluted to a give a stock solution with a concentration of ≈ 60 µmol kg^{-1}. Adding 40.9 g of NaCl per kg of stock solution matches the ionic strength to that of seawater (0.7 moles kg^{-1}). This stock solution was stored in an amber glass, aluminium foil wrapped bottle to exclude light, and used for all experiments. 0.1 M pH buffers covering the BGC indicators working range (pH = 3.0 - 5.5) were prepared from formic acid / sodium formate (pH = 3.0 to 4.0) and acetic acid / sodium acetate (pH = 4.5 to 5.5). The ionic strength of these buffers was brought close to that of seawater (0.7 moles kg^{-1}) by addition of NaCl. Buffer recipes were produced using an internet based buffer calculator provided by the University of Liverpool (http://www.liv.ac.uk/buffers/buffercalc.html). The recipes employed are given below in Table 3-2.

Buffered indicator samples were prepared by diluting ≈ 14.00 g of BCG solution with ≈ 40.00 g of each pH buffer as triplicate solutions measured using 5 figure balance (±1 mg) giving final concentrations for photometry of ≈ 20 µmol kg^{-1} with respect to BCG. As the indicator is a weak acid and can affect solution pH, indicator aliquots are accurately measured to keep BCG concentration consistent between solutions. BCG concentrations were chosen to avoid deviation from the Beer-Lambert law associated with high absorbances. The maximum permitted absorbance was 1.00. The pH of the buffered indicator solutions was verified with a high precision pH electrode and pH meter (Orion 8102BNUWP ROSS Ultra and Orion 3 Star, both manufactured by Thermo Scientific). The apparatus was calibrated with certified pH buffer solutions (pH 3.01, 6.01 and 9.201, Fisher) covering the range of interest. When the calibration was checked using the same certified solutions, deviations from the certified pHs were 0.017, 0.0036, -0.0132 respectively, with standard deviations of 1.1 x 10^{-3} pH or less. Five measurements of each buffered BCG solution were made.

Buffer target pH	Buffer composition	Amount of acidic component / mols	Amount of basic component / mols	Mass of NaCl required to increase ionic strength to 0.7M / g
3.0	Formic acid / sodium formate	0.0795	0.0204	39.79
3.5	Formic acid / sodium formate	0.0551	0.0448	38.36
4.0	Formic acid / sodium formate	0.0279	0.0720	36.77
4.5	Acetic acid / sodium acetate	0.0555	0.0444	38.38
5.0	Acetic acid / sodium acetate	0.0283	0.0716	36.79
5.5	Acetic acid / sodium acetate	0.0111	0.0888	35.78

Table 3-2 – Recipes used in the preparation of buffers for the RGB-PD pH measurement experiment

Correction for the higher ionic strength of mixed indicator and buffer solutions was made using a TRIS pH Certified Reference Material (CRM, from the laboratory of A. Dickson, Scripps Institute of Oceanography). Mean corrected pHs were 2.680, 3.146, 3.637, 4.151, 4.660, 5.163 with standard deviations not exceeding 4 x 10^{-3} pH between triplicated solutions. Potentiometric pH measurements are not affected by the optical properties of the solutions, so this served as an independent means for determining solution pH to detect any deviation within triplicated solutions, however absolute measurements of pH by potentiometry in seawater media are not straightforward. This is because the high ionic strength of the solutions raises potentials across the liquid junction of the electrode.

3.4.3 Apparatus

The experimental apparatus for spectrophotometric pH measurements was assembled in a modular arrangement (Figure 3-3(b)). LEDs (Luxeon Rebel, Phillips, λmax of 454 and 620 nm) were used as light sources, driven by a constant current supply (Buckplus,

Luxdrive). The constant current supplies are specifically designed for use with the Luxeon Rebel LEDs, and maintain steady light output. They also allow control of light intensity by using an external variable resistor (max 5 kΩ). The LEDs draw current at up to 350 mA, producing intense light and significant heat output. Thermal regulation of the LEDs was achieved by mounting them on printed circuit boards coupled to heat-sinks. SMA optical fibre fittings were then aligned with the LEDs using an x, y, z optical stage and attached with epoxy resin. The LED light sources were coupled to a commercial 1 cm thermostatic cuvette holder (CUV-TLC-50F, Ocean Optics) via a bifurcated optical fibre, and sample temperature was maintained at 25°C. A second bifurcated fibre allowed simultaneous coupling of two optical detectors for comparative measurements. The detectors used were a conventional CCD spectrophotometer (HR2000+, Ocean Optics) and the RGB-PD (TCS3414CS, ams AG) mounted on an evaluation board (TCS 3414EVM, ams AG). RGB-PD integration time and gain were set to 400 ms and 64x, and the brightness of the LEDs adjusted such that the reference signal recorded was approximately 90% of the saturation level for both channels. The spectrophotometer required a 10 ms integration time to achieve 90% saturation, and every 40 spectra were averaged resulting in an effective measurement time of 400 ms. Wavelength accuracy of the spectrophotometer was validated with a holmium oxide certified reference solution (Starna Scientific Ltd, Essex UK). A custom holder was machined from poly(methyl methacrylate) (PMMA) to couple the optical fibre from the cuvette holder directly to the photodiode evaluation board, such that the exit light was focused on the photosensitive area. An in-house thermistor temperature probe designed by Mr Andy Harris monitored sample cuvette temperature via a data acquisition card (NI PCI-6289, National Instruments). With the light source powered off the outputs of the RGB-PD channels were zero, however a dark current correction was necessary for the spectrophotometer.

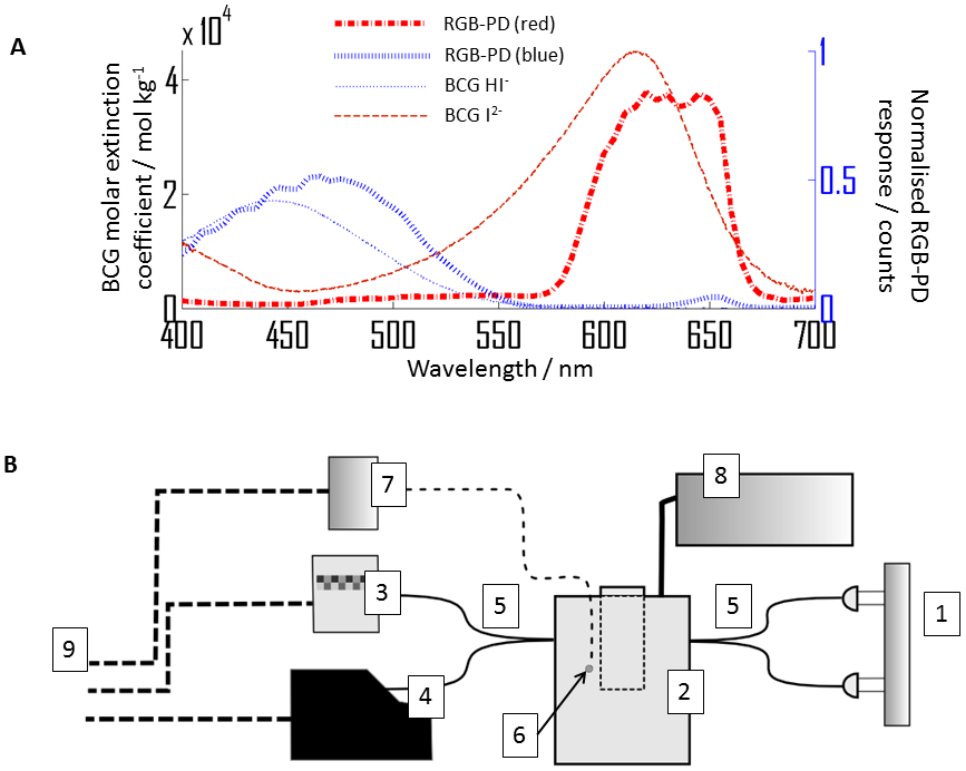

Figure 3-3 - TCS3414 optical response and experimental setup. (a) Data showing the wavelength dependent response of the photodiode (obtained from manufacturer) together with the spectral variation in molar extinction coefficient (ϵ, obtained experimentally, Section 3.4.6) for the BCG indicator. (b), Schematic used in assessment of the RGB-PD as a replacement for a commercial spectrophotometer, showing 1) LED power supply, 2) thermostatic cuvette holder, 3) RGB-PD evaluation board 4) spectrophotometer, 5) bifurcated optical fibres, 6) thermistor, 7) thermistor controller, 8) controller for cuvette holder, 9) connections for data acquisition and control by computer.

3.4.4 Bromocresol green molar extinction coefficient (ϵ) determination

Molar extinction coefficients (ϵ) of BCG were determined according to the procedure described by Martz and co-workers [29]. High ionic strength (0.7 M) acidic (HCl, pH ≈ 1) and basic (NaOH, pH ≈ 9) standard solutions of BCG were produced with pH values at least 3 units different from the pKa_2 of the indicator (≈ 4.5). Varying the concentration of BCG in the solutions allowed ϵ values to be determined from their absorbances according to the Beer Lambert Law. Practically, BCG concentrations of ≈ 0, 5, 10, 15, and

20 μmol kg^{-1}, and ≈ 0, 2, 5, 7, and 9 μmol kg^{-1} were used for the acidic and basic solutions respectively. Photometric measurements were performed simultaneously using both spectrophotometer and RGB-PD. The spectrophotometer is capable of sub-nanometre discrimination of wavelength and so ϵ values can be confidently reported at a specific wavelength e.g. ϵ_{615nm}^{I2-} for the extinction coefficient at 615 nm for the I^{2-} BCG species. As measurements with the RGB-PD are significantly broader in bandpass, these are labelled as "red" or "blue" in subscript to signify the photodiode channel used e.g. ϵ_{red}^{I2-} for the extinction coefficient determined with the red photodiode channel for the I^{2-} species. All results were processed in MATLAB. Additionally the experiment was repeated using a white light source (LS-1, Ocean Optics) and spectrophotometer to obtain whole spectrum values of ϵ for both I^{2-} and HI^{-} species for use in an optical model. The nominal path-length for the cuvette used was 1 cm, though not verified experimentally. Additionally it is possible that there will be variation in the channel bandpass between individual RGB-PDs. Quoted values of ϵ will be therefore specific to the apparatus and cuvette used in this system.

3.4.5 Optical modelling

The theoretical performance of the experiment was modelled (MATLAB), based upon rearrangements of the Beer-Lambert law, and the optical properties of the LED light source, BCG indicator, and detector. For a given pH, the protonation state of BCG could be predicted and converted into absorption spectra from the determined ϵ values according to the Henderson-Hasselbalch equation $pH = pKa + \log_{10}([I^{2-}] / [HI^{-}])$. Square brackets denote concentration of I^{2-} and HI^{-}. RGB-PD response was then predicted based on spectral data supplied for each channel of the photodiode by ams AG (Unterpremstatten, Austria). The spectral response of the RGB-PD in relation to the molar extinction maxima is shown in Figure 3-3(a), indicating the matching of absorbance and detection peaks. In the case of the RGB-PD and BCG, the peaks show similar FWHM and an offset of around 10–15 nm, so careful selection of a narrower band light source was necessary to obtain good quality photometry. A model emission spectrum approximating a LED was generated using a normalized Gaussian function. Convolutions of model light source, detector, and absorbing indicator were obtained for both the HI^{-} and I^{2-} species. This was done by multiplying normalized molar extinction coefficient, LED Gaussian and the photodiode channel response together. Over a range

of LED peak wavelengths and the integral of the resultant was calculated. The most desirable LED was deemed to be that which would yield the largest integral, with a narrow emission peak. A selection of suitable LEDs were purchased, and recorded emission spectra applied to the optical model to determine which gave the best theoretical performance.

3.4.6 Bromocresol green molar extinction coefficient (ϵ) determination

Molar extinction coefficients (ϵ) were obtained by measuring the absorbance of several concentrations of the BCG indicator in both acidic and basic solutions. This was performed using a tungsten white light (broad spectrum) source (LS-1, Ocean Optics) and spectrophotometer (Ocean Optics) for wavelengths between 400 nm and 700 nm to provide data for the optical models. The BCG ϵ values were calculated from the slope of a linear fit of absorbance versus indicator concentration at each wavelength measured. The results are used in Figure 3-3(a) and Figure 3-4 to demonstrate the matching of BCG absorption peaks to the RGB-PD red and blue channel response spectra. BCG (ϵ) values for performing photometric pH measurements were then re-measured using the chosen LED light sources with both the spectrophotometer (Ocean Optics), and RGB-PD. The BCG ϵ values were again calculated from the slope of a linear fit of absorbance versus indicator concentration. For the LED based system, molar extinction values of 43200, 368.2, 2280, 18190 mol^{-1} kg cm^{-1} (to 4 significant figures (S.F.)) were determined with the spectrophotometer for ϵ_{615nm}^{I2-}, ϵ_{615nm}^{HI-}, ϵ_{444nm}^{I2-}, ϵ_{444nm}^{HI-} respectively. The corresponding values determined with the photodiode were 36800, 771.9, 3062 and 15590 $mol^{-1}kg^{3}cm^{-1}$ (to 4 S.F.)for ϵ_{red}^{I2-}, ϵ_{red}^{HI-}, ϵ_{blue}^{I2-}, ϵ_{blue}^{HI-} where “red” and “blue” signify the RGB-PD channels used to approximate the 615 nm and 444 nm spectrophotometer bands . These results are specific to the equipment and particular batch of BCG used. Caution should be exercised in further use of these values for pH determination so values of ϵ are reported here for completeness. There is a more significant difference in the HI^- and I^{2-} ϵ values at both the 444nm/blue and 615nm/red wavelengths for the spectrophotometer than the RGB-PD. This indicates that the spectrophotometer measurements are more selective for the species of interest and therefore less prone to overlapping of the HI^- and I^{2-} spectra at these wavelengths. In theory this should allow the spectrophotometer to resolve smaller changes in pH than the RGB-PD by increasing the dynamic range.

3.4.7 Light source selection and outcome of optical modelling

Careful selection of LED light sources would be necessary to achieve the best performance of the RGB-PD. For simulated LED spectra, wavelengths of maximal LED optical intensity (λ_{max}) of 460 nm and 620 nm gave the greatest overlap integral for the HI^- and I^{2-} measurements respectively. The availability of LEDs with specific emission spectra is limited, and variation occurs between batches of components. Although the Luxeon Rebel LEDs used were binned according to peak wavelength, selection by bin number was not possible when ordering small quantities (<1000 units). The spectral output of the LEDs selected differed slightly from the ideal values, having emission maxima at 452 nm and 626 nm rather than 454nm and 620nm. The suitability of the chosen LEDs is shown in Figure 3-4, which shows convolution of the LED with the photodiode filter for HI^- and I^{2-} measurement. The measured ratio of combined optical component FWHM to molar extinction coefficient FWHM are 1/6 and 1/5 for the red and blue channels respectively, somewhat larger than the 1/10 ratio desired.

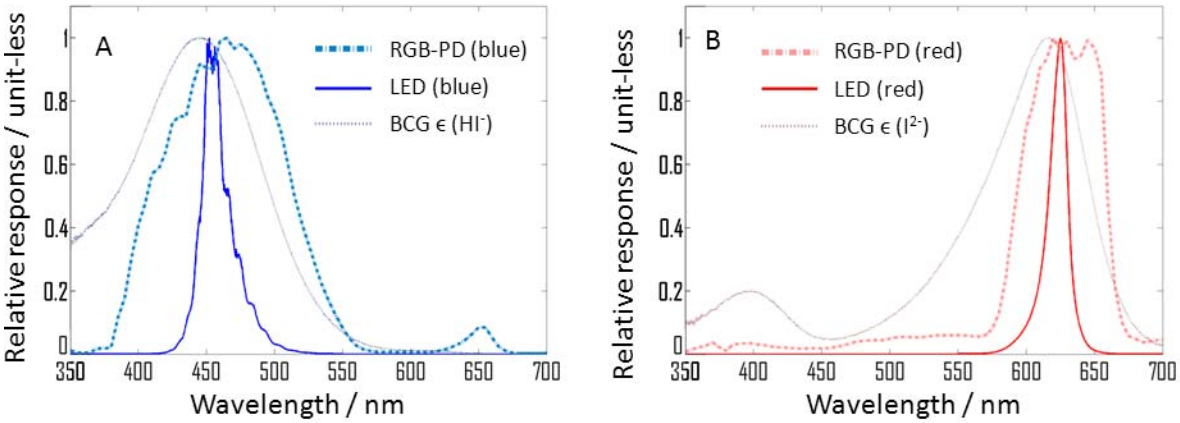

Figure 3-4 - Spectra of the chosen LED, RGB-PD channel, and the corresponding BCG species being measured, for (A) monoprotonated HI^- BCG species, and (B) the I^{2-} BCG species. The specificity of the optoelectronics for the species being measured is largely governed by the LED spectra which are much narrower than the RGB-PD filters. All spectra presented are normalised for the purposes of comparison.

For the LEDs selected, the model predicted agreement between measurements undertaken using the Ocean Optics spectrophotometer and RGB-PDs at pH = 4.5 which is close to the pKa_2 of BCG, and at the edges of the working indicator range at pH = 3.0 and 5.5 (Figure 3-5(a)). The most significant modelled difference between

spectrophotometer and RGB-PD derived pH of ≈ 0.01 was observed around pH = 3.0 (Figure 3-5 (a)).

3.4.8 Comparison of RGB-photodiode and spectrophotometer pH measurements

The pH of the buffered indicator solutions was calculated from experimental absorbance measurements made using both the RGB-PD and spectrophotometer. The individual concentrations [HI^-] and [I^{2-}] are calculated from the relevant absorbances using Equations (2.9) and (2.10). Measurements of the buffers in the absence of BCG were used as the blank references required for calculation of absorbance (equation (2.6)). Sample cuvettes introduced into the holder were thermally equilibrated for 10 minutes before light measurements, made at the relevant wavelengths over a period of 1 minute.

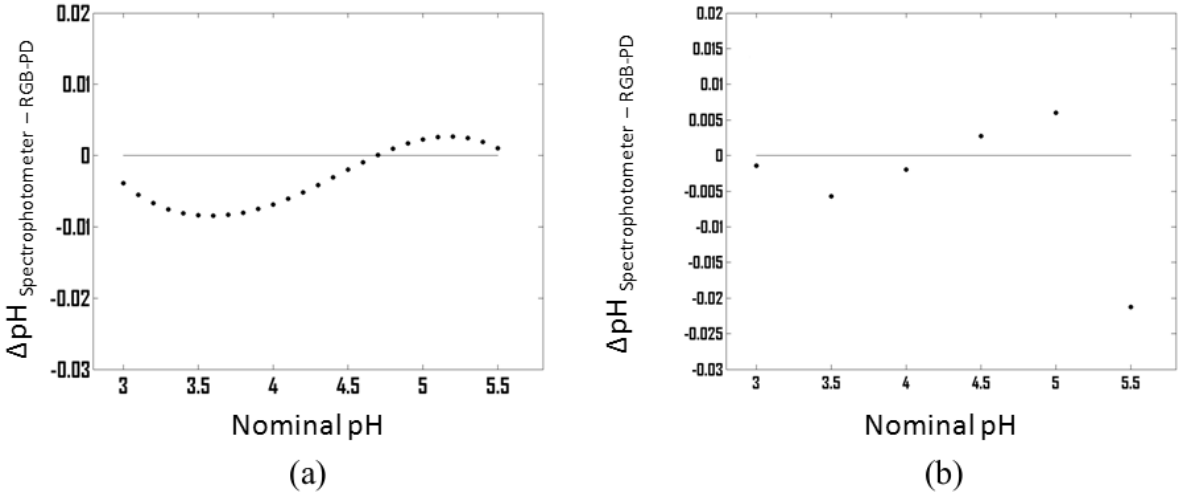

Figure 3-5 - Difference between pH values measured by spectrophotometer and RGB-PD, simulated (a) and experimental (b). The "Nominal pH" used for the x-axis is the theoretical pH of the samples calculated from the buffer recipes used in their preparation. The standard deviations of replicate pH measurements with RGB-PD and spectrophotometer are given in Figure 3-6 (a).

Both model and experimental results showed close agreement between pH determined by spectrophotometer and RGB-PD (Figure 3-5(a), (b)). The majority of experimentally determined pH values differed by less than ±0.007 pH, although greater difference (0.022 pH) was observed for the pH = 5.5 buffer. This distinctive pattern of discrepancies is also observable in modelled results (Figure 3-5 (a)), which predict similar agreement between the RGB-PD and spectrophotometer detection methods. The difference

between RGB-PD and spectrophotometer measurements lies in the wavelength specificity of measurements. The spectrophotometer has a narrow bandpass, which gives good wavelength specificity, Hence the relationship between absorbance and concentration for the I^{2-} and HI^{-} species closely approximates the beer lambert law with the spectrophotometer. The RGB-PD has a wider bandpass, and so the relationship between concentration and absorbance does not approximate the beer lambert law as well for the spectrophotometer measurements. This causes variations in the values of $[I^{2-}]$ and $[HI^{-}]$ obtained through photometry, which in turn affect pH. The effect becomes most pronounced at pHs distant from the pKa, as in these regions the absorbances due to I^{2-} and HI^{-} are more extreme, with one being high, the other being low, at which point photometry with the RGB-PD becomes most challenging.

The pH = 5.5 measurements have the largest difference between spectrophotometer and RGB-PD, and there is a significant difference between the modelled and experimental results where the model predicted agreement to within 0.001 pH yet a difference of ≈0.02 was observed. The pHs chosen for experimental measurement are at the edge of the generally accepted working range of the BCG indicator (around 1 pH unit from the pKa_2), and so disagreement at these points would be expected. The working range of the indicator is simply the pH ranges over which changes in pH can be resolved with the equipment being used. The use of a literature value for the pKa_2 of the BCG indicator (4.479) is justified here as any difference between this and the pKa_2 specific to the batch of BCG used would affect both spectrophotometer and RGB-PD determined pH equally. Thus no difference to $\Delta pH_{Spec\text{-}RGB\text{-}PD}$ would occur if the literature value were wrong. However should the true pKa_2 be substantially different, the pH = 5.5 measurements may be outside the indicator working range. pKa_2 can be estimated from the experimental data collected; the Henderson Hasselbalch equation can be rearranged to give:

$$\text{Log}\,([I^{2-}]/[HI^{-}]) = pH - pKa$$

Plotting Log $([I^{2-}]/[HI^{-}])$ against pH should produce a straight line with gradient 1 and intercept the x-axis at pH=pKa. This was performed using both the nominal pH of the buffers and corrected pH values from potentiometry for $[I^{2-}]$ and $[HI^{-}]$ measured using the spectrophotometer. A linear best-fit line is then used to estimate pKa_2. The pKa_2 values determined were 4.58 and 4.46 for the nominal and potentiometric pHs, which suggests that the pH 5.5 measurement is at the edge of the working range of the

indicator. The same could be said for the lower end of pH, which should be outside the working range of the indicator at pKa – 1.

After calculating the concentrations $[I^{2-}]$ and $[HI^{-}]$ from absorbances at red and blue wavelengths according to equations (2.9) and (2.10), pH is determined according to the Henderson Hasselbalch equation. If the calculation of one or more of these concentrations is offset in the RGB-PD compared to the spectrophotometer, it can have a significant effect on $\Delta pH_{Spec\text{-}RGB\text{-}PD}$. The most significant effect arises from smaller of the two concentrations at a given pH. At pH = 5.5 $[HI^{-}]$ is around 10 times smaller than $[I^{2-}]$, and the offset in these concentrations between spectrophotometer and RGB-PD ≈ 1.0 x 10^{-7} μmol kg^{-1} or 10% of the smaller HI^{-} measurement. The actual absorbance contribution of HI^{-} at pH = 5.5 will be ≈ 0.03 Abs and ≈ 0.0016 Abs in the blue and red channels respectively, with the very low concentration in the red channel arising from this having the smallest molar extinction coefficient. The contribution from HI^{-} to absorbance in the red channel is similar to the standard deviation associated with the measurement (see following Section 3.4.9) and therefore cannot be resolved. As the offset in both the larger and smaller of the two concentrations is the same, the sensitivity to this offset and so the deviation at pH = 5.5 comes predominantly from $[HI^{-}]$. The same effect is not seen in the pH = 3.0 measurement where the lowest absorbance contribution of any species is 0.006 Abs, at least 3 standard deviations above the background noise level (3.4.9). While the offset in concentrations between spectrophotometer and photodiode for $[HI^{-}]$ was similar to that seen at pH = 5.5, the offset in the smaller $[I^{2-}]$ concentration was found to be extremely low at around 1.0 x 10^{-10} moles kg^{-1} at pH = 3, and explains why this measurement has such good agreement between RGB-PD and spectrophotometer. This level of agreement at pH = 3.0 is suspiciously low, requiring absorbance measurements to agree to within 0.0005 Abs. From this perspective the good agreement at pH = 3 is more unusual than the poor agreement at pH = 5.5.

The difference between modelled and experimental results could be caused by the supplied RGB-PD spectral response data being slightly different to the properties of the photodiode. In addition, the model only accounts for offsets in determined concentrations of HI^{-} and I^{2-} which arise from the overlap of RGB-PD, LEDs and BCG, and not for example stray light bypassing the cuvette path length. Differences between the observed and modelled results may also arise from error sources such as impurities in the indicator, temperature offset, and error in the determined molar extinction

coefficients used. The standard deviation arising from replicate pH measurements of solutions was < 0.007 pH for both RGB-PD and spectrophotometer measurements, better than 0.23% Figure 3-6(a). Variations in the concentration of BCG between replicates can affect pH precision. As BCG concentration was controlled to within ±0.1% and the buffer concentrations used were high compared to BCG, pH measurement precision in this case is limited by the error introduced through cuvette replacement.

At pH= 5.5 the majority of BCG indicator exists in the I^{2-} form giving a strong absorbance in the red photodiode channel. At higher absorbances, photodiode measurements are prone to a non-linear response that causes underestimation of the concentration of the species measured. Correcting for underestimation of $[I^{2-}]$ causes an increase in $pH_{RGB\text{-}PD}$ according to the Hendersson Hasselbalch equation, increasing the magnitude of $\Delta pH_{Spec\text{-}RGB\text{-}PD}$. This means that non-linearity cannot explain the deviation, and is supported by the fact that the model, which includes these effects, did not exhibit this.

Potentiometric measurements were made as an independent means to identify errors due to photometry. The standard deviation of potentiometric pH measurements of solutions (< 0.004 pH) is similar to those made by spectrophotometry (Figure 3-6(a)). The offset between potentiometric and RGB-PD pH measurements was large at ≈ -0.2 for all except the pH = 3 measurement (-0.06 pH, Figure 3-6(b)). A constant offset between the two methods could originate from an incorrect value of $pKa_{2(indicator)}$ used in the spectrophotometric calculation, or from the calibration of the pH electrode.

At pH = 3 although spectrophotometric methods strongly agree (Figure 3-5), there is a deviation from the linear offset between potentiometric and spectrophotometric results (Figure 3-6(b)). From closer examination of experimental data, the photometric data shows strong linearity across the entire dataset, however both spectrophotometer and RGB-PD show identical deviations from linearity at pH = 3. The cause of this is unclear, and discrepancies in measurements small. It may be that a coloured contaminant affects photometry but not pH, and is present only in the pH = 3 sample.

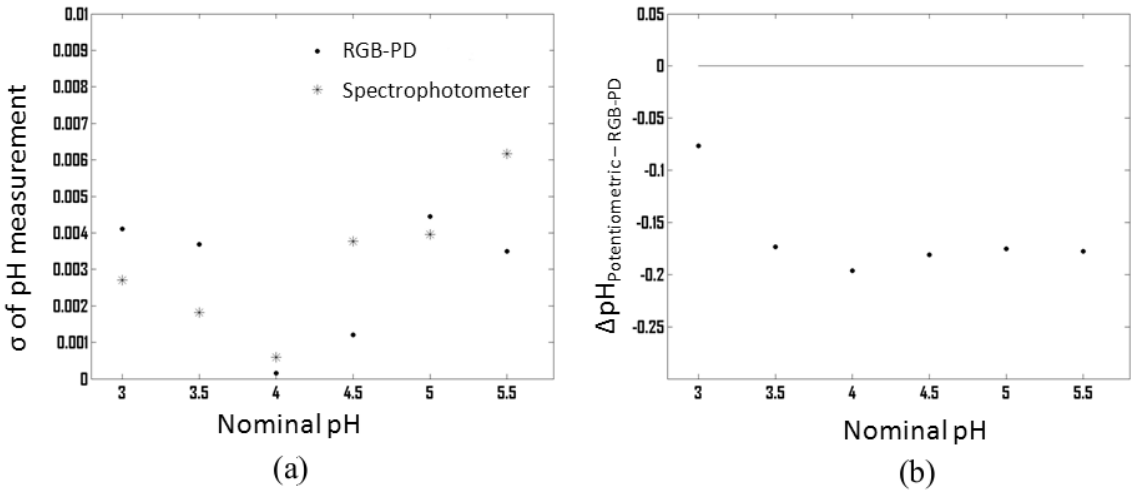

Figure 3-6 – pH error, and difference between pH measured by potentiometry and RGB-PD. (a) Standard deviations (σ) of RGB-PD and spectrophotometer pH measurements, (b) difference between potentiometric and RGB-PD measurements. The "Nominal pH" used for the x-axis is the theoretical pH of the samples calculated from the buffer recipes used. Both measurements were made at a constant 25°C in a thermostatic cuvette holder (photometric) or water bath (potentiometric).

The stated indicator purity was ≥90%. Previous work has raised the issue of sulfonephthalein indicator purity, which can cause pH offset of up to 0.01 pH [26, 104, 105]. High purity sulfonephthalein dyestuffs are not readily available. As a practical solution to the issue, Yao et al. suggest retaining a portion of indicator used for comparison to high purity indicators [104]. HPLC methods offer a means of purifying indicator, though this requires considerably effort and expense if equipment and expertise are not available [104, 105].

3.4.9 Noise associated with RGB photodiode and spectrophotometer measurements

To compare the noise associated with light measurements by RGB-PD and spectrophotometer, time domain fluctuations made over a 7-hour period were analysed. The data used in this analysis is provided on the attached CD-ROM. This measurement provides the combined light source, detector, and system noise for the specific setup used. The integration time and gain of the RGB-PD (400 ms, 64x), and integration time and number of averaged spectra for the spectrophotometer (10 ms, 40 averages) were the same as those used in all other experimental measurements. Around 1.5 times more data

points were recorded from the RGB-PD evaluation board than would be expected given the integration time and experimental duration. Inspection of the data revealed that this was due to duplication of a data point around once every second. This was found to have also occurred during pH measurements, but will not have affected comparison of RGB-PD and spectrophotometer, as a 1-minute average of the signals from both devices was used in pH calculation. To assess the noise associated with the approach, a 1 minute moving average was applied to the observed signals, and the random error in absorbance measurements calculated by propagation of error. The standard deviations for a 0.5 absorbance (Abs) measurement with the red (615 nm) and blue (444 nm) channels were 4.6 and 1.3 milli-absorbance units (mAbs) respectively for the spectrophotometer, and 0.80 mAbs and 0.66 mAbs for the RGB-PD.

Although the standard deviation of RGB-PD measurements were at least half those of the spectrophotometer, noise introduced by the use of a replaceable cuvette was a more significant source of error. This was determined by repeating 9 measurements with a single pH 4.5 BCG solution. The spectrophotometer measurements had mean and standard deviations of 0.394 Abs and 0.0022 Abs at the red wavelength, and 0.212 Abs and 0.00178 Abs at the blue. The RGB-PD measurements had similar means and standard deviations of 0.347 Abs and 0.00151 Abs in the red channel, and 0.197 Abs and 0.00128 Abs in the blue. As the purpose of the work is to examine whether comparable performance can be achieved with the RGB-PD, this was deemed acceptable. Fluctuations due to temperature changes over the time scale of photometric determination were not specifically examined, but will have been accounted for in the 7 hour signal measurements. These are therefore not significant in their contribution to photometric uncertainty in comparison to the error introduced by cuvette replacement.

3.4.10 Uncertainty analysis of pH measurements with the RGB-Photodiode

Section 3.3 describes a method of uncertainty analysis used in assessment of the RGB-PD. This type of analysis is useful in understanding the spectrophotometric pH measurement results described in Section 3.4.8. Figure 3-7 shows the outcome of this analysis, and Section 3.3.4 gives full details of how this is calculated. The contribution to uncertainty from individual parameters used in the determination, along with the overall uncertainty in pH ($U_c(pH)$) is shown. The horizontal pH axis highlights how these uncertainties vary with the pH of the solution. This analysis incorporates the spectral effects caused by using the RGB-PD with the LEDs particular to the experimental setup.

In addition, uncertainties associated with molar extinction coefficients vary with the absorbance caused by each species of BCG, and therefore vary with pH at constant [BCG]. These uncertainties are first calculated, stored as a lookup table, and the appropriate values are called for each specific pH measurement made. Details of the calculation are given in Appendix A 1.8, the lookup table is included on the attached CD-ROM.

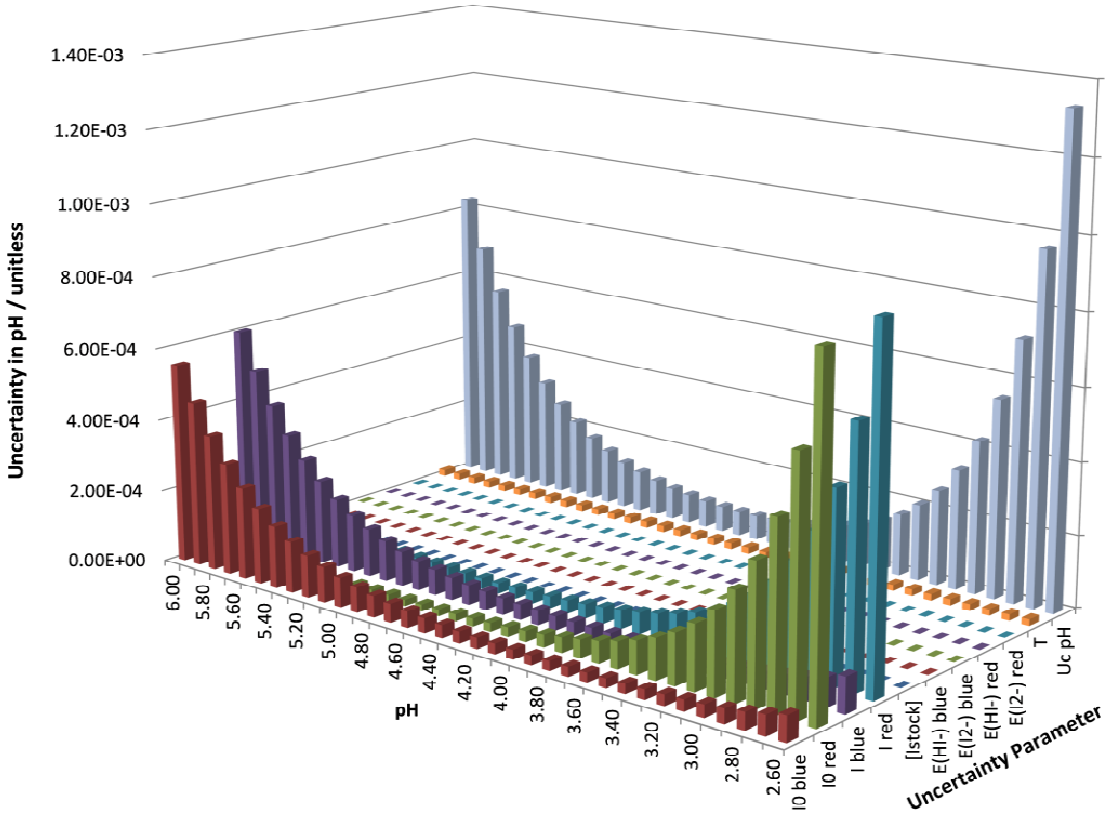

Figure 3-7 - Uncertainty analysis for pH measurements made using the RGB-PD. Uncertainty changes depending on the pH being measured, so is calculated in 0.1 pH intervals between 2.6 and 6.0. The depth axis shows the individual parameters analysed for their contribution to uncertainty, and the total uncertainty in the pH measurement – $U_c(pH)$. Uncertainty introduced by the pKa_2 of BCG indicator is equal at all pHs and so not shown here. Individual uncertainties are summed as squares, then square rooted to give $U_c(pH)$.

Uncertainty in the RGB-PD pH measurement ($U_c(pH)$) varies considerably with the pH of the solution. As expected, the uncertainty is at its lowest close to the pKa_2 and becomes significantly worse when measuring more than 1 pH unit away from this. It was

decided not to include uncertainty due to pKa_2 of the indicator as the contribution of this to $U_c(pH)$ is uniform across the entire pH range. pKa_2 uncertainty therefore does not affect $\Delta pH_{Spec\text{-}RGB\text{-}PD}$. If pH measurements are to be reported, it is recommended that $U_c(pKa_2)$ should be included in calculation of $U_c(pH)$ At pH ≤ 3.00, the HI^- form of the indicator dominates, and the largest uncertainty comes from the light intensity measurements I and I_o in the red channel which corresponds to the lower concentration I^{2-} species. Conversely at pH ≥ 5.00 the largest uncertainty comes from intensity measurements of low concentration HI^- in the blue channel, with the majority of the indicator in the I^{2-} form. Other sources of error including temperature fluctuations have a far lower effect on the pH uncertainty. This supports the analysis of the discrepancy at pH=5.5, but goes no further toward explaining why the pH = 3.00 measurement agreed so well between spectrophotometer and RGB-PD. A list of parameters used in the analysis with the magnitude of their associated values and errors is given in Table 3-3 below.

Parameter	Value	Uncertainty
E 615nm I2	38990 $mol^{-1} kg cm^{-1}$	pH dependent[1] 0.91 - 1.99 x 10^{-6} %
E 615nm HI	780 $mol^{-1} kg cm^{-1}$	pH dependent[1] 4.50 - 9.96 x 10^{-5} %
E 444nm I2	3560 $mol^{-1} kg cm^{-1}$	pH dependent[1] 0.99 – 2.18 x 10^{-5} %
E 444nm HI	14530 $mol^{-1} kg cm^{-1}$	pH dependent[1] 2.40 – 5.34 x 10^{-6} %
T	25 / ℃	0.01 ℃[2]
I 444 nm	pH dependent	1 / counts[3]
Io 444 nm	65000 / counts	1 / counts[3]
I 615 nm	pH dependent	1 / counts[3]
Io 615 nm	65000 / counts	1 / counts[3]

Table 3-3 - Errors used in the analysis of systematic errors associated with pH measurement using the RGB-PD by Kragtens method, as shown in Figure 3-7. The sources of contributing uncertainties are (1) separate calculation, given in Appendix A 1.8, (2) obtained from thermostatic cuvette holder datasheet, (3) estimated, as data unavailable.

3.4.11 Conclusions from RGB Photodiode pH measurement

The RGB-PD shows excellent potential as a replacement for conventional photometric detectors for both single and multiple-wavelength measurements. The footprint of the detector is reduced from 150 cm^2 to 0.01 cm^2 when compared to the Ocean Optics HR2000+ spectrophotometer. The standard deviation associated with absorbance measurements without cuvette replacement were between 1.3 – 4.6 mAbs for the spectrophotometer, and 0.66 – 0.80 mAbs for the RGB-PD, therefore photometric performance is improved with respect to noise. When a replaceable cuvette in employed, the precision associated with absorbance measurements is similar for the two methods. The RGB-PD is encapsulated in a polymer as a single component, and is therefore likely to be more rugged than the spectrophotometer. Although RGB-PDs were primarily intended to monitor display screen equipment and ambient light for consumer electronics applications, I have demonstrated that they have clear potential for use in

analytical chemistry. The properties of in-built filters are not customizable in readily available components, which gave an optics to absorber FWHM ratio of ~1/5, somewhat larger than the desired 1/10. Nevertheless in this instance the combination of light source, absorber, and detector performed well, agreeing with pH measurements made with a conventional spectrophotometer (Ocean Optics) to within 0.01 pH between pH = 3 and 5. It is possible that a small number of units with customized filters could be produced for a specific application, or existing properties modified by applying additional optical filters to the system, though such changes would be accompanied by increased unit costs. The precision of pH measurements of (σ = 0.007 pH) showed that with further characterization, the RGB-PD could potentially be used with BCG for spectrophotometric pH measurement for total alkalinity titrations, which require < ±0.01 pH precision for monitoring of ocean acidification. For the application examined here, the RGB-PD and LED based system has demonstrated a 400-1000 times reduction in the cost of detector components.

3.5 RGB–Photodiode for measurement of total alkalinity using Bromocresol Green indicator

The first part of this chapter identified the potential of the RGB-PD/LED based optical system for total alkalinity (TA) measurement. Section 3.4 demonstrated its utility and shortcomings in the measurement of pH with bromocresol green (BCG) indicator over the range of pH relevant to TA determination by acid titration. The question remains whether this device is suitable for measurement of pH within alkalinity determination, and whether further application to the tracer monitored titration (TMT) method is possible. TMT requires monitoring of total indicator concentration by the photometric apparatus to quantify amount of acid added.

The following section focusses on answering these questions using a largely numerical approach. Modelling TA titrations provides data to combine with an RGB-PD optical model. From these modelled titrations and their interpretation by the optical system, uncertainty analysis quantifies the error that will be associated with TA measurement. The approach treats systematic and random sources of error separately, and individual contributions to overall uncertainty are evaluated by propagation of error.

3.5.1 Previous work by the originator of the method

Martz included an examination of TMT's sensitivity to errors in different parameters based on equilibrium and mixing models, and determined the most error prone inputs to the non-linear least squares (NLLS) routine [29]. In summary, to deliver a precision of 0.1 %RSD in TA (< 3 μmol kg^{-1} for typical oceanic TA values), the precision in absorbance achieved with the optical system had to be better than ± 0.0005 in 0.5 - 1.0 absorbance units, and uncertainty in $pKa_{2(ind)}$ (where $Ka_{2(ind)}$ is the indicator's second dissociation constant) better than ± 0.001. The temperature dependence of pKa_2 requires either accurate temperature measurement and determination of pKa_2 as a function of temperature with a combined error less than ± 0.001, or thermostatting of the titration to within ±0.05 °C. The substantial difference between the optical system proposed herein compared to that of the system used in the original TMT method published by Martz highlights the prudence of undertaking a new uncertainty analysis. The following sections outline this error analysis strategy.

3.5.2 Implications from pH measurement work

The pH measurements made using the RGB-PD highlight some important considerations for its use in determination of TA, particularly if the TMT methodology is used. The TMT method follows acid additions by measuring $[BCG]_{total}$ throughout the titration and comparing this to the concentration of BCG in the titrant stock, made up of acid and indicator in known concentrations. The dilution factor for BCG in the sample is therefore equal to that of acid. With the TMT method disagreement between the true concentration of BCG in the sample and that measured by photometry using the RGB-PD leads to error in the determined amount of acid added in titration. BCG concentration was kept constant in the pH measurement experiment, and deviation introduced in its determination through photometry can be calculated from the sum of individual concentrations of BCG species [HI^-] and [I^{2-}] used in pH determination for both the spectrophotometer and RGB-PD measurements. The results of this are given in Figure 3-8.

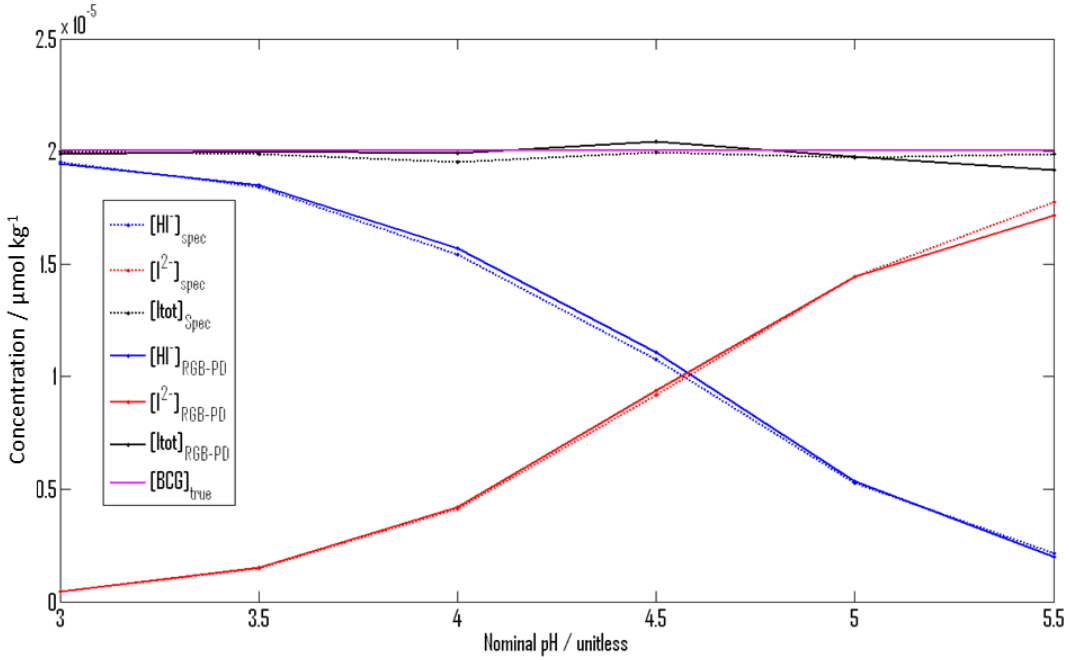

Figure 3-8 – Discrepancy in measurement of BCG concentration in pH experiments between spectrophotometer and RGB-PD, including individual acidic and basic forms [HI^-] and [I^{2-}] and total BCG indicator, [Itot]. The true concentration of BCG determined from masses used is shown for comparison.

Disagreement in the total indicator concentration [Itot] is most significant close to pH = pKa_2 (≈ 4.5) and especially at the pH = 5.5 measurement. In general the RGB-PD estimates of $[BCG]_{total}$ tended to be higher than those of the spectrophotometer. The spectrophotometer $[BCG]_{total}$ tends to be closer to the true value than the RGB-PD determined [BCG]. Figure 3-8 above clearly shows that this offset is small but not constant across all pHs, which could cause a titration curve to become misshapen. Non-linear least squares (NLLS) analysis for TA with outlier rejection, as suggested for the TMT technique, would likely reject a large number of points within the curve rather than consider the whole dataset. Although the analysis of the disagreement in measured pH at 5.5 was ascribed to differences in the determination of the lower concentration HI^- species, the large difference in [Itot] stems mainly from an overestimation of the larger [I^{2-}] term by the RGB-PD.

The TMT method identified the most trusted region of the model used in NLLS to be between pH = 3 and 4. In both the modelled and experimental results for pH measurement with the RGB-PD described in 3.4.8 there is a systematic deviation in

measured pH for measurements away from the pKa_2. The noise associated with photometric measurements is superior for the RGB-PD compared to the spectrophotometer (Section 3.4.9), and comparable to those observed in the TMT optical system. The absorbance noise associated with the RGB-PD photometry measurements is ≈ 0.0008 absorbance units (Abs) at its worst with cuvette replacement excluded, close to Martz's requirement of 0.0005 Abs.

Therefore, the pH measurement experiment highlights two main areas of concern for use of the RGB-PD as an optical detector for TMT. Firstly, the RGB-PD may miscalculate $[BCG]_{total}$ at or around the pKa_2 of BCG, leading to errors in TA. The offset of the measured TA curve will likely vary over the pH range of the titration, compromising the NLLS. Offsets in the measured pH may further complicate TA analysis. Just how objectionable these effects will be to TA determination can be examined by further uncertainty analysis.

3.5.3 Titration Modelling

Total alkalinity titrations were modelled to examine the theoretical performance of an RGB-PD based TMT analyser. From the titration data, the spectrophotometric intensities associated with RGB-PD measurement can be predicted, and the titration curve recalculated as if this had been obtained experimentally. Uncertainty associated with RGB-PD TMT measurements can then be calculated. Artificial alkalinity standards containing only carbonate species will be used to assess the prototype system, so the model reflects this. For titration of a carbonate only alkalinity standard in a closed cell system, the relationship between added acid titrant (A_{acid}) and $[H^+]$ is expressed according to equation (1.19).

For real seawater, additional terms for nutrients and species conservative with salinity have to be included. These are given in equation (1.11). The concentrations on the right hand side of equation (1.19) can be expressed entirely in terms of $[H^+]$, carbonate dissociation constants and DIC (3.4) [48].

$$TA - A_{acid} = \frac{DIC \cdot K_1^*[H^+]}{[H^+]^2 + K_1^*[H^+] + K_1^*K_2^*} + \frac{2 \cdot DIC \cdot K_1^*K_2^*}{[H^+]^2 + K_1^*[H^+] + K_1^*K_2^*} + \frac{K_w}{[H^+]} - [H^+] \quad (3.4)$$

When equation (3.4) is rearranged to equal zero by subtracting *TA*-A_{acid} from both sides, determination of the roots of the expression with respect to $[H^+]$ is possible. The single, positive, real root will equal $[H^+]$, allowing calculation of pH at any point in an alkalinity titration for a solution with known TA and DIC. The relationship can be modified to account for the dilution of sample by titrant with a dilution factor D (3.5) based in this case on the flow rate *(f)* of the syringe pumps (3.6). Some terms from equation (3.4) are contracted to simplify equation (3.5), and these are linked by colour coding. Added acid (A_{acid}) is equal to titrant acidity (*Acidity)* multiplied by the dilution factor.

$$0 = [HCO_3^-] \cdot (1 - D) + 2[CO_3^{2-}] \cdot (1 - D) + [OH^-] - [H^+] - (TA \cdot (1 - D)) + (Acidity \cdot D) \quad (3.5)$$

$$D = \frac{f_{titrant}}{f_{titrant} + f_{sample}} \quad (3.6)$$

For $NaHCO_3$ alkalinity standards, TA = $[NaHCO_3]$ The DIC term used need only be within 10% of its true value, so is taken as ≈ TA. Determination of the roots of equation (3.5) is performed using the *fzero* function in MATLAB, as suggested by Prof Andrew Dickson of UCSD by personal correspondence. *Fzero* finds the root of a continuous function of one variable, in this case $[H^+]$ in (3.4) [132]. The inputs used for *fzero* are titrant acid concentration (*Acidity*), flow-rates of titrant and sample, TA, DIC, K1, K2, Kw and an initial estimate as well as upper and lower bounds for $[H^+]$. An alternative to *fzero* is the *roots* function in MATLAB, which first requires rearrangement of (3.4) into a quartic polynomial of the form $a[H^+]^4 + b[H^+]^3 + c[H^+]^2 + d[H^+] + e = 0$. This will output four roots, one of which should be real and positive, the value of $[H^+]$. I found it was simpler and more convenient to use fzero. Figure 1-2 is a good example of a titration curve generated using this method, highlighting how other solution parameters can be calculated once $[H^+]$ is obtained. A full example of the titration model code is included in Appendix A 1.3.

3.5.4 Uncertainty analysis for TMT with the RGB-PD

Uncertainty analysis is introduced in Section 3.3. The aim of uncertainty analysis in here is to predict the performance of the RGB-PD for TMT analysis of total alkalinity. As

stated in the literature review (Chapter 2), the generally accepted level of precision of TA measurements required for ocean acidification experiments is ± 1 μmol kg^{-1}.

A reasonably complete idea of the design of an RGB-PD based TMT system can be formulated, based on the general requirements of titration apparatus, the pH measurement work, and the original TMT system design. The optical system used is taken directly from the pH measurements, and analyses presented here are based on its characteristics.

3.5.5 Treatment of systematic errors

The treatment of systematic errors is outlined in Section 3.3.4. Only the numerical method was applied to the determination of U_c(TA), as this was the simplest to implement. The U_c(TA) calculation was based on equation (3.4) and repeated across the range of pHs encountered during a typical titration to identify the most trusted pH range over which TA measurements could be made. A full example of this code for calculation of U_c(TA) is included in Appendix A 1.10.

The errors used in determination of U_c(TA) were obtained where possible from datasheets and the literature. Concentration errors for the titrant were parameterised from smaller uncertainty calculations. A significant complication was that in using the RGB-PD system, errors arising through deviations from the Beer Lambert law would vary depending on the individual concentrations [HI^-] and [I^{2-}]. These concentrations themselves vary with pH, and TMT increases the total BCG concentration in the sample as acid titrant is added. To account for this, the predicted uncertainty in molar extinction coefficients over a large concentration range was calculated from the spectra of RGB-PD channels, LEDS and BCG indicator. Storing these as lookup tables of indicator concentration *vs* uncertainty allows retrieval of the appropriate uncertainty in ϵ when required during uncertainty analysis. Invariably the required error value falls between two points in the lookup table, overcome by linear interpolation. An example of lookup table calculation is given in Appendix A 1.8, an example of the lookup table is provided on the attached CD-ROM. The method uses a linear range of pHs, and from a simulated titration curve the associated dilution values (D) as given in equation (3.5). From these two numbers, a given titrant composition, and the spectral data used in previous pH models, the RGB-PD-based TA uncertainty is predicted at each pH. Analysis of a 30 pH point titration takes approximately 5 minutes using a PC with a 2.4 GHz processor (Intel Core 2). The results are given below in Figure 3-9.

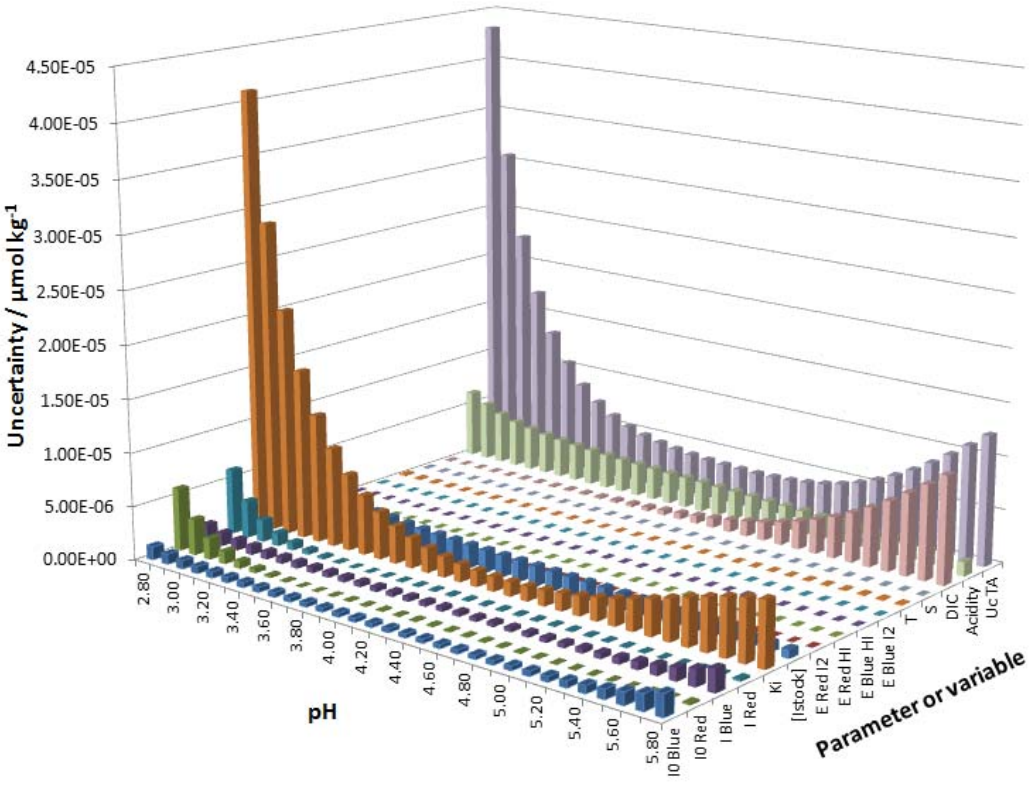

Figure 3-9 – Uncertainty analysis based on systematic errors associated with tracer monitored titration with the RGB-PD. As the titration progresses pH moves from high to low. The combined standard uncertainty in total alkalinity (U_c(TA)) at each titration point varies with pH. The standard uncertainty associated with each parameter is evaluated separately; U_C(TA) is calculated as the root of the sum of squared individual uncertainties. An explanation of parameters, and error values is given in Table 3-4.

The general shape and magnitude of TA uncertainties agrees with those determined in the analysis performed by Martz [26]. The carbonate parameters K1 and K2 and the water dissociation constant K_w are not included in this analysis as these were incorporated as temperature and salinity dependant expressions[15]. Martz showed that only K1 contributed significantly to the overall uncertainty (up to 5 µmol kg^{-1} at pH = 5), which would not greatly affect the outcome of the analysis performed here. Between pH ≈ 3.7 and 5.0 Uc(TA) does not exceed 5.0 µmol kg^{-1}, which may indicate that this is the most useful region for TA measurement with an RGB-PD based system. Large uncertainties arise from the parameters related to the titrant (Acidity, Ki, [Istock]) and photodiode measurements, which is unsurprising given how the analytical weight of the TMT method is focussed on these. At higher pH, where carbonate species HCO_3^- and CO_3^{2-} predominate, DIC is also a significant source of uncertainty. Overall, the anticipated

performance determined here, in general agreement with the previous work by Martz, strengthens the case for the use of the RGB-PD for TMT. The values and sources of error used in the uncertainty analysis used to generate Figure 3-9 are given in Table 3-4.

Parameter	Uncertainty in parameter/ Absolute value (percentage in parentheses)	Source of uncertainty estimate
$[I_{stock}]$ Concentration of indicator in titrant	1.02×10^{-8} µmol kg^{-1} (0.05%)	Calculated by error propagation from performance of balances used in preparation
S Salinity	1.08×10^{-3} (0.0027%)	Calculated by error propagation from performance of balances used in preparation
DIC dissolved inorganic carbon	25 µmol kg^{-1} (1%)	Suggested value from original method [26]
Acidity $[H^+]$ in titrant	7.98×10^{-6} µmol kg^{-1} (0.1%)	Calculated by error propagation from performance of balances used in preparation
I & I0, red and blue Intensities associated with RGB-PD measurement	1 count (0.015 to 0.15%)	No data was available in datasheet – based on assumption that intensities measured are close to true value
Ki Indicator equilibrium constant	0.045 (1.00 %)	Reference [26]
T Temperature	0.01 ℃ / (0.04%)	From water bath controller datasheet (TE-10D, Bibby Scientific U.K.)
ϵ, HI^- and I^{2-}, red and blue	Lookup table used, maximum 5×10^{-6} %	Simulation of inaccuracy of ϵ based on RGB-PD spectra.

Table 3-4 – Errors used in the determination of uncertainty in TA over the TMT titration pH range arising from systematic errors. These correspond to the parameters shown in Figure 3-9, the middle column gives the absolute value and percentage value of errors. The right hand column gives sources for the error values chosen.

3.5.6 Treatment of random errors

For the numerical approach to random error analysis of TMT determination, titrations are simulated with random errors applied to appropriate parameters, and then evaluated as for experimental data. Repeating the procedure several times allows fluctuations in TA measurement to become apparent. Achieving this for an RGB-PD based system is very similar to the approach used in systematic error analysis, and is described in Figure 3-10. The sources of error accounted for are fluctuations in temperature during the titration,

and photometric noise from the photodiode measurements. Temperature fluctuations automatically affect all equilibrium constants, as these are expressed in their temperature dependent forms. By specifying the number of titration points considered, the simulation resolution can be adjusted. Normally distributed random numbers generated with appropriate mean and standard deviation create the desired noise in parameters. The model applies this to the temperature used to calculate each titration point. The spectrum of BCG expected for each titration point is then generated, and RGB-PD measurement simulated from the spectra of LEDs and photodiode channels. Another normally distributed random number applied to each photodiode intensity value simulates the measurement noise. This is repeated until 100 sets of photodiode data have been collected, the error being different and random in each set. These are then analysed using the NLLS routine (Appendix A 1.5), allowing calculation of mean and standard deviation values predicted for TA measurement.

As described in Section 3.3.5, propagation of random errors is assessed here by a purely numerical approach, in line with previous studies [29, 90]. To achieve this, titrations are simulated with random errors applied to appropriate parameters, and then evaluated as for experimental data. Repeating the procedure several times allows fluctuations in TA measurement to become apparent. Achieving this for an RGB-PD based system is very similar to the approach used in systematic error analysis, and is described in Figure 3-10. The sources of error accounted for are fluctuations in temperature during the titration, and photometric noise from the photodiode measurements. Temperature fluctuations automatically affect all equilibrium constants, as these are expressed in their temperature dependent forms. By specifying the number of titration points considered, the simulation resolution can be adjusted. Normally distributed random numbers generated with appropriate mean and standard deviation create the desired noise in parameters. The model applies this to the temperature used to calculate each titration point. The spectrum of BCG expected for each titration point is then generated, and RGB-PD measurement simulated from the spectra of LEDs and photodiode channels. Another normally distributed random number applied to each photodiode intensity value simulates the measurement noise. This is repeated until 100 sets of photodiode data have been collected, the error being different and random in each set. These are then analysed using the NLLS routine (Appendix A 1.5), allowing calculation of mean and standard deviation values predicted for TA measurement.

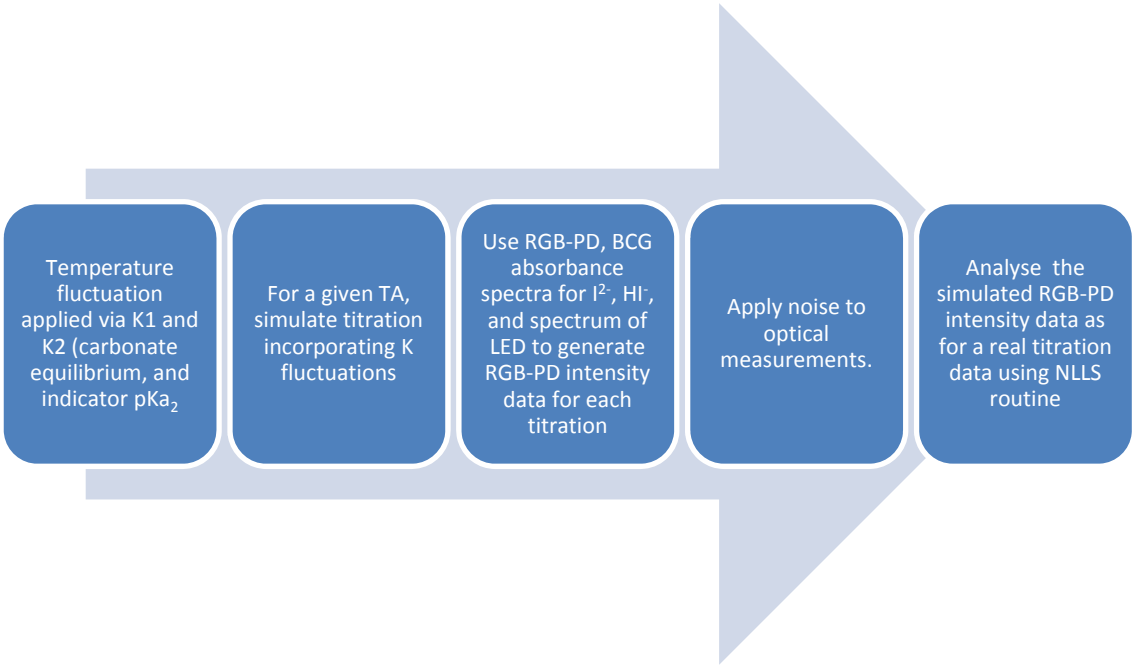

Figure 3-10 - Method for examining random errors. Process is repeated to achieve pseudo-replicate results for statistical analysis.

The noise analysis conducted during the pH experiment in Section 3.4.9 provided the source of error for the photodiode measurement. Temperature error data came from the datasheet of a water-bath temperature controller (Techne TE-10D, Bibby Scientific U.K.).

The NLLS routine outlined in Section 1.5.2 typically includes a filter which rejects titration points should their squared residual (r^2) value exceed a given threshold. The random error analysis does not exclude data points, as by interpreting the full set of data a "worst case" scenario of the effect of the included errors is examined. Several repeats of the analysis with errors at up to 10 times their measured or reported values were used to check the effect of underestimating errors. This was examined individually and in combination. The range of oceanic total alkalinity spans 2000 - 2500 µmol kg^{-1}, so analysis was performed at these extremes. The results are shown in Table 3-5.

Temperature uncertainty / °C	Photodiode uncertainty (%)	pH range handled by NLLS	2000 µmol kg^{-1} TA mean	2000 µmol kg^{-1} TA std	2500 µmol kg^{-1} TA mean	2500 µmol kg^{-1} TA std	Percent difference 2000 µmol kg^{-1} sample	Percent difference 2500 µmol kg^{-1} sample
0.01	0.004	full	2276	3.0	2798	1.5	88	89
0.1 (10x)	0.004	full	2275	3.0	2798	1.5	889	894
0.1 (10x)	0.04 (10x)	full	2278	35	2797	16	88	894
0.01	0.004	4-5 only	2175	0.76	2690	0.76	92	939
0.1 (10x)	0.004	4-5 only	2175	0.82	2690	0.79	92	939

Table 3-5 – Results from the analysis of random errors performed for titrations of 2000 and 2500 µmol kg^{-1} samples. 30 titration points were used in the simulation.

For a given temperature and photodiode measurement uncertainty, the results of the 2000 and 2500 µmol kg^{-1} are given, along with the standard deviation obtained from the 100 repeats of the simulation. The percentage changes are calculated from TA(input) / TA(mean simulated). In general the alkalinities obtained from TMT simulation are approximately 200 – 300 µmol kg^{-1} larger than those used to generate the initial titration curve. If the percentages are the same for the 2000 and 2500 µmol kg^{-1} simulations, the response of the instrument should be linear across the range of total alkalinities examined. The difference between the two is about 1 %, so measurement with the RGB-PD introduces some non-linearity in determined TA over the oceanic TA range. If a single alkalinity of CRM were used to examine the discrepancy, this effect would not be noticed. The results of the RGB-PD pH measurement work (Section 3.4.8) showed that pH measurements close to the pKa_2 of the indicator showed the lowest discrepancies compared to spectrophotometer measurements. Restricting the pH range over which NLLS is performed to close to the indicator pKa_2 was therefore examined and found to reduce TA discrepancy (to 92% of the nominal value), and standard deviation (< 1 µmol kg^{-1}) of measurements. The predicted standard deviation of TA samples analysed using the RGB-PD based system is less than 3 µmol kg^{-1}, and increasing the error in temperature alone to 10x its reported value has little effect on this. A 10-fold change in photodiode error results in a corresponding 10-fold increase in TA standard deviation. Working with 30 titration points, 100 runs can be analysed in less than 1 minute using a PC with a 2.4 GHz processor. The computational load increases significantly when several hundred or more points are considered.

Titration curves can be reconstructed from the simulated photodiode data by calculating pH and dilution factor *D*. This can be compared with the simulated data fed into the RGB-PD model, with Figure 3-11 showing an example of this.

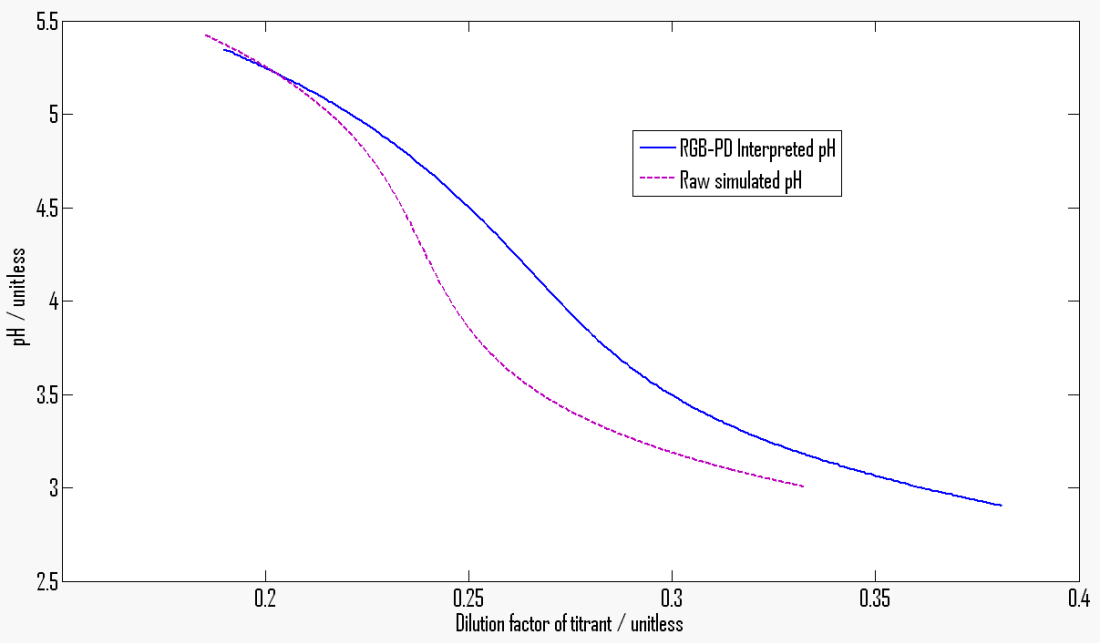

Figure 3-11 - Difference between the raw simulated titration curve (dilution factor D vs pH) and the curve predicted where the RGB-PD has been used to measure the indicator. The RGB-PD distorts the curve, giving it the characteristics of a more alkaline sample.

The difference in titration curves could pose problems for the NLLS method, which will try to fit a poorly conditioned model to the titration curve data when determining TA. Because the simulated titration NLLS did not reject any data, fitting the model to the predicted photodiode response still resulted in a reasonable result for TA determination. Care will have to be taken in implementing the NLLS to real titration data, particularly with regards to rejecting data which falls outside the modelled values. A tight threshold was used in the original method for data rejection [26]. This may have to be made more flexible when performing TA analysis. Figure 3-11 shows that the RGB-PD interpreted data appears to require more titrant to acidify the sample. This explains why the model overestimated TA.

The fact that measurement of a single alkalinity CRM would not detect the non-linearity of the response shows that the response of the system needs to be characterised with a series of samples of known alkalinity. The simplest way to do this is to prepare samples of known alkalinity, or to compare the response of the system to a series of samples analysed with a trusted TA analysis instrument. Once the system is characterised CRMs measured periodically during analysis can monitor any discrepancy. Interestingly the random error analysis identifies a potential systematic error that would associated with the system, and that is not apparent from systematic error analysis. This arises because

of the way that the RGB-PD response spectra are incorporated into the simulation, and is a useful consequence of using at least two different approaches in examination of uncertainties. In conclusion, the precision associated with TA measurements is predicted to be excellent and of a suitable level for ocean acidification studies, being typically less than 3 μmol kg^{-1}. The system is relatively insensitive to temperature fluctuation, however photodiode noise has a more significant effect. The technique used did not study fluctuations in photometric measurements brought about by changes in background absorbance and other solution effects such as refractive index change. These would affect the TA precision achievable. Restricting the pH range considered by the NLLS had the effect of reducing offset and improving precision.

3.5.7 Conclusions from Error Analysis, and implications for the use of an RGB-PD based TA instrument

Error analysis techniques examining the RGB-PD as a replacement photometric detector generally showed agreement with error sensitivities previously highlighted by Martz for the TMT system [26]. The analysis predicts that precision associated with TA measurements meets the requirements of ocean acidification studies, having a standard deviation close to 0.1% TA, and less than 3 μmol kg^{-1}. A similar approach has been used by other workers [26, 29, 90]. Systematic error analysis identified that the offset in TA is comparable to Martz's system, however the random error analysis identified a more significant offset of around 200 μmol kg^{-1}. This is reasonably linear across the oceanic range of TA values, and in theory characterising the system with standards or checking it against an established instrument will compensate for this. This arises due to the polychromatic nature of the light used in photometry.

The RGB-PD based system is far cheaper (< $5 USD) and smaller than the main alternatives available, which are CCD spectrophotometers, or a bespoke optical system designed specifically for the task [29, 112, 115]. These contribute significantly to the overall cost of a system. Reducing the cost associated with the instrument allows purchase of more individual instruments and therefore more extensive measurements to be made. The clear potential of RGB-PDs as photometric detectors in this role, coupled with the promising performance demonstrated in this chapter makes a strong case for the development and testing of them in a prototype TA analyser. The following chapter

cover the design considerations, fabrication and testing of such a device, along with an evaluation of its performance and the potential for future development.

3.6 Declaration for Chapter 3

The work presented in Chapter 3 is my own with a few important exceptions that I must declare.

The thermistor controller used in the experimental determination of pH by RGB-PD and spectrophotometer in Section 3.4 was designed and built by Mr Andy Harris, electronics engineer in the Ocean and Technology Engineering group at the National Oceanography Centre, Southampton.

The spectral response data for the RGB-PD, used in Figure 3-3 was supplied by ams AG (Unterpremstatten, Austria), and used in all optical models for the photodiode. Prof Andrew Dickson of UC San Diego provided advice for modelling total alkalinity titrations, recommending the use of MATLAB and the fzero function. I fully developed the code used in alkalinity titration models based on this method and TA theory.

The NLLS routine used for analysis of modelled titration data in Section 3.5 was developed by Todd Martz and supplied by his doctoral supervisor, Prof Michael DeGrandpre, (University of Montana) in the form of a Microsoft Excel spread sheet and VBA program. Dr Ed Waugh provided assistance with the initial conversion of this to a MATLAB format. All NLLS analyses performed were derived from this.

I performed all experimental work, assembly of the experimental setup, and assembly of the electronics associated with the LED light sources. All MATLAB models were written by me, with the caveats expressed above.

The work described in Section 3.4 has formed the basis of a manuscript entitled "**RGB photodiodes as detectors for spectrophotometry: Examination with a colorimetric pH assay**". This was submitted to Optics Express and has progressed through the first round of review. I am first author, and my supervisory panel – Dr Matthew Mowlem, Prof Eric Achterberg and Dr Doug Connelly, along with Dr Ed Waugh, all commented heavily on the text of this manuscript. All are co-authors on the manuscript

Chapter 4

Measurement of total alkalinity by spectrophotometry with an RGB-photodiode detector

4.1 Introduction

The purpose of the research presented in this chapter is to examine the suitability of the red green and blue photodiode (RGB-PD) as a detector in spectrophotometric measurement of total alkalinity (TA). Total alkalinity is essentially determined from a series of pH measurements made following known additions of acid to a seawater sample (Section 1.5). The advantages of a spectrophotometric technique (Section 2.4.4), and the suitability of an RGB-PD (TCS3414CS, ams AG) for pH measurements over the range required for TA measurement (Chapter 3) has been identified. Furthermore, error propagation studies performed in Section 3.5 showed that an RGB-PD based TA system could perform measurements with the generally accepted level of precision (0.1 %RSD) required for ocean acidification studies using the tracer monitored titration (TMT) method described by Martz et al [29]. The benefits in size and cost reduction associated with the RGB-PD device over the current photometric systems are useful in the development of future analysis devices for environmental monitoring.

This chapter examines the quality of seawater TA measurements made with a prototype RGB-PD based analyser. The main intention behind the experiments is to prove the concept of RGB-PD detectors for TMT titration and alkalinity determination. Should the system fall short of the desired performance examination of the causes should dictate whether improvements are possible. The titration system aims to use apparatus and

techniques that could be easily adapted into a fully automated, portable instrument. The work undertaken is therefore a step toward delivery of a viable system rather than fabrication of an advanced, field-tested instrument. The choice of apparatus for the examination of the RGB-PD is not straightforward. There must be flexibility to cope with changes to system design if required, and yet components must not compromise the quality of measurements needed. Microfluidic technology is employed to take advantage of rapid prototyping of analysis devices, and brings with it the potential for further miniaturisation. This is the first time this technology has been used in TA determination, and has shown great potential for the development of underway systems and in situ sensors for oceanographic analytes [71, 133]. Prior demonstration of microfluidic technology for oceanographic measurements coupled with the predicted precision for RGB-PD TMT measurement being better than 3 μmol kg^{-1} across the TA range of ocean waters shows the potential for this type of device.

4.2 Experimental Approach

TMT is based on a closed cell titration, where the CO_2 liberated during titration cannot leave the system by diffusion, or by equilibration with a headspace of air. This requires that both reaction and photometry occur in a sealed vessel. The design challenges posed by such a vessel have already been discussed in Section 2.2.1. The original TMT method utilised an actively stirred reaction chamber fabricated from metal where titrant would gradually displace sample [26]. Another solution is to take advantage of microfluidic technologies, which have recently generated considerable interest for their potential of miniaturising analysis devices in the fields of environmental monitoring and point of care diagnostics [80, 114]. The use of optical measurements such as absorbance spectrophotometry within these system is commonplace [134]. The National Oceanography Centre, Southampton has developed an in-house capability to fabricate microfluidic wet-chemical analysers for ocean science applications [135], and these have been demonstrated as suitable for long term in situ oceanographic measurements [133]. The reduced size of the RGB-PD makes it an extremely attractive detector for use in these microfluidic devices and indeed some research combining the two has already been conducted. Here a microfluidic device has measured absorbance of differently coloured dyes using a RGB-PD and LED based detector [126, 127]. A device incorporating LEDs and microfluidic technology has been developed for measurement of oceanic pH.

This system has since been deployed at sea as an underway system with excellent results (precision of 0.001 pH) [71]. As it is likely pH and TA systems will eventually be deployed in tandem for full carbonate system measurements, it made sense having these share common components. These microfluidic devices are manufactured from (poly)methyl-methacrylate, which has a good impermeability against diffusion of CO_2 gas [136]. I therefore decided to use a microfluidic system based on the pH analyser described above for examination of the RGB-PD as a detector for TMT. TA analysis has not been performed using either a microfluidic system or a RGB-PD, so there is significant novelty in the development of this system.

4.3 System Design

4.3.1 Mixing and Chip Design

The TMT method relies on high quality photometry to determine both pH and the amount of acid added. To achieve this sufficient light must pass through the microfluidic flow cell to the RGB-PD detector. The light output of the LEDs is limited (maximum of ~300 mW), therefore light throughput is maximised by using short path lengths, and wide channels. The bromocresol green (BCG) indicator used in TA determination is sufficiently soluble in water that a high absorbance titrant can be prepared, and therefore a 1 cm flow cell is used in the microfluidic chip. The flow cell is cut to 700 µm x 700 µm, which is wider than the diameter of the optical fibres used (600 µm). The same flow cell path length is used in the pH experiments detailed in Chapter 3.

Efficient mixing in microfluidic channels is difficult, as the small channel size means that flow is invariably laminar. Mixing therefore occurs through diffusion and dispersion rather than through turbulence [137-139]. For the TMT method, it is crucial that sample and titrant be well mixed for each titration point. The microfluidic pH system uses a ≈ 2m serpentine (a fluidic channel that undulates back and forth in a series of 'U' shapes to accommodate a long channel length in a relatively compact space) to achieve effective mixing [71]. TMT uses photometry to quantify the amount of acid added, and carry-over of sample from previous titrations can severely disrupt this. Concerned that the serpentine would increase the volume of sample required for flushing this feature was removed. Mixing is performed by stopping flow and waiting for diffusion to occur in the stationary liquid within the flow cell. This greatly adds to the analysis time per sample, but is acceptable for a proof of concept instrument.

The calculation of the time required for diffusive mixing is challenging, as the diffusion constant for the specific species being studied must be known. Generally large molecules diffuse more slowly than small, so the calculation of mixing time focussed on BCG indicator – the largest molecule in the mixture (≈ 10x molecular mass of other species). A best estimate for the molecular radius of BCG was obtained using Avogadro molecular mechanics software to estimate the molecule's morphology, which is then measured across the widest point. A radius of 0.5 nm (1 nm diameter) was obtained. A table of molecule "sizes" and diffusion constants was taken from Squires and Quake (2005), from which Figure 4-1 was created [137]. The spreadsheet from which this plot is produced is included in the attached CD-ROM.

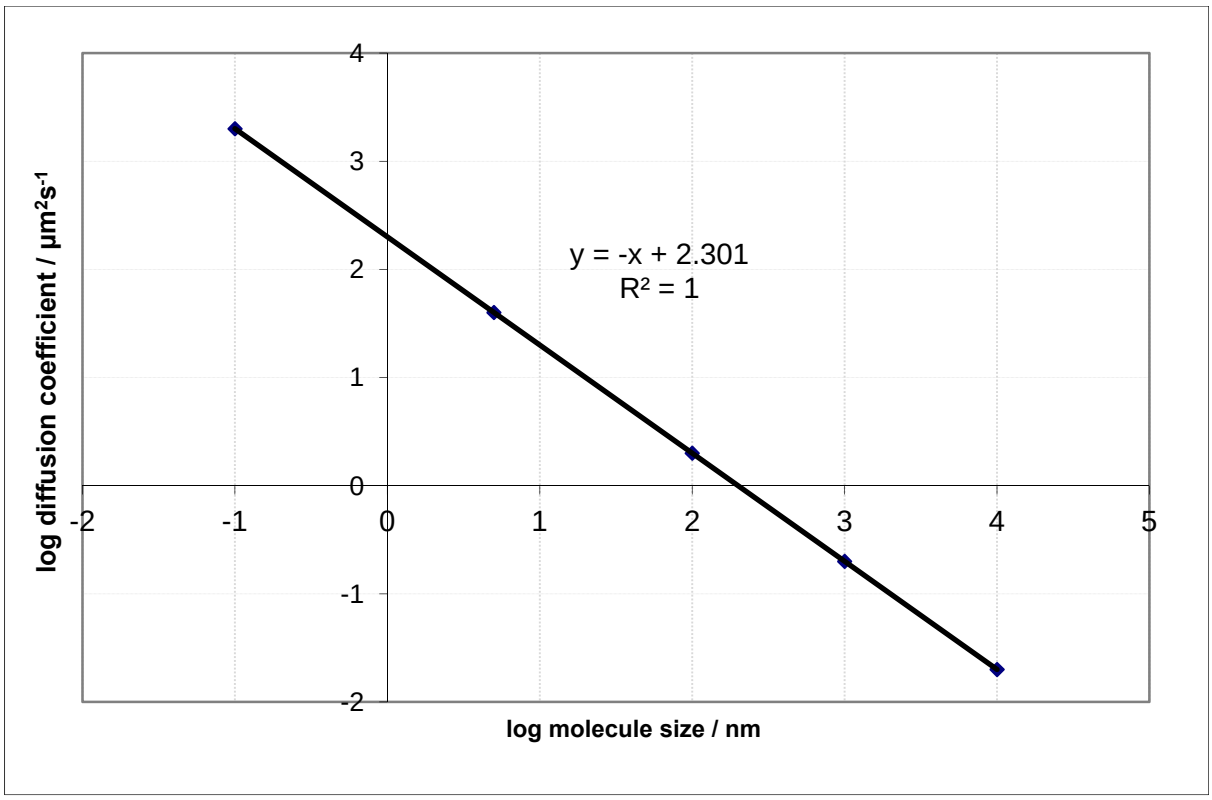

Figure 4-1 – Relationship between a molecule's 'size' and its diffusion coefficient at room temperature, plotted from data provided in Squires and Quake [137]. A linear relationship exists between the log (base 10) of molecule size and the log of diffusion coefficient D_i.

The molecules diameter was taken to be what is meant by "size". Once the diffusion coefficient D_i ($\mu m^2 s^{-1}$) is obtained, the time taken for mixing in seconds, t_m can be calculated according to equation (4.1), where x is the distance (in μm) over which diffusion has to take place, typically the channel width. The D_i values in Figure 4-1 are only valid at room temperature.

$$t_m = \frac{x^2}{D_i} \quad (4.1)$$

The pH system is designed such that the BCG indicator flows in the centre of the channel. The value for x used was therefore 350 µm, predicting a mixing time of around 10 minutes. An alternative to the plot is to use the Stokes-Einstein equation (4.2) which derives the diffusion coefficient D_i ($m^2 s^{-1}$) from molecular radius m_r, Boltzman constant k_b (JK^{-1} or $kg\ m^2\ s^{-2}\ K^{-1}$) , viscosity μ_w(kg s m) , and temperature T (K).

$$D_i = \frac{k_b T}{6\pi m_r \mu_w} \quad (4.2)$$

Assuming the molecular radius given above, the Stokes-Einstein equation predicts a shorter mixing time of around 4 minutes. The above calculations are worst case scenarios, as neither considers the fact the BCG is a charged molecule in a polar solution with high concentrations of other ions. According to Valko, *"it is impossible to associate the diffusion coefficient of an ion in an electrolyte solution with its molecular size or its mobility unless the concentrations or concentration gradients of all ions present in the solution are known"* [140]. Rather than attempt further calculation based on the known concentration gradients, the pragmatic solution is to simply accept the 4 minute mixing time and examine photometry data to determine whether this is adequate.

Full details of the microfluidic chip manufacturing process used are given in Ogilvie et al., and Floquet et al. [108, 135]. Briefly, the microfluidic chip is manufactured from a PMMA substrate. Grey-tinted PMMA is used to exclude stray light and maintain linearity according to the Beer Lambert law. The substrate is machined to create fluidic channels of 250 µm x 250 µm, and a wider absorption flow cell of 700 µm x 700 µm x 1 cm. Through holes are cut to mark fluid inputs and valve locations for micro-inert valves (LFNA1250125H, Lee Products Ltd, UK.) which are used to control the fluid. Interference fittings for optical SMA fibres are machined at a precise depth to align optical fibres with the flow cell. The overall shape is then cut out, and this base piece is solvent bonded to a lid using chloroform exposure, heat, and pressure. Small holes cut for fluidic inputs are tapped with a thread, and valve connections cut. Mounting holes are included for a

waterproof cap, which protects the valves when the chip is immersed in a water bath. The chip schematic used is show in Figure 4-2 below.

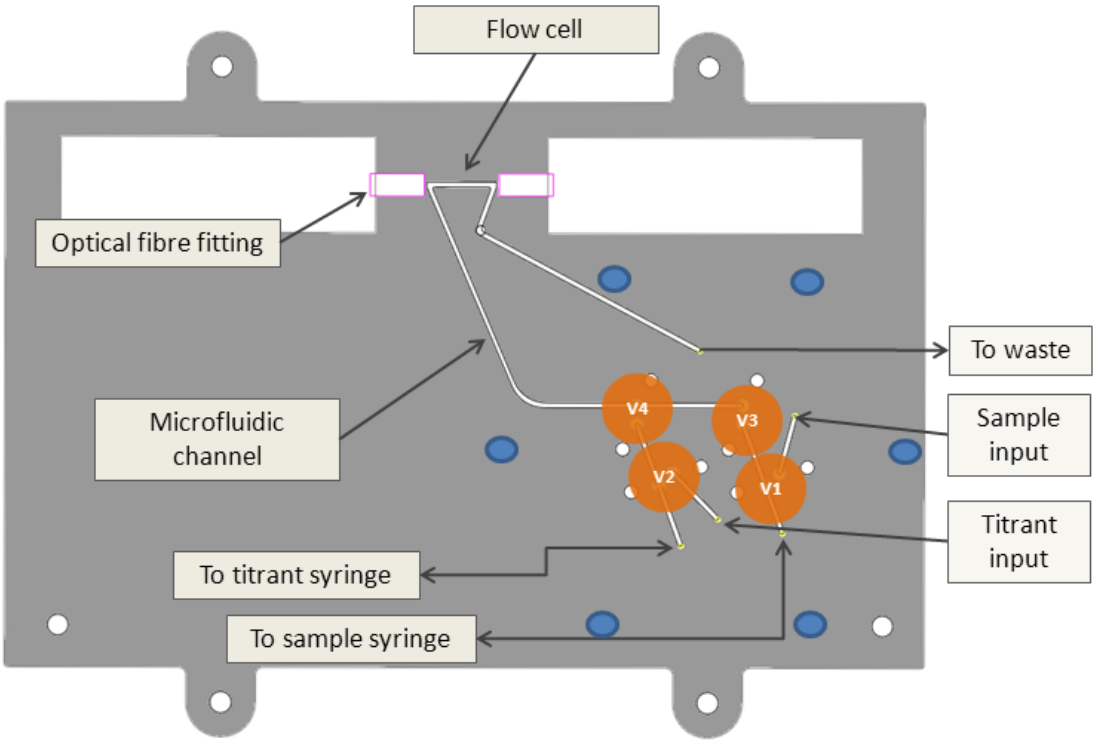

Figure 4-2 – Schematic of the microfluidic chip for the RGB-PD TMT system. V1-V4 are the valves used in combination with syringe pumps for fluidic control. The microfluidic channel (white line) directs fluid to the flow cell for mixing and photometry. Blue circles are mounting holes for a waterproof cap to protect the valves. The two white rectangles at the top represent voids to accommodate the fibre's large SMA ferrules.

Fluid in the microfluidic pH system is pumped with precision syringe pumps (Nanomite, Harvard Apparatus, UK.), which are able to resolve flow rates of between 3.30 nl hr^{-1} and 1900 µl min^{-1} to within 0.05%. TMT relies on photometry to determine both pH and the amount of acid added during titration. Using syringe pumps provides a backup for determining acid added if the RGB-PD measurement gives poor results. In this case the RGB-PD will only be used for pH measurement, not titrant quantification.

4.3.2 Apparatus and assembly

The entire system is housed within a thermostatic water-bath. A steel frame keeps the microfluidic chip immersed under water and the electronic components dry. The water

bath's lid completely covers the experimental setup to exclude external light and help maintain temperature. When modifications, inspections, and repairs need to be made, the entire frame can be lifted out of the water bath without dismantling the system.

The optical system comprises the light source and RGB-PD detector setup used in the pH work described in Section 3.4. Additionally the epoxy-bonded LED/heat-sink assemblies are housed in an aluminium box. This is because some light leaks though the epoxy resin, and interferes with the RGB-PD. Light from the LEDs is combined using a 20 cm bifurcated fibre, and routed through the flow-cell to the RGB-PD assembly by 600 μm optical fibres (M29L01, Thor Labs). As the microfluidic chip is immersed in a water bath, the optical fibres are permanently bonded to the chip using a UV-Cured optical adhesive (Norland optical adhesive 68). This has a refractive index which matches the PMMA chip substrate, and prevents water disrupting the interface between chip and fibre. Titrant and sample are pumped through the system using two syringe pumps (Nanomite, Harvard Apparatus, UK.) which drive glass syringes (Gastight, Hamilton Company, USA). The syringes feature inert materials, employed here to cope with the corrosive seawater/acid solutions being pumped. Titrant, sample and waste are transported to the chip by 1/16" PTFE tubing. Sample is stored and waste collected in 1 litre fluid bags (Flexboy, Sartorius, UK.). Titrant was stored close to the syringe pumps in an aluminium foil covered 125 ml Nalgene bottle. A graphic of the apparatus setup is given in Figure 4-3 below.

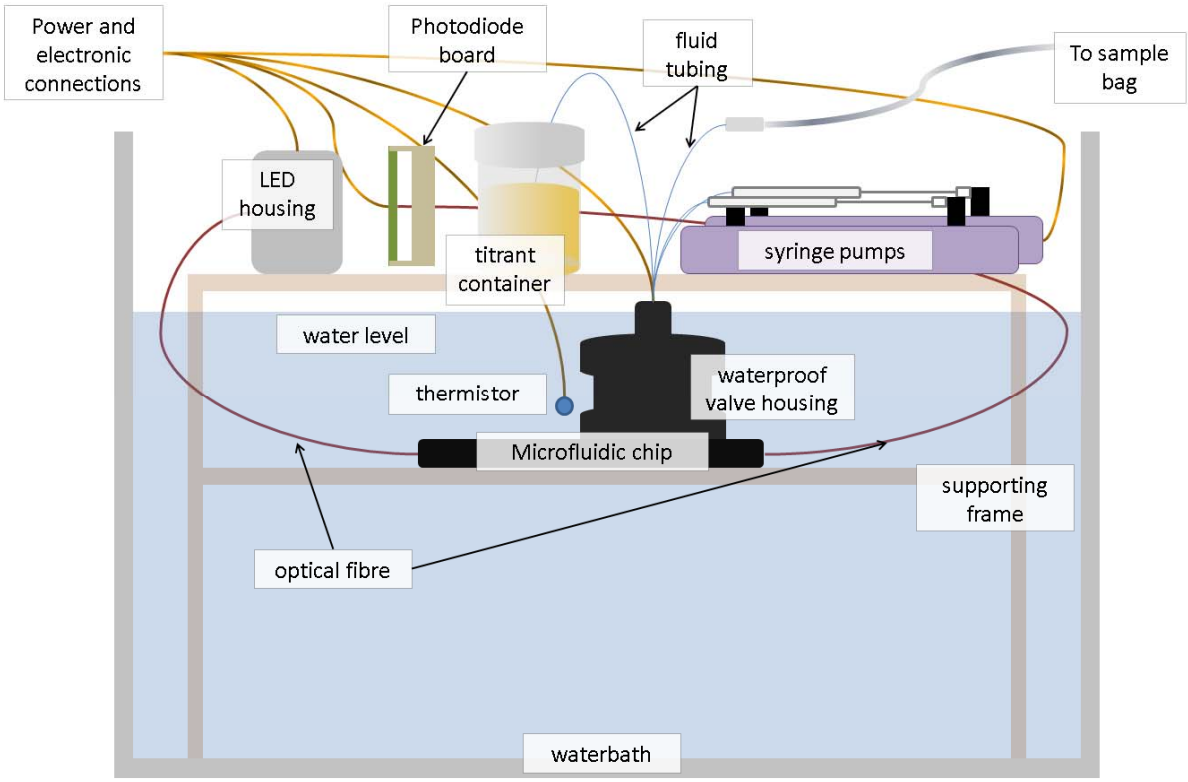

Figure 4-3 - Schematic of the apparatus setup used in the examination of the RGB-PD as a photodetector for TMT analysis of total alkalinity. The RGB-PD / LED setup is identical to that used in the pH work described in chapter 3.

The apparatus is operated from a PC running LabVIEW software (National Instruments) providing the overall control. This includes valve actuation, temperature measurement, syringe pump operation, and extraction of RGB-PD data. The on-chip valves are actuated by a custom-built unit developed by Mr Andy Harris. The electronic control unit also has the ability to monitor temperature via three waterproof thermistors which are attached to the chip. The specific LabVIEW code evolved from previous work within the research group which I heavily modified for TA work. The two syringe pumps are operated via two separate serial ports on the PC. This allows simultaneous starting of the syringe pumps which is important for the intended titration experiments. Directly integrating the RGB-PD measurement into LabVIEW was problematic, so the evaluation module from pH work was used and operated with its proprietary software. This writes irradiance data continuously to a text file on the PC. To record a photodiode measurement LabVIEW simply reads a specified number of lines from the end of this

text file. The RGB-PD was always operated with maximum integration time (400 ms) and gain (64x), and LED brightness adjusted so that blank measurements were within 90% of the saturation level for each channel. LabVIEW can operate a timed sequence of events, so valve operation, pumping, and RGB-PD readings were timed and synchronised according to experimental requirements. The precise sequence of events required careful optimisation, as detailed in Section 4.5. LED intensities and water bath temperature were set at the start of the experiment.

4.3.3 Power consumption

The power consumption associated with the instrument was estimated by summing the power ratings of individual components obtained from their data sheets. These are provided in Table 4-1, with power given in Watts (W).

Component	**Power consumption / W**
Water bath thermo-regulator	1150
Control PC	120
Syringe pumps (x2)	36
Valves (x4)	3.6
LEDs (x2)	0.7
RGB-PD	0.011
Total	**1310**

Table 4-1 – Calculation of power consumption of the microfluidic TMT system.

4.4 Solution Preparation

Solutions prepared for the titration work are similar to those described in the pH experiment in Chapter 3. A stock solution of bromocresol green (BCG, ACS reagent grade, Sigma Aldrich) was prepared by dissolving ≈ 0.4 g of solid in ≈ 1000 g of ultrapure water (Milli-Q, Millipore) and this batch was used for all titration experiments. Exactly as in the pH experiment, the molar extinction coefficients (ϵ) were measured from a BCG concentration series measured in acidic and basic solutions.

Alkalinity standard samples for titration were prepared from $NaHCO_3$ (Fisher, analysis grade). A ≈ 0.2000 mol kg^{-1} $NaHCO_3$ stock was prepared from solid $NaHCO_3$ and Milli-Q

water. Aliquots of this were then diluted in artificial seawater (Milli-Q + 0.7 mol kg^{-1} NaCl, analytical reagent grade, Fisher) and preserved with saturated $HgCl_2$ solution (200 µl per litre of standard). Alkalinity standards with concentrations between 2000 and 2500 µmol kg^{-1} were used for all determinations. For the specific examination of RGB-PD performance in TMT, repeat runs of 6 $NaHCO_3$ alkalinity standards were conducted with alkalinities in the range between 2000 µmol kg^{-1} and 2500 µmol kg^{-1} in steps of 100 µmol kg^{-1}. Preparing all solutions from a single stock solution of $NaHCO_3$ reduces the potential of variability between standards. Sufficient volume of each standard was prepared to allow at least 5 replicate analyses.

4.4.1 Titrant Composition

The acid titrant was prepared using HCl (volumetric analysis standard, Fisher) and the BCG stock solution with ionic strength adjusted to seawater salinity (0.7 M) using NaCl (Fisher). An ampoule of certified 1 M HCl (±0.003M) is diluted to a 0.1 mol kg^{-1} working stock solution, and a portion of this used to prepare the titrant. The concentrations of BCG and HCl in the final titrant must be tailored according to the alkalinity range of the samples, the optical path-length, and the flow rates that can be achieved with the syringe pumps. This is required to resolve the titration curve for all samples. A sample at the high end of the TA range needs to be acidified to pH = 3, and yet the absorbance due to the HI^- species in the indicator must not exceed 0.7 Abs. Conversely for a low concentration TA sample, despite adding enough titrant to achieve good photometry, the sample must not be acidified below pH = 5.5. Preliminary work used several titrant formulations, but the final system characterisation experiment used concentrations of ≈ 6.8 mmol-kg^{-1} and 80 µmol-kg^{-1} for HCl and BCG respectively. A litre of titrant was sufficient to perform required analyses several times over. A more in depth discussion of how the specific flow rates were chosen is given in Section 4.5.

The BCG stock solution is more dilute than that described Martz as much of the BCG remained un-dissolved at the recommended concentration [29]. Addition of a small quantity of NaOH allows rapid dissolution of even large quantities of BCG in water [141]. This was not used due to observed bleaching of colour in dilute NaOH/BCG solutions, and concern it would complicate the titrant composition. Other sulfonephthalein indicators such as bromocresol purple, and bromophenol blue may have improved water solubility, and are suitable for alkalinity measurement [28, 59]. Their spectra do not however match as well with the RGB-PD response as BCG, so are not considered here.

4.4.2 Determination of molar extinction coefficients (ϵ)

Molar extinction coefficients (ϵ) for BCG associated with the microfluidic flow cell were determined as described for the pH characterisation work in Chapter 3 Section 3.4, but were extended to cover a wider range of BCG concentrations, giving at least 0.7 Abs in the dominant absorption peak for I^{2-} and HI^{-} respectively. At least 13 different concentration of BCG were used in each determination. Non-linear deviations from the Beer Lambert relationship were minimal for all ϵ determinations, with the exception of $\epsilon(HI^{-})_{red}$ which deviated strongly from linearity with BCG concentrations above 30 μmol kg^{-1}. This is related to the weakest absorption band for bromocresol green. The values of ϵ determined for the microfluidic flow cell were 31320, 299.0, 3252, and 13450 for $\epsilon(I^{2-})_{red}$, $\epsilon(HI^{-})_{red}$, $\epsilon(I^{2-})_{blue}$, and $\epsilon(HI^{-})_{blue}$ respectively. These are reported here for completeness, as these values are dependent on the precise flow cell length, BCG batch, and specific light source/detector system used.

4.5 Design of the titration routine

Following the production of a microfluidic instrument with the necessary apparatus to perform titrations, the specific method by which a titration could be performed needed to be designed. The simplest method was to measure each titration point with a single injection of titrant and sample. Starting with a ratio of titrant to sample which achieves a pH somewhere above the equivalence point (pH >5), the flow rate of the titrant is increased with each successive step until the pH drops below pH = 3. A pause between the end of the injection and photometric measurement allows time for thermal equilibration and mixing of the sample and titrant. The total number of titration points between pH = 5 and pH = 3 can be tailored by changing the increment by which titrant flow rate is increased. Using this method the entire volume of the chip either side of the flow cell is filled with a uniform mixture of sample and titrant. Theoretically this means that there will be no net diffusion of dissolved species such as CO_2 in and out of the flow cell. The downside is that sample run time will be long – assuming 5 minutes per titration point for 10 to 30 points, the analysis will take ≈ 1 - 2 ½ hours. Commercial systems by comparison can process a sample in less than 10 minutes (Total Alkalinity Titrator, Apollo Scitech Inc). Blank reference measurements were taken at the start and end of the titration series. Referencing between each sample is preferable, but complete flushing was found to require at least 10x 1 ml injections, which would add considerably

to the analysis time. To provide larger flushing volumes, a 1000 µl and 500 µl syringe was used for sample and titrant respectively.

4.5.1 Video analysis of flow characteristics in the microfluidic chip

To optimise the titration routine I performed video analysis of the flow through the chip. This was done with water and a blue dye (erioglaucine). Erioglaucine is not a pH indicator, and chosen as I was only interested in how the flow profile varies with flow rate. Using a light box as a backlight gave an extremely clear view of what was happening in the flow cell under different flow regimes. The dye was diluted until there was good contrast between it and the blank yet still somewhat transparent to the backlight, concentration not being accurately measured. The camera (Optio WG-1 GPS, Pentax) was positioned on PMMA spacers approximately 2 cm above the flow cell, with the horizontal plane of the image at about 40° to the cell long axis due to the proximity of the valves. The majority of analysis is done by eye, reviewing the video to determine the spatial distribution of dye and water. The video files used for analysis are provided on the attached CD-ROM. Images can be extracted from the video (Figure 4-4), allowing numerical calculation of the two dimensional absorbance distribution across the flow cell (Figure 4-6). The figure shows the area over which two dimensional photometry was performed (red rectangle). Measurements of an adjacent area of the chip substrate (yellow rectangle) compensates for changes in the background light level and the response of the camera. The two areas are identical in size.

During titration 10x 1 ml flushes were required to flush coloured sample from the system and return to the reference level. In video analysis, removal by flushing with water of a mixed dye solution clearly shows that faster flow rates (1800 µl min^{-1}) were most efficient (Figure 4-5). Whether this was due to flow characteristics through the channel or simply that a given volume was flushed more quickly with a fast rate was not examined.

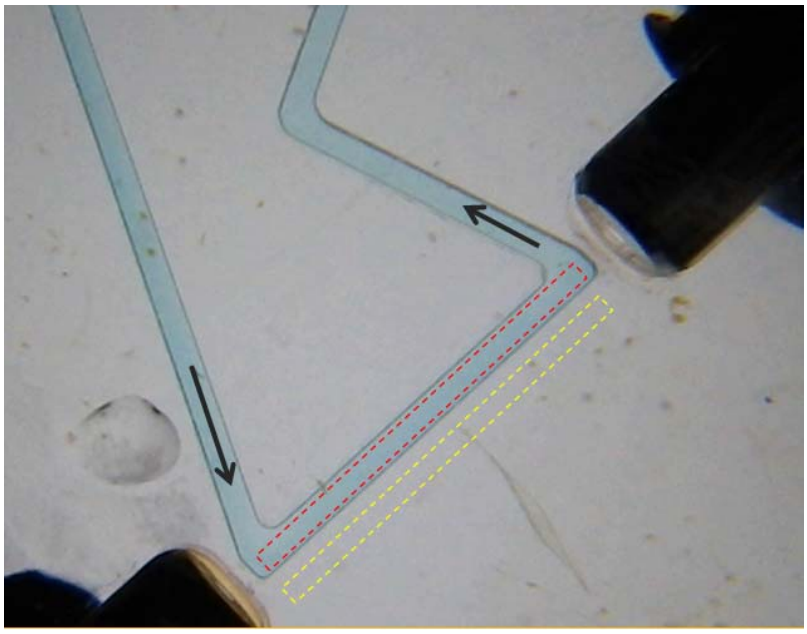

Figure 4-4 – The microfluidic flow cell as it appears in video analysis, lit from behind with a fluorescent backlight and filled with a coloured dye (erioglaucine) and water in place of titrant and sample. In the image these have mixed by diffusion for a few minutes. The dark coloured objects SW and NE of the image are the SMA connectors of the optical fibres which direct light through the flow cell (700 µm x 1 cm) for photometry. Black arrows indicate flow direction. The red (flow cell) and yellow (reference) rectangles show the areas used for 2D photometry.

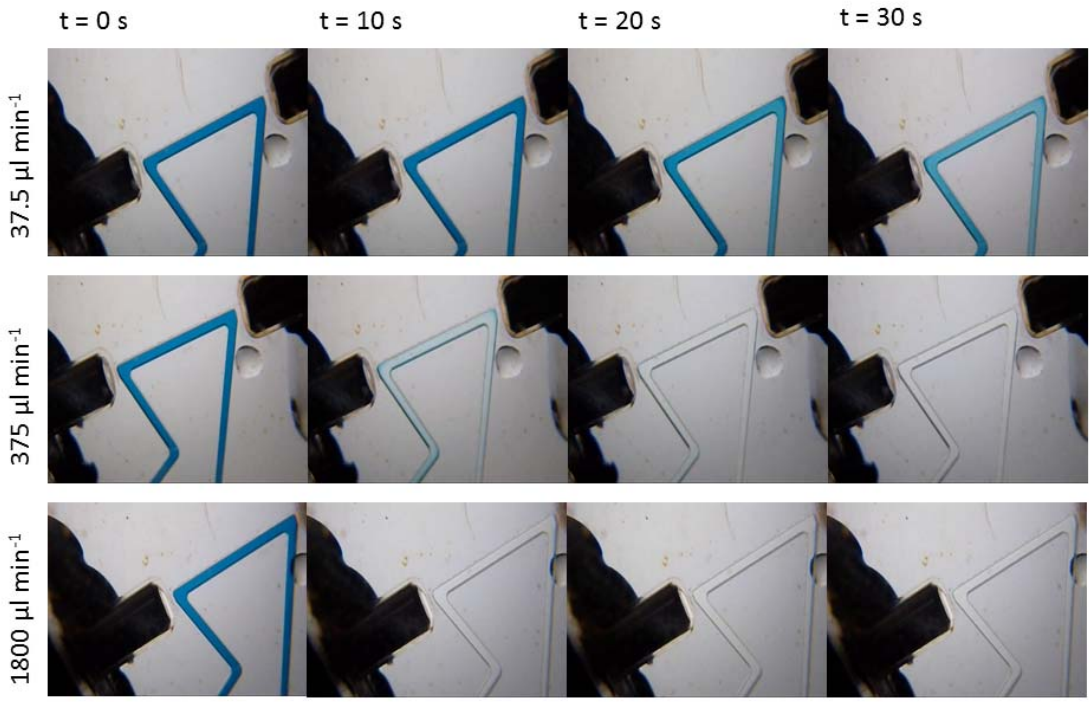

Figure 4-5 – Still frames from videos of the microfluidic system, showing flushing at 0, 10, 20, and 30 s for 3 different flow rates. To reduce the sample analysis time, the flow rate that takes the least time to flush is preferable, which in this case is the fastest flow rate (1800 µl min^{-1}).

During a titration the sample and indicator are flowed together, with the indicator introduced into the centre of the channel. The optimum flow rates at which this could be performed were also examined. Faster flow rates (up to 1800 µl min^{-1} sample, 900 µl min^{-1} dye) resulted in unpredictable distributions of dye and water within the channels, in some cases (900 µl min^{-1} sample, 450 µl min^{-1} dye) a pulsating eddy of dye formed at the outside of the first (i.e. upstream) corner in the flow cell (video included in attached CD-ROM). The distribution of dye and sample within the flow cell dramatically shifted when flow was halted by valve closure. This would result in uneven dye distribution through the flow cell. In the most extreme case, with dye and water flow rates of 450 µl min^{-1} and 1800 µl min^{-1} respectively, when the flow was stopped dye would be aggregated downstream of the flow cell and then slowly diffuse back into the flow cell. This would set up a visible concentration gradient over the longitudinal axis of the flow cell (Figure 4-6 (a) and CD-ROM). During titration this would result in an uneven distribution of indicator through the flow cell, and a gradient in pH. Photometry with the RGB-PD would measure the average of this gradient, resulting in inaccurate measurement of pH and total indicator concentration. Both these measurements are important for TMT.

By contrast using 10x slower flow rates (180 and 45 µl min^{-1} for water and dye respectively) the distribution of dye throughout the flow cell was greatly improved (Figure 4-6 (b)).

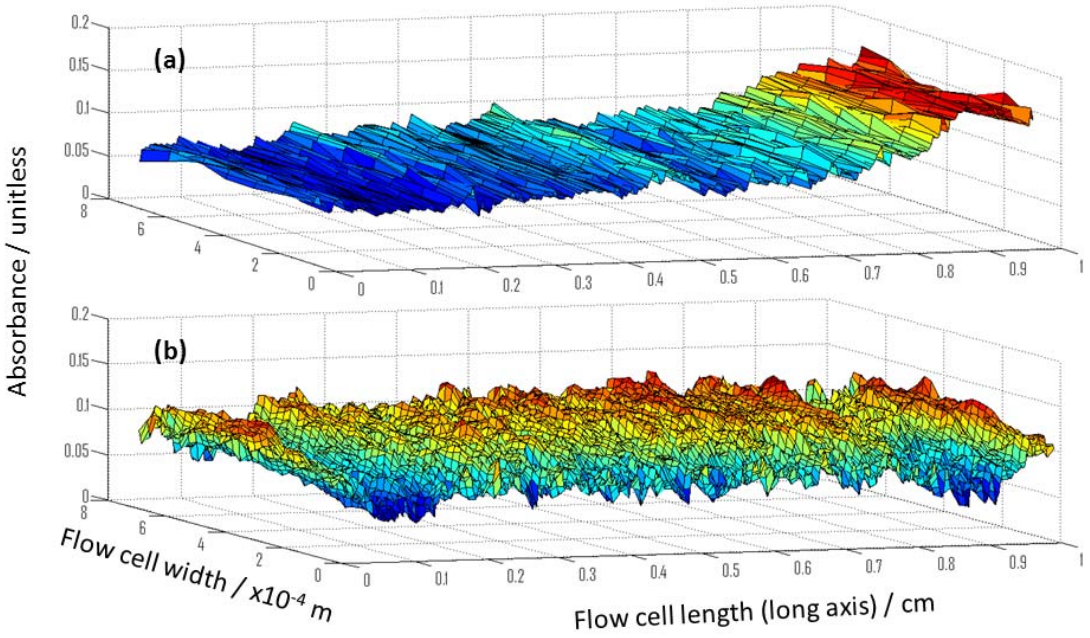

Figure 4-6 – Results from 2D photometry performed on the flow cell from the red-channel pixels of images extracted during video analysis. Titrant and sample are replaced with blue dye (erioglaucine) and water. Image (a) shows absorbance from dye and water flowed at rates of 450 µl min^{-1} and 1800 µl min^{-1} respectively, followed by ≈ 1 minute of stationary diffusive mixing. Image (b) shows the result from respective water and dye rates of 180 and 45 µl min^{-1}. Colours highlight the highest (red) and lowest (blue) absorbance in each sub figure.

Should the titration method use fast injection rates to speed up the time taken to process a sample, the video analysis shows this is likely to result in unusual flow patterns within the flow cell, and possibly even extreme concentration gradients within the cell. The volumes injected were of the order of 1250 µl or more, which is far in excess of the internal volume of the microfluidic chip (≈ 10 µl).

4.5.2 Improved titration method

In an effort to overcome the detrimental effects observed in the video analysis, a new titration regime was developed in LabVIEW, drawing on the observations made during the video analysis. This is based on a fast flush with approximately 800 µl of blank

sample, followed by slow injection of titrant and sample in the desired ratio. The short flush with blank is a compromise of flushing efficiency, sample consumption, and total analysis time. At this point a reference measurement is made, to examine whether injection of such a small volume can be used for more regular blank referencing in photometry. Next 200 µl of sample and between 50 and 100 µl of titrant, depending on the desired titration ratio, is injected. The combined flow rate of these does not exceed 270 µl min^{-1}. Because the syringe pumps cannot report on when their injection is complete, LabVIEW calculates the time taken for injection once the inject command is sent to the pumps. When this time elapses, minus a short safety margin, the valves into the chip are closed and remaining sample and titrant allowed to flow back into their reservoirs. This is a convenience which allows the same volumes to be aspirated and injected irrespective of the titrant to sample ratio used. This also ensures the syringes always return to their fully empty position, allowing LabVIEW to progress the titration by looping through a series of instructions, incrementing the titrant flow rate with each loop. Photometric measurements are made after a 5 minute wait when injection is completed. Each step in the loop is described as a "state" and these continually recorded to a log file for the purpose of fault finding. Once titration has completed, the chip is flushed with 10x 1ml of blank sample to achieve a full blank measurement. Full details of the titration scheme used in examination of the RGB-PD are shown in Table 4-2 below.

State	Description	Valve Operation			
		V1	V2	V3	V4
0	Starting State – Stop syringes \ all valves closed \ wait for user to press start button. Set working directory and start logging experimental data	closed	closed	closed	closed
1	Initialise system – all valves closed	Closed	Closed	Closed	Closed
2	Reverse both syringe pumps	Closed	Closed	Closed	Closed
3	Set pump fill rates fast for filling \ open valves 1 and 2	Open	Open	Closed	Closed
4	Set pump volumes to 1000 µl sample \ 100 µl titrant	Open	Open	Closed	Closed
5	Fill both pumps, wait 28 s for sample to fill	Open	Open	Closed	Closed
6	Close valves 1 and 2, open valve 3 for sample	Closed	Closed	Open	Closed

	flush				
7	Reverse syringes	Closed	Closed	Open	Closed
8	Set sample syringe inject rate within LabVIEW (fast)	Closed	Closed	Open	Closed
9	Send sample inject rate to sample pump	Closed	Closed	Open	Closed
10	Set and send sample inject volume to 800 µl	Closed	Closed	Open	Closed
11	Send run signal to sample pump	Closed	Closed	Open	Closed
12	Wait for sample syringe to flush chip, record RGB-PD and thermistor data.	Closed	Closed	Open	Closed
13	Prepare inject volume, 200 µl sample, 100 µl titrant	Closed	Closed	Open	Closed
14	Send inject volumes to both pumps.	Closed	Closed	Open	Closed
15	Send inject rates to both pumps, 100 µl/minute for sample, titrant depends on titration point, up to 50% of sample inject rate. Open valve 4. *Note: if titration is complete valve 2 is opened instead to flow titrant to reservoir and chip flushed with just sample*	Closed	Closed	Open	Open
16	Signal both pumps to inject	Closed	Closed	Open	Open
17	Wait for sample to finish injecting	Closed	Closed	Open	Open
18	Close valves 3 and 4, open valve 2 to flow remaining titrant back into the reservoir	Closed	Open	Closed	Closed
19	Close all valves. Wait 5 minutes for mixing by diffusion	Closed	Closed	Closed	Closed
20	Record RGB-PD and thermistor data to specific files. Go to state 1	Closed	Closed	Closed	Closed

Table 4-2 - "State machine" used in the modified alkalinity determination routine used to examine the RGB-PD, including actuation of valves. .

4.6 Performance of the prototype RGB-PD titration system

4.6.1 Reference flushes and temperature measurement

The titration routine developed in Section 4.5 performs a full flush at the end of each titration for the purpose of a photometry blank reference. Between each titration point, a small injection of blank sample is performed to remove the previous titration mixture. A separate reference was taken at this point to examine whether these injections could be used for blank referencing. This is also performed for each of the 10 full blank reference flushes taken at the end of the titration series. Figure 4-7 compares the intensities recorded for quick references taken during titration with those taken during the post-titration flushing injections. Only the RGB-PD red channel is examined as any remaining indicator will take the I^{2-} form due to the excess of alkaline sample present during these injections. It is clear that indicator left over from the previous titration mixture is carried over into these "in between" reference measurements. As the titration progresses, the concentration of BCG ([BCG]) is increased, and this is apparent in the reference signals made between each titrant injection. The absorbance from BCG reaches a maximum of around 0.02. When the titration is finished and the chip flushed for blank measurement with blank sample only, the "in between" references show much greater stability.

The presence of indicator in blanks injected between each titration point shows that referencing at the end of the flushing series will be most effective. The poor removal of the previous titration mixture also shows that titration points will become progressively contaminated with the previous sample which will affect total alkalinity determination. The presence of additional titrant means that by the TMT method the total alkalinity of the sample will be over-estimated. A rudimentary examination of the data show that during the mid-point in the titration cycle (close to the equivalence point) the amount of added acid required could be overestimated by as much as 33 μmol kg^{-1}. This could cause an equivalent overestimation of TA. As the carryover increases as the titration progresses, the overestimation of added acid will also increase. Thus the sample will effectively appear to have a higher TA as the titration progresses, and will distort the titration curve, affecting the NLLS regression used to determine TA.

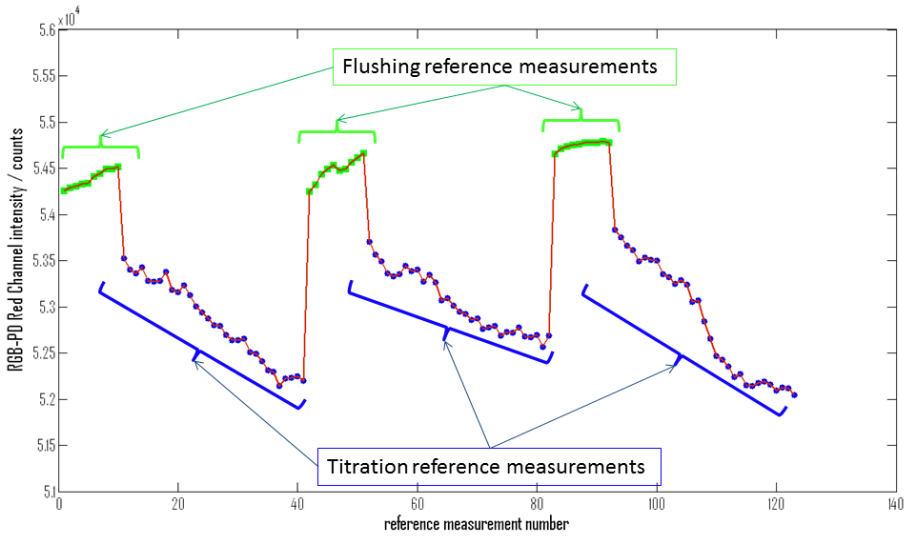

Figure 4-7 - Examination of the reference measurements made during each injection, specifically looking at the red RGB-PD channel raw data. Green data points highlight the references made during the full blank flushes (no titrant injected) made after each full titration is completed. Blue data points are references made during the quick flushing step between injections during titration.

Indicator carryover was anticipated as an issue, and had to be tolerated as full flushing between each titration point would result in an excessively long sample processing time, of the order of 5 or more hours per sample analysed. The amount of sample consumed would also increase to ≈ 300 ml. It is possible that by modifying the system to include a higher capacity (≈ 10 ml per injection) pump would allow such measurements to be made in a much shorter time. A low precision syringe pump would be sufficient for this. The existing system would however have to be modified to accommodate the extra pump input by either including a 3 way valve at the position of the sample syringe to accommodate the third pump on the same fluidic line, or a redesign of the microfluidic chip to include a third syringe input with associated valves.

Initial temperature measurement with the thermistor system was excellent, however after a few days of immersion the signal would suddenly drop. The thermistors were potted in epoxy resin at the end of thin connecting wires, and water ingress was found to be responsible for the signal change. Despite removal, drying, and re-coating with epoxy resin, the same drop in signal following immersion for several days was observed. Automated temperature logging was therefore abandoned. The water bath was relied upon for temperature control. Manual measurements with a probe were used to check

that the temperature provided by the water bath was reasonable. Given that this probe was uncalibrated, and the water bath temperature controller brand new and therefore recently certified, it was decided that the water bath 'set' temperature would be used in analyses. This was deemed acceptable due to the high performance of the bath (± 0.01 °C) and the relative insensitivity of TA measurement predicted by error analysis in the previous chapter (Section 3.5). The temperature used for all titrations was 27.00 °C

4.6.2 Total alkalinity determination with the RGB-PD

The RGB-PD based titration system was used to analyse 6 samples for total alkalinity using the TMT method. The samples were $NaHCO_3$ standards with alkalinities between 2000 μmol kg^{-1} and 2500 μmol kg^{-1} in 100 μmol kg^{-1} increments, prepared in 0.7 moles kg^{-1} NaCl to approximate seawater ionic strength. Five replicate measurements were made of each sample, giving a total of 30 titrations performed to characterise the system. For each of these titrations, 31 injections of titrant and sample were performed, the titrant incrementally increased with each new injection. This was followed by 10 injections of sample alone to flush the system and provide a reference measurement for photometry. The photometric titration data was processed using a non-linear least squares method in MATLAB, the full code of which is provided in Appendix A 1.5. To remove outliers and poor quality titration data, a series of rejection filters are applied. Firstly pH measurements outside the range pH = 3.0 to 5.5 are ignored, as are absorbances below 0.01 Abs or above 0.8 Abs. A best-fit titration curve is found, and the residual differences between this and the experimental data are calculated, as shown in Figure 1-5. Residuals with squares larger than a chosen threshold are rejected, and the titration curve evaluated a second time ignoring these points. Martz set the R^2 threshold based on the theoretical value required for titration precision of < 0.01% at approximately 1×10^{-11} mol^2 kg^{-2}, or an absolute residual difference of around 3 μmol kg^{-1}. This would reject almost all the data collected with the RGB-PD, and so a less stringent 8×10^{-8} mol^2 kg^{-2} filter was applied. With these rejection criteria the NLLS uses at least 15 titration points, with the exception of the 2400 and 2500 μmol kg^{-1} analyses, which used 10 or fewer titration points for 7 out of the 10 replicates. The results of these analyses are shown in Figure 4-8 below. Tabulated data is provided in Table 4-3, and is also provided on the attached CD-ROM.

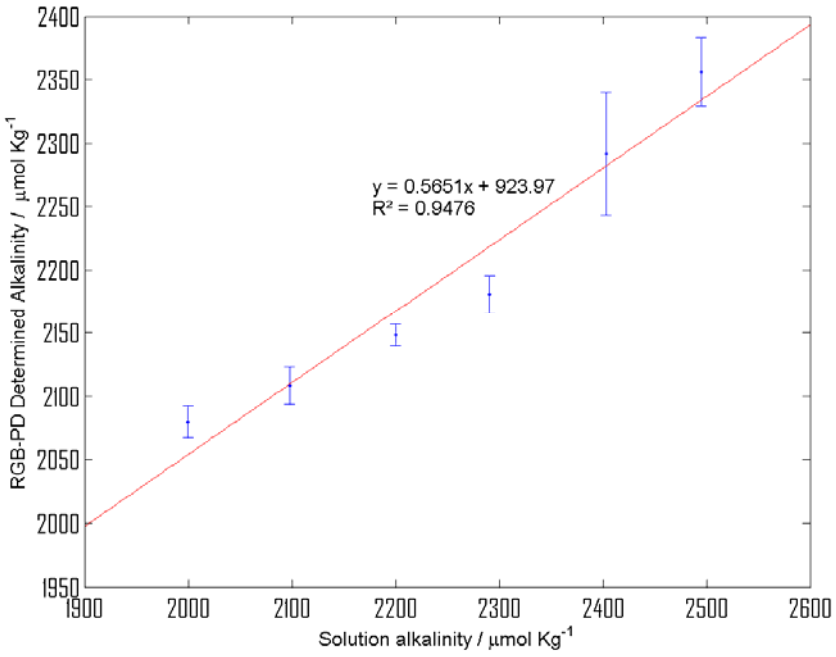

Figure 4-8 – Alkalinity determined by TMT (added acid quantified by photometry) using the RGB-PD based microfluidic system for a series of alkalinity standards including error bounds of ± 1 standard deviation (σ) (data in blue). A linear fit (red line) is applied to the data to highlight correlation, including equation and R^2. The maximum standard deviation is 21 µmol kg^{-1} for the 2500 µmol kg^{-1} standard.

The RGB-PD system exhibits a linear response across the oceanic range of total alkalinities, with precision better than ± 21 µmol kg^{-1}. The four lower concentrations have precisions better than ± 13 µmol kg^{-1}. The samples analysed ranged in TA from 2000 µmol kg^{-1}, to 2500 µmol kg^{-1}. However, the TA range obtained by analysis with the prototype system covered just ≈ 2180 – 2360 µmol kg^{-1}. Essentially the TA of the lowest concentration sample is over estimated while the highest concentration is under estimated. This means that when TMT analysis is employed, the instrument's response is compressed compared to the samples measured, in this case a series of samples spanning 500 µmol kg^{-1} being interpreted as having a span of only ≈ 180 µmol kg^{-1}. Precision associated with TA measurements may therefore be levered unfavourably by the compressed scale. Where repeat measurements of TA for a single sample are made, the standard deviation of measurements is effectively larger than the absolute values. In the worst case the ≈ 0.4 times compression of the dynamic range means the standard deviation associated with measurement may be as much as 112 µmol kg^{-1} for the 2400 µmol kg^{-1} measurement, rather than 49 µmol kg^{-1}.

		Determined Alkalinities from TA system / μmol kg^{-1}						
Nominal TA / μmol kg^{-1}	Solution TA from masses / μmol kg^{-1}	Run 1 / μmol kg^{-1}	Run 2 / μmol kg^{-1}	Run 3 / μmol kg^{-1}	Run 4 / μmol kg^{-1}	Run 5 / μmol kg^{-1}	Mean / μmol kg^{-1}	σ / μmol kg^{-1}
2000	2000	2065	2079	2076	2096	2088	2080	12
2100	2098	2101	2101	2113	2132	2095	2109	15
2200	2200	2157	2153	2140	2155	2139	2149	9
2300	2291	2191	2155	2192	2182	2182	2181	15
2400	2403	2324	2330	2323	2223	2258	2292	49
2500	2495	2328	2349	2358	2346	2401	2356	27

Table 4-3 – Tabulated data from the TMT TA determination

I conclude therefore that the RGB-PD is capable of TMT measurements of TA with precision better than 50 μmol kg^{-1}, with absolute precision values reported better than 21 μmol kg^{-1}. Chapter 3 demonstrated that pH measurement with the RGB-PD was excellent, and uncertainty analysis predicted that performance for TMT TA determination should be better. It could be that poor determination of acid additions are to blame, and as the performance demonstrated here is less than desired, it is useful to decouple the pH and added acid determinations for TA measurement.

A benefit of using the syringe pumps is they offer a backup to tracer monitored acid dosing, as the amount of added acid can be determined from the pump flow rates instead. By this method the RGB-PD is only used to determine pH. To examine this, the titration data was reprocessed as before with the exception that syringe pump flow rates were used for acid quantification. The LabVIEW program designed automatically logs flow rate data as part of the titration routine. The results of this analysis are shown in Figure 4-9 below for comparison with the TMT experiment. There are two differences that are immediately apparent when flow rate data are used. Firstly the linearity of the instrumental response to alkalinity standards over the range examined is improved. Secondly the magnitude of the instrument's response is expanded, with almost 500 μmol kg^{-1} difference between the highest and lowest determined alkalinities. Determined TA values are close to the standards being measured, and the gradient of the best fit line is close to 1. Tabulated data is provided in Table 4-4, and the attached CD-ROM.

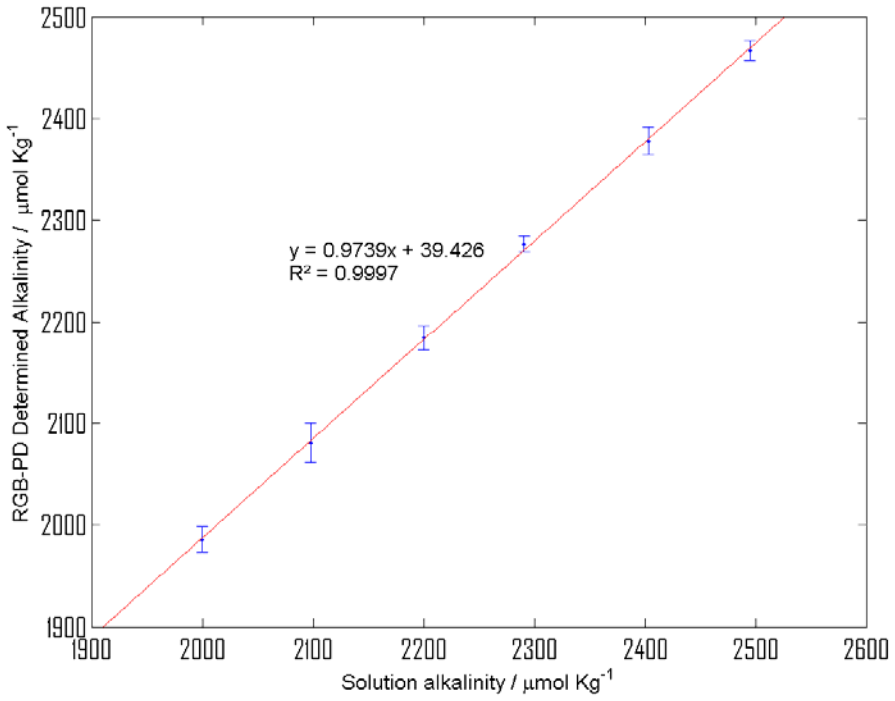

Figure 4-9 – Alkalinity determined using syringe flow rates for titrant quantification (not TMT), pH measured by RGB-PD (data in blue, including errors bounds ± 1 sd). A (red) line of best fit is applied, showing equation and R^2. Maximum standard deviation = 19 µmol kg^{-1}). Error bounds appear smaller in this figure compared to the TMT data plot (Figure 4-8) because of the expanded range in determined TA values.

The difference between the TMT and flow rate based TA determination is in the means of acid quantification. This must therefore be responsible for the difference in the observed results. In TMT, this is achieved by measurement of total indicator concentration which is proportional to acid concentration in the mixed titrant. The specific cause of the observed behaviour therefore arises from the RGB-PD measurement of combined [I^{2-}] and [HI^-] concentrations to yield [BCG]. This effect was observed in the pH determination work (Figure 3-8). The lower alkalinity samples determined TA values appear to be overestimated while larger alkalinities are under-estimated. Over estimation of TA by the TMT method was predicted during uncertainty analysis (Figure 3-11), and it appears that the magnitude of this effect varies with sample TA. The carryover of indicator identified in reference measurements (Figure 4-7) would also result in an overestimation in the measurement of the amount of acid added, and hence overestimation of TA. Further work is necessary to isolate the effects on TMT of these

factors, separating RGB-PD concentration determination issues from those of fluidic effects introduced by the microfluidic architecture.

The residual rejection criterion for the flow rate based TA determination was increased to 2 x 10^{-7} mol^2 kg^{-2} to give the best results. This means that the fit is less stringent regarding the removal of outlying titration data points, which have residuals (compared to the fitted NLLS model) which exceed the rejection threshold. On one hand increasing the rejection threshold allows more experimental data to be included when performing the model fit. The caveat is that the determined TA is more likely to be influenced by experimental errors. Increasing the rejection criteria for the TMT data did not significantly improve results. It is preferable that as much of the experimental data as possible is included in the analysis of TA, and this was used to justify increasing the rejection criterion in this case. With this modification a greater amount of titration data was used for all analyses without compromising precision. At least 25 titration points were used in the analyses of replicates from all alkalinity standards. The poorest precision measured was better than for the TMT method (± 19 μmol kg^{-1}), and the remaining 5 determinations had precision better than ± 13 μmol kg^{-1}. The magnitude of imprecision directly obtained from the analyses is similar for both the TMT and flow rate methods. With no compression of determined TA dynamic range when flow-rate data are used, the precisions associated with these data are not unfavourably leveraged. Imprecision due to pH will be the same for both methods, therefore the determination of added acid is responsible for the differences in determined TA scales.

		Determined Alkalinities from TA system						
Nominal TA / μmol kg^{-1}	Solution TA from masses / μmol kg^{-1}	Run 1 / μmol kg^{-1}	Run 2 / μmol kg^{-1}	Run 3 / μmol kg^{-1}	Run 4 / μmol kg^{-1}	Run 5 / μmol kg^{-1}	Mean / μmol kg^{-1}	σ / μmol kg^{-1}
2000	2000	1980	1990	1967	2000	1992	1986	13
2100	2098	2069	2102	2079	2097	2056	2080	19
2200	2200	2199	2191	2180	2183	2167	2184	12
2300	2291	2285	2286	2273	2272	2268	2277	8
2400	2403	2400	2370	2383	2370	2368	2378	14
2500	2495	2462	2482	2455	2466	2470	2467	10

Table 4-4 - Tabulated data from flow rate based TA determination

4.6.3 Comparison to uncertainty analysis

Uncertainty analysis in Section 3.5.4 predicted better precision for the TMT method than was observed experimentally. Analysis of random errors suggested an uncertainty of 3 μmol kg^{-1}, and the uncertainty from systematic errors generally better than 10 μmol kg^{-1}. TMT TA precision was found to be between 9 – 49 μmol kg^{-1}. This does not take into account the compression of dynamic range observed. That the variability of real samples is expected to be greater than calculated uncertainty has already been discussed (Section 3.3.2).

A number of factors may be responsible for this difference in TA precision by TMT analysis. One or more crucial sources of uncertainty may have been overlooked. No term is included for fluctuations in the syringe pump flow rates, and the effect of indicator carryover between samples is ignored. In fact no fluidic properties such as mixing were incorporated into the uncertainty analysis.

Individual uncertainties used in U_c(TA) determination may have been underestimated. The supplied photodiode spectrum may not be representative of the photodiode incorporated into the instrument. It is possible to check this using monochromated light at discrete wavelengths by using, for example, a broadband light source and several different bandpass filters. Full characterisation of the RGB-PD could be performed with a sweepable monochromator such as a prism, and a broadband light source. The time, cost, and complexity involved in performing this characterisation challenging, and was not performed for these reasons. Outsourcing this task to a specialist is a pragmatic solution to address this.

Determined parameters of acidity, molar extinction coefficient ϵ, and indicator dissociation constant pKa_2 rely on the experimental procedure used in their determination are subject to the effects of human and instrument error. This is not accounted for in uncertainty analysis. Finally the microfluidic design introduces the challenges of flushing dead volumes and poor mixing characteristics. The value of errors associated with measurements and parameters used were based on experimental results and published data with the exception of RGB-PD irradiance measurement uncertainty. This was assumed to be very good (1 count in 65,000). With a suitable calibrated light source and graduated neutral density filters the validity of this assumption can be tested.

The time, cost, and complexity involved make this characterisation challenging, and was not performed for these reasons. Because the titrations are examined over a wide range of pH values, the resolution of the titration curve becomes limited when a narrow band of pH values is studied, so rejection of high pH (> 4.5) data results in poor precision as this dramatically reduces the number of points considered. Repeating the experiment with much higher resolution of titration data would allow examination of this effect.

The carryover of indicator in the "in between" reference measurements discussed at the beginning of this section is a likely source of error for added acid determination in TMT measurement. At the end of the titration, this represents up to a 2.5% overestimation in $[BCG]_{total}$ which will influence the determination of the amount of acid added. This is a worst case estimation, as by removing residual indicator the flushing period is performing as intended, and subsequently less indicator will carry through to the titration mixture injected after the flushing period. Uncertainty analysis predicted a 5 μmol kg^{-1} uncertainty in each titration point arising from a 0.1% uncertainty in acidity, and therefore a 2.5% overestimation is significant. This would have the effect of shifting the determined total alkalinity curve if the carryover of indicator is constant, or distorting the curve if it varies. Improvements to the design of the microfluidic chip in future embodiments of the instrument should focus on removal of dead volume - space where solution can collect and avoid being flushed. One solution has been to build low dead volume valves directly into the chip [142-144]. A simpler approach is to increase the flushing volume of blank sample between titration points, although as discussed earlier this consumes extra sample and takes time. As this issue stems mostly from the use of a flow cell type apparatus, this approach was not the most effective for examining the performance of the RGB-PD for TMT determination of TA. The use of microfluidics clearly brings both benefits and disadvantages. Small volumes of sample and the ability to rapidly develop a precision engineered prototype system allowed the RGB-PD detector for TA to be examined quickly and with reasonable precision. Mixing and flushing were however problematic, and greatly added to the time taken to analyse a single sample.

In spite of this these results are extremely encouraging. The RGB-PD was not designed for this type of application, however the performance of this first generation device has shown great potential. This is the first chemical analyser based on an RGB-PD which uses the colour discrimination of channels for simultaneous measurement at two wavelengths. Additionally RGB-PDs and microfluidics have not yet been used for TA

determination. The performance fell short of target specifications of precision and analysis time identified in Section 2.5 , and the probable causes are examined, yet in spite of this measurements of total alkalinity were clearly demonstrated.

4.7 Apparatus reliability for automated measurements

Although several reliability issues were encountered when using the instrument, analyses were generally able to progress without constant operator intervention. The most common modes of failure arose from two main causes, human error and individual component failure. By examining the causes behind failed or improperly executed titrations, future development of instruments can be guided to mitigate these, and will be interesting to developers of any instrument based around the components used here. The common modes of failure, along with mitigation strategies are given in Table 4-5.

Mode of failure, description, *suggested mitigation*	Results in total titration failure?
Human Errors	
Failure to open closure on sample storage bag *Operator checklist item / add auto-sampler*	Yes
Do not set RGB-PD software to write to file *Operator checklist item / incorporate RGB-PD reading directly into LabVIEW code*	Yes
RGB-PD evaluation board power LED left on *Operator checklist item / Physical removal of power LED from board.*	No
Improper fitting of lid allowing ambient light to reach photodiode *Optically isolate RGB-PD board / operator checklist item*	No
Individual component failures	
Syringes not starting *Fit sensors to detect syringe movement / position. Use more powerful syringe pumps / Operator can check movement at start.*	Yes

Syringe fails during titration *Replace syringe / different pump /full mode not known*	Possible
RGB-PD communication failure *Permanently solder to serial converter / read evaluation board from LabVIEW or use I²C interface*	Yes
Water bath temperature failure / low liquid level *Ensure sufficient temperature difference above ambient or fit chiller / check water level regularly or fit level monitor*	No

Table 4-5 - Common modes of failure of the RGB-PD TA system, and suggested mitigation strategies (italics).

The instrument is fully automated once experimentation starts. Changing of samples is however still performed manually, followed by restarting the instrument. In this manner the instrument was run without significant interruption for 13 days while TA determination was being performed. When changing samples it is easy to neglect crucial tasks that will compromise the experiment. A bag containing the new sample needs connecting to the fluidic input, and is sealed with a plastic clip (Figure 4-10). If the clip is not removed sample cannot be delivered to the system.

Figure 4-10 - Sample storage bag similar to the one used for alkalinity measurement. The close up shows one clip open, one closed.

4.7.1 RGB-PD Power LED

If the RGB-PD evaluation software is restarted following power off or failure, this automatically illuminates a small green power LED close to the RGB-PD (Figure 4-11). This can be switched off in software, but is easy to forget and creates a small (< 0.03% at maximum sensitivity) background light signal. The power LED is green, and the red and blue RGB-PD channels are relatively insensitive to it. The interference introduced was less than 30 counts in 55000 (Figure 4-12). Interference would be further reduced if more light were passed through the flow cell allowing a lower gain and integration time to be used with the RGB-PD.

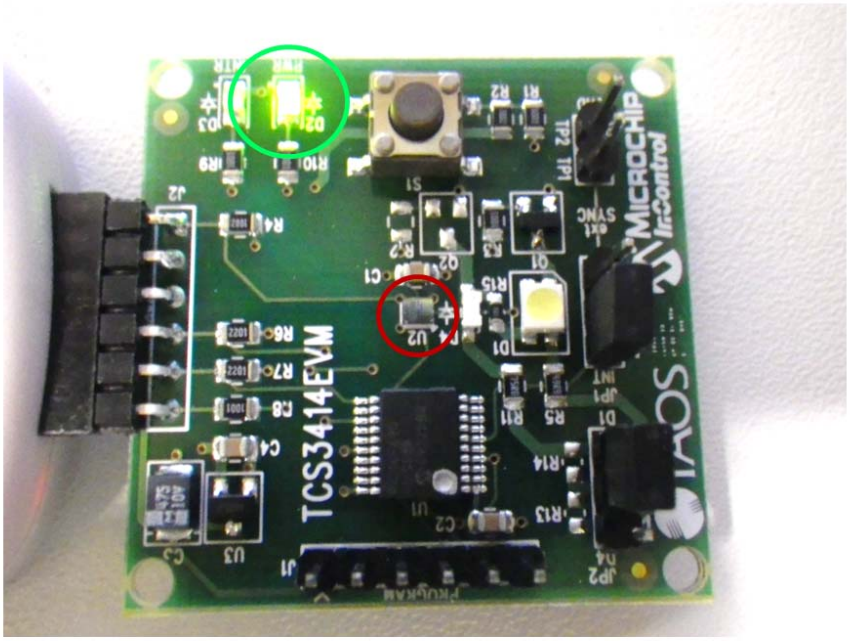

Figure 4-11 - Location of the green power LED (green circle) on the TCS3414EVM evaluation board, relative to the RGB-PD (red circle).

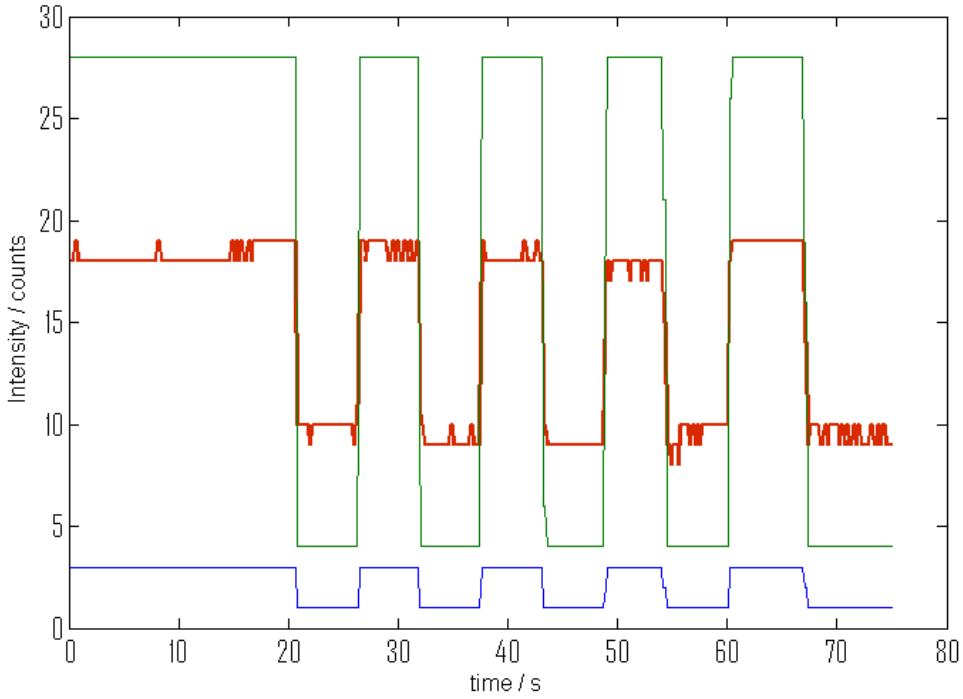

Figure 4-12 - Interference in the red, green, and blue RGB-PD channels caused by switching the power LED on and off. At this integration time and gain the signal due to the photometric LEDS would be 55000 counts or more.

4.7.2 Data logging with TCS3414 EVM software

Before titration commences, the TCS3414 EVM software must also be set to log RGB-PD data to a text file. Failure to do so will go undetected by the LabVIEW software, which simply reads the end of the previous text file. This may not be noticed until the titration data is processed. LabVIEW is also set to record all data in such a way (every file with a unique time and date stamp) that neglecting to provide a new directory to write to will store multiple titrations in the same directory. This would be simple to rectify, modifying the LabVIEW program to check for unchanging photodiode data and existing files.

4.7.3 Stray light from

A stainless steel lid excludes ambient light from the experimental setup. The lid is removed for inspection once titration starts to ensure movement of both syringe pumps. Failure to ensure it is closed properly can result in ambient light leakage to the photodiode.

4.7.4 Addressing reliability and quality issues

The above issues were largely addressed by way of a checklist, which the operator is required to run through when starting a titration. This also addressed mundane issues such as failure to empty the waste bag.

RGB-PD titration system start-up checklist
Reagents and sample
Sample bag connected to inlet
Bubbles purged from sample fluidic line
Sample fluidic fittings tight
Sufficient titrant in reservoir
Titrant aspiration tube submerged
RGB-PD set up
LED power adjusted to give ≈ 90% of saturation
Previous data logging file copied and saved under appropriate filename
Start data logging
Water bath and waste check
Check water bath temperature

Empty waste bag if needed
LabVIEW control setup
Set up folder for experimental data, and copy location to LabVIEW code
Start the titration program
Check data is being recorded in the experimental data folder
Start the titration routine
Ensure the syringes are moving, and no fluid leaking.
Close water bath lid, visually inspect to ensure the seal is good

Table 4-6 – Operators checklist when performing TA analysis with the RGB-PD microfluidic TMT instrument.

Removal of the power LED would remove this vector of failure. Concerned that the evaluation board could be damaged in the process, I opted not to perform this modification. Other, more accessible LEDs in the light sensitive parts of the system were covered with black tape, and with care this could also be applied to the power LED. Modification of the LabVIEW code to look for static photodiode data would prevent failure to initiate RGB-PD data logging. It is more likely in future embodiments of the system that the functionality to control the RGB-PD directly from LabVIEW would be implemented instead.

4.7.5 Individual component failure

Individual component failure was a significant problem encountered during operation of the RGB-PD TA system, mainly because in comparison to human errors these issues were harder to prevent. It was common for communication error to cause the RGB-PD control program to suffer a fatal error and shut down, terminating the logging of data with no ability to restart if communication was restored. Though no specific data was kept of this occurrence, 11 of the 94 data log files stored from TA determination had suffered this fault (≈ 12%). The true figure is likely to be higher, as if the fault was noticed early on in experimentation, the data log file would simply be overwritten with the new data. The origin of this is unknown, but was reproduced by gentle distortion of the connection between the RGB-PD evaluation board and the supplied USB/serial converter. As this is a detachable connection, permanently soldering the two components together would create a more rigid connection. It is not known however whether this is the definite cause of the failure. This fault became apparent before the

system was run fully autonomously, where occurrence of the fault would be noticed immediately. Attaching the PD board and the serial converter to a plastic backing created rigidity in the connection and appeared to reduce the occurrence of the fault. Once the system was fully automated and housed in the water bath, only 2 of the 33 experimental runs performed experienced failure due to the RGB-PD communication issue (6%). This affected 1 of the 6 experimental runs used to produce Figure 4-8 and Figure 4-9. Directly controlling the RGB-PD via its I^2C interface, or direct communication via LabVIEW to the evaluation board is a better long term approach.

4.7.6 Syringe pumps

The use of syringe pumps and syringes caused significant problems for titration, often becoming stuck when the system was restarted. Invariably this occurred at the titrant syringe, which also experienced significant corrosion by the seawater / HCl titrant mixture (Figure 4-13). Whether the corrosion itself caused the failure is not known, however it would be prudent to replace the syringe before this is experienced. Checking the integrity of the PTFE plunger integrity around once every week would allow the problem to be noticed before it resulted in failed titration runs. The head of the syringe showed significant corrosion, indicating that liquid had entered the barrel. This is concerning, as it can contaminate the titrant, and may leak onto sensitive equipment. Contamination of the titrant would be cumulative over time, and complicate long term operation of the system in a remote environment. Occasionally the titration would finish, and one of the syringe pumps would appear out of phase with the other (i.e. one full, one empty, where they should both be empty). This potentially means that one syringe has stuck part way through the titration and injection has occurred with just one syringe. If the syringe starts moving again there is a chance that it may, for example, begin pumping liquid from the chip back to the titrant reservoir contaminating all further titrations. In the worst case the syringe pump may fail again, go back into phase, and the error go entirely un-noticed. Where this happened, both the recent titration data and the titrant itself would be discarded. To some extent this was mitigated by checking for syringe movement at the start of the titration run, as once moving the syringes would rarely fail from that point on. This therefore became a checklist item. Frustratingly this requirement means that even if an auto sampler is added to the system, titrations cannot be easily run remotely. The syringe pumps cannot give feedback on their state to the controlling program. Fitting magnets to the syringe pusher, and position sensors (Hall effect sensors) along the throw of the syringe would enable this. LabVIEW is able to

monitor this type of device to detect any syringe errors. The system could stop and alert the operator, thus securing the integrity of the titrant reservoir.

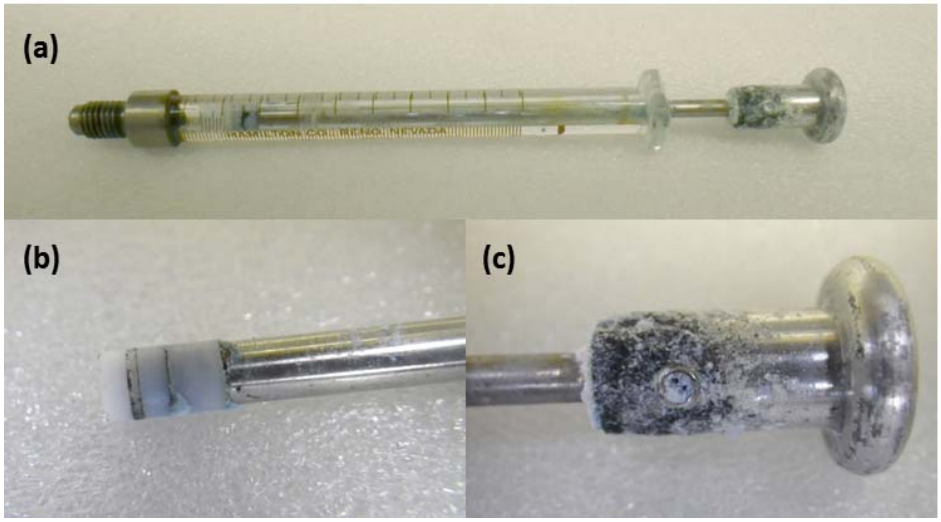

Figure 4-13 - Corrosion of the titrant syringe (a), around the PTFE tip of the plunger (b) and head (c).

Thermistor failure has already been discussed in Section 4.6.1. Uncertainty analysis showed temperature measurement error was one of the less important contributions to TA measurement uncertainty (Section 3.5), in agreement with the findings of Martz who identified that temperature effects only began to significantly affect precision at 0.05 °C. Some temperature problems were also encountered in using the water bath. The original plan was for TA measurement at 25 °C, however with ambient temperatures in the laboratory higher than expected this was increased to 27 °C. If this had been anticipated a chiller unit could have been employed allowing operation at standard temperature.

Documenting the common modes of failure encountered during TA determination with the microfluidic RGB-PD system allows improvements in the design for a second generation device. Removing the human error factor would significantly improve reliability and performance. Improved LabVIEW code, photodiode interfacing, reduction of stray light sources and better sample handling would also help. Introducing a single dark current measurement (RGB-PD response in the absence of the light source) would help mitigate power LED and ambient light issues. This will require electronic control of the LEDs, or a shutter being introduced into the optical line to isolate the detector from the light source.

Removal of the need for a water bath would be useful. Examination of operation at ambient temperature, as is performed for pH, is an interesting solution to that needs further investigation [71]. The temperature dependence of seawater equilibrium constant must be known for the range of ambient temperatures for this approach to succeed. Electronic temperature control such as a Peltier device or heating resistor would make for a more portable system in place of a water bath [145].

The continued use of the syringe pumps needs careful consideration, given their reliability and limited feedback for control purposes. Some of these issues are peculiar to the model used, and the convenience and versatility of using syringe pumps mean that they are likely to be employed in future microfluidic titration devices. In the TA determination performed, the flow rate based measurement was superior to the TMT based measurement. If flow rate methods are pursued instead of TMT, considerable convenience would be lost by abandoning syringe based pumping.

4.8 Conclusions from Chapter 4

Previous chapters identified the need for measurements of the oceanic carbonate system, and specifically of the carbonate parameter total alkalinity (TA). An extremely small and cheap alternative detector for spectrophotometry (RGB-PD) exhibited excellent potential for measurement of TA as discussed in Chapter 3. Chapter 4 demonstrated how measurement of TA has been achieved with the RGB-PD in a first generation auto analysis instrument. The RGB-PD detector was combined with microfluidic technologies to produce a novel TA analyser capable of precision between 10 and 50 μmol kg^{-1} over the range of oceanic seawater alkalinities, depending on the analysis method used. The analysis methods differed in their mode of acid quantification, the first using tracer monitored titration (TMT), the second using syringe pump flow rates.

The device works by mixing of a seawater sample (in this case an artificial alkalinity standard) in varying ratios with a premixed indicator/acid titrant to perform a titration. Using microfluidics complicates mixing, as the flow in microfluidic systems is invariably laminar. Flow injection analysis with a turbulent regime would improve this, but increases size and reagent/sample consumption. Complete mixing was calculated to take ≈ 4 minutes in the microfluidic flow cell by diffusion alone, which places a time constraint on how fast the titration can be progressed.

Video analysis of the visible flow within microfluidic channels guided the development of the most effective titration technique. This included fast flushing of the chip at 1800 µl min^{-1} to purge the previous sample, followed by slow injection of the next sample and titrant plug. After flushing and mixing, spectrophotometry with the RGB-PD collects photometric data of BCG. Of the two acid quantification methods used, the flow rate method gave results with better accuracy (-14 to –28 µmol kg^{-1}) and precision TA standard deviations of ± 8-19 µmol kg^{-1}. Absolute values of precision for the TMT method were similar, but degraded by compression of the total alkalinity dynamic range. This means effective precisions for TMT-determined TA are made worse. Shortcomings in the system design cannot be ruled out for their role in preventing accurate acid quantification, resulting in the poor performance of TMT analysis. Common modes of instrument failure highlight the importance of avoiding human error when designing future versions of the instrument, which was a significant problem despite the fact that the titration for each sample was run autonomously. The use of syringe pumps gave a useful alternative method for quantifying acid, however they were also responsible for several failures of the system, and their continued use requires scrutiny.

This device is the first device to incorporate either an RGB-PD, or microfluidic technology for analysis of seawater total alkalinity. The analysis was fully automated once a sample had been loaded. The results are encouraging (≈ 1 %RSD precision for the flow rate method), and the proof of concept of the use of these technologies in this application is a significant step towards provision of small, affordable, rugged, and automated instruments for monitoring the oceanic inorganic carbon system.

4.9 Declaration for Chapter 4

I performed the entirety of the experimental and theoretical work described in chapter 4. There are however several instances where I must acknowledge the efforts, assistance, and work of others.

The microfluidic chip described in Section 4.3.1 is the culmination of a significant research effort by many workers at the Centre for Marine Microsystems. Their contributions are best described in the publications regarding the development of fabrication techniques and their use in the production of oceanographic wet chemical analysers [71, 108, 133, 135]. Though not directly involved in the development, I had some involvement in work that guided the design of these microfluidics. My early work under the direction of Dr Cedric Floquet involved the use of clear substrate microfluidic chips. We identified the effect stray light had on photometry, which provided part of the impetus for the use of tinted substrates in microfluidic chip manufacture. It was at my request that a microfluidic flow cell able to accept SMA optical fibres for photometry was developed, and this was later incorporated into the pH system. I specified the design of the microfluidic chip used here – a modification of the existing pH system developed by Victoire Rerolle, with no serpentine mixer. The pH system's waterproof valve protection cap was retained.

I adapted the heavily modified LabVIEW code used to control the prototype TA system from a core program developed for the pH system by Victoire Rerolle, which itself evolved from considerable contributions by other members of the research group. The specific functionality I introduced was:

- The ability to control two syringe pumps with simultaneous start over two COM ports
- The incrementing of titrant injections relative to sample as the titration progressed.
- The ability to flush with blank between titration injections
- Timing the syringes and actuating valves for consistent injection.
- The reading of the RGB-PD data file for spectrophotometric measurement, and writing this to text files for ease of input into MATLAB.
- The writing of log files and state files to assist troubleshooting.

Valves and thermistors were controlled via an electronic interface developed in-house by Mr Andy Harris.

The specific NLLS routine used to analyse titration data was adapted from that described by Martz (2005) [26], and was supplied to us by Prof Michael DeGrandpre in the form of a Microsoft excel file with visual basic routine. With help from Dr Edward Waugh, this was converted for use in MATLAB. This formed part of the analysis routine used for models and experimental data.

Chapter 5

Conclusion and future work

5.1 Conclusion

The overall aim of this project was to improve automated seawater total alkalinity (TA) determination for the examination of ocean acidification (Section 1.6). with the work presented here addressed this by examining new technologies to improve instrumentation rather than by development of a new analytical method, as it was hypothesised that recent technological advances would facilitate the achievement of the overall aim. The two main technologies examined are microfluidics for fabrication of the analyser, and a readily available optical detector capable of measurement at multiple wavelengths (a red green and blue photodiode (RGB-PD)).

5.1.1 Literature review (Chapter 2)

The majority of the aims and objectives outlined for Chapter 2 in Section 1.6.1 were addressed. Scientific literature relevant to TA determination was examined to identify key innovations and successes in TA determination and address the aims and objectives outline for Chapter 2. Comprehensive guidelines exist for the measurement of TA by acid/base titration [48], and current methods are able to achieve the required quality of TA measurements (Figure 2-2).

The availability of instruments to make TA measurements is limited in comparison to other carbonate variables however [55, 70, 78, 79]. The key area in which innovation is required for seawater TA determination is therefore development of instrumentation rather than improvement of the quality of analytical techniques. This is because there is

a need to resolve long-term changes in carbonate chemistry, and it is important that researchers have instruments that can be deployed beyond the laboratory, and for long periods of time. It was decided to focus on this therefore, and research into the possibility of improving existing techniques was limited. Several workers have begun to address this [29, 85], and more advanced systems are approaching maturity [84].

The most suitable TA analysis methods for development were identified as those based on spectrophotometry rather than potentiometry (Section 2.3.2). Titration methods which involve purging with an inert gas were rejected as this would limit deployment opportunities of a future instrument, and for this reason open cell titration (Section 1.5.3) and single step titration (Section 2.3.1) were deemed unsuitable for development. In hindsight, this decision to reject the single step method is not necessarily justified. An alternative to the inert gas purge is the use of gas exchange between liquids across a membrane. Although this increases complexity in instrument design, this approach would address many of the issues encountered in the microfluidic system developed here (Chapter 4) such as indicator carryover between samples and long analysis times.

The tracer monitored titration (TMT) method developed by Martz was selected as the most suitable method for further development [26, 29, 84]. This technique removes the need for quantification of titrant and sample masses or volumes, and has been demonstrated for measurement of seawater certified reference materials. Here bromocresol green (BCG) indicator is used to measure both pH and the amount of acid added for each step in titration. This has the opportunity to greatly simplify the apparatus required for titration, but do so by placing additional burden on the spectrophotometric apparatus.

A target specification for a new automated TA instrument was compiled, based on the required precision for ocean acidification measurements (1 – 2 μmol kg^{-1}), and the assumption that this first generation device will be a bench top instrument. The components and techniques used are to be chosen such that future development of the instrument for remote deployment or in situ deployment is possible.

5.1.2 Spectrophotometric detection system (Chapter 3)

The overall aim of chapter 3 was to identify the most suitable components for spectrophotometric measurement of TA 1.6.2. The use of the TMT technique places

additional requirements on the spectrophotometric system, as this is also used for acid quantification. The precision of absorbance measurements for this technique must be ± 0.0005 Abs or better. In the original method this prevented the use of a conventional spectrophotometer. Opportunities for size and cost reductions presented by modern technologies were examined. This was partly to promote uptake of the technology by researchers (See aims in 1.6.1) and improve the feasibility of future in situ deployment (Section 2.5). Technologies considered include microfluidics and modern optoelectronic such as photodiodes [114].

Measurement of pH using bromocresol green is necessary for TMT, and the objectives for chapter 3 specified that measurement of pH with the selected optical detection system should be performed. To measure pH from BCG, the light absorption at two wavelengths is measured. These wavelengths corresponded to colour sensitive channels in a red green and blue photodiode (RGB-PD TCS3414CS, ams AG). This type of device has previously been used for high quality analytical photometry, yet no study has yet examined using the individual colour channels in an assay which requires discrimination of more than one colour [126, 127]. As such it is a new type of detector for both TA and pH measurement, satisfying an objective specified in Section 1.6.2. The RGB-PD in the role of detector for pH measurement was found to agree with a commercial spectrophotometer to within 0.01 pH between pH = 3.0 and 5.0. The precision was ±0.007 pH, and the device is 400-1000 times cheaper than the spectrophotometer, costing <$10 compared to the several thousand dollar price of a modular CCD spectrophotometer. The RGB-PD device is significantly smaller than the spectrophotometer (0.01 cm^2 footprint compared to 150 cm^2, and less than 2 mm in height, compared to 4.5 cm). Discrepancies were observed in BCG species concentration determination, and hence also pH measurement with the device, when compared to a spectrophotometer. This can potentially affect the ability of the device to perform total alkalinity measurements by TMT. Measured variability associated with RGB-PD absorbance measurements was determined to be 0.00080 Abs and 0.00066 Abs for the RGB-PD red and blue channels respectively, close to the 0.0005 Abs required for the TMT method.

Uncertainty analysis was used to examine the theoretical performance of the RGB-PD for TA determination by TMT. A titration model was used to propagate random and systematic errors associated with TMT measurement by the RGB-PD. Uncertainty in TA

measurements was comparable to those calculated in the original TMT study [26]. Uncertainty introduced by systematic errors associated with measurements and parameters ranged from 8 - 20 μmol kg^{-1} for individual titration points across the range of pHs measured during titration. The pH region with lowest uncertainty in TA was between pH = 3.8 – 5.2. Predicted precision by analysis of random errors in temperature and photometry were identified as being 3 μmol kg^{-1} or less, but would rise proportionally with increased photodiode measurement errors. This falls just short of the ± 1 – 2 μmol kg^{-1} precision target specification identified from the literature review (Table 2-4), and is due to RGB-PD based sensor performance falling short of the required 0.0005 Abs. It is noted in Section 3.3.2 that the true variability in experimental measurements will be greater than the calculated uncertainty. The cost and size advantages of the RGB-PD were used to justify further experimentation, in addition to the fact that the shortfall in performance was small. It was also noted that exploration of these type devices had not been performed, and the predicted performance was still better (0.2 %RSD for the predicted performance vs ≤ 1.0 %RSD for those referenced) than for other recent natural water alkalinity measurement techniques[60, 61, 85]. The use of an RGB-PD for this purpose had also not been reported in the literature. In hindsight it would have been better to choose a more suitable detector for validation of the microfluidic titration system examined in Chapter 4. The aims and objectives for Chapter 3 (Section 1.6.2) were completely addressed through the work undertaken.

5.1.3 Microfluidic TMT analysis system incorporating the RGB-PD detector (Chapter 4)

The overall aim of Chapter 4 was to design and build an analysis system capable of measuring total alkalinity, meeting the target specifications outlined in Table 2-4 at the end of Chapter 2. The intended microfluidic design was implemented, based on a spectrophotometric pH system developed by Victoire Rerolle [71]. The microfluidic device is manufactured from (poly)methyl-methacrylate which has good impermeability against diffusion of CO_2 gas [136], important for the closed cell titration system required in the design specification. Fluid was pumped by precision syringe pumps, and the instrument run automatically from a PC once a sample was introduced. Power consumption for the bench top instrument was 1.310 kW.

The system used static diffusive mixing which took 4 minutes per titration point, with 31 titration points forming a single titration. This resulted in an analysis time per sample of

at least 2.5 hours due to the diffusive mixing. This was tolerated in this experiment as titration performance, not sample through-put, was being examined. This falls short of the 20 minute sample processing time identified in the target specification, but is sufficient to be able to resolve tidal variability in TA.

The analysis method was optimised as intended. Video analysis of the flow profile through the microfluidic chip was used to optimise the titration cycle. Slow flow rates (<270 µl min-1) were favoured for injection, while fast flow rates (1800 µl min^{-1}) were used for flushing.

Artificial alkalinity samples ($NaHCO_3$ in a 0.7 mol kg^{-1} NaCl background) with TA = 2000, 2100, 2200, 2300, 2400, and 2500 µmol kg^{-1}, were analysed with the RGB-PD system with 5 replicates of each sample. Certified reference materials (CRMs) and real seawater samples were not analysed as intended due to a lack of time. Alkalinities determined by TMT had precisions between ±9 - 29 µmol kg^{-1} (± 1 - 2% RSD). The system gave a linear response (R^2 = 0.9476), but compressed the dynamic range of the alkalinities to 40% of that the sample set. This gives a corrected precision of up to ± 112 µmol kg^{-1}. When flow rates were used in place of TMT for acid quantification the linearity (R^2 = 0.9997), precision (±8 – 19 µmol kg^{-1}), and accuracy (-14 to – 28 µmol kg^{-1}) improved. The problem with TMT performance can be attributed to acid titrant quantification problems. These arise due to the accuracy of RGB-PD determination of BCG species concentrations, and interference caused by previous coloured sample remaining in the dead volumes of the microfluidic chip. A summary of how well the instrument satisfied the design specifications outlined in Table 2-4 is given below in Table 5-1.

Specification	**Target performance**	**Achieved performance**
Deployment environment	Capable of underway measurement onboard ship.	Shore based laboratory only
Size	60cm x 60cm x 60cm for a bench top instrument	Achieved, though electronics were separated from fluidics in case of spillage.
Power consumption	3 kW (assuming mains power available)	1.310 kW
Endurance	Up to 1 month	At least 13 days

pH Measurement method	Spectrophotometry	Spectrophotometry (with RGB-PD)
Precision of TA measurement	σ = 1 - 2 µmol kg^{-1} , or better than 0.1 %RSD over the range of oceanic TA	8 – 19 µmol kg^{-1} using flow rates 25-112 µmol kg^{-1} using TMT (corrected for compression effect)
TA Measurement range	2000 – 2500 µmol kg^{-1}	2000 – 2500 µmol kg^{-1}
Open / closed cell (reaction cell type)	Closed cell	Closed cell
Analysis time per sample	20 minutes	2.5 hours
Amount of sample consumed per analysis	< 100 ml, allowing multiple measurements for 1 litre of collected sample.	40 ml
Amount of titrant consumed per analysis	< 1 ml, allowing 1000 measurements for a 1 litre reservoir	< 3 ml

Table 5-1 – Comparison of target specifications and those achieved in the TA analysis instrument produced

Common modes of failure encountered during experimentation are documented to aid in future design improvements. Human errors can largely be addressed through engineering and procedural controls. The components with which failures were most commonly encountered were the titrant syringe pump, thermistors, and RGB-PD evaluation board.

Overall the performance of the RGB-PD in the role of detector for TA determination is encouraging, though the TMT based measurement performance was very poor. In attempting to produce a fully functional analysis instrument within the time available, the experiments performed could not fully characterise the microfluidic architecture for TA titration, or the RGB-PD for TMT analysis, as these individual contributions cannot be separated. Further work is therefore necessary to determine whether these approaches should be pursued.

5.2 Opportunities for future work

Chapter 4 outlines further experiments which can be performed to further evaluate the RGB-PD. The experiments performed proved the concept of using the RGB-PD for TA measurement, however performance fell short of predictions from uncertainty analysis.

5.2.1 Improvements to flushing

The most likely cause was interference caused by remnants of previous sample and titrant mixtures. These can exist in corners of the micro fluidic chip which are poorly flushed between titration points It therefore makes sense to first examine whether modifications can improve this situation, and deliver better quality titration. The simplest approach is to increase the flushing efficiency between titration points. Ten 1 ml flushes completely removes the previous titration mixture, as shown by the full flushes performed at the end of a titration cycle. It is important to note that there is a minimum 30-second pause after each 1 ml injection for the end of cycle flush, which allows diffusion of previous coloured sample from dead volumes within the chip. More than 10 ml may be required to achieve the same flushing efficiency in a single injection, and it is estimated that the time taken per analysis could rise to at least 5 hours. An additional reference measurement between each titration point is achievable with this method, and allows improved rejection of drift in the light source and detector during titration. Drift was not examined in the experiments performed. If increased flushing proves impractical, the design can be reverted to the chamber method described by Martz to fully assess the potential of the RGB-PD [26]. This would completely remove the effect of dead volumes within microfluidic channels, but would require considerable time and effort.

Isolation of the effects of sample carryover and mixing in the microfluidic chamber from the spectral discrepancies introduced by the RGB-PD is necessary to determine the cause of poor performance of TMT determinations. With complete assessment of the RGB-PD performance as outlined above, refinement of the microfluidic design can reduce the dead volume space within the chip. The video analysis used in chapter 4 (see attached CD-ROM) gave insight into the two dimensional flow profiles and mixing characteristics of the chip. Extending this to three dimensions using laser techniques or flow simulations can influence future microfluidic designs to reduce dead volume and improve mixing and flushing.

5.2.2 Improvements to system design

Several improvements for system design to cope with experimental issues are suggested in Section 4.7. Direct interfacing with the RGB-PD is recommended to address the issues encountered when using the evaluation board. These included communication issues, and failures originating from human errors in the operation of the evaluation board as many data acquisition operations had to be initiated manually for each sample run. Reducing operator workload through software and engineering improvements is necessary for remote operation and reduces the influence of human error.

Reducing individual component failure is important for long term deployments. A new method of temperature measurement is needed as thermistor based measurements failed. This meant no temperature logging was performed during titration, which is important for correction of equilibrium constants in TA determination.

5.2.3 Syringe pumps

The syringe pumps used occasionally became stuck which would prevent pumping. No method for detecting this was implemented in the experiment, and the syringe pumps used cannot report on their status. As discussed in section 4.7.6, if the syringe pump begins moving again out of phase with the titration cycle, it may contaminate the reagent by aspirating sample from the chip and pumping this to the titrant reservoir. A Hall effect sensor is a magnetic field detector that could be used to monitor the behaviour of the pumps. By mounting a small magnet on the syringe pump's pushing arm, and a hall effect sensor at either end of the pump's throw, LabVIEW could be programmed to check for syringe movement and stop the experiment if the syringe stalls.

5.2.4 Improvements to photometry

Improved flushing may not improve the linearity of the RGB-PD response, nor the dynamic range compression encountered when this was used for TMT (Section 4.6.2). The titration model used to fit experimental data in the non-linear least squares (NLLS) takes no account of the spectral response of the RGB-PD. Based on the simulations of RGB-PD performed, the NLLS model can be modified to account for this. As can be seen from Figure 3-11, a large difference exists between the simulated titration curve, and the curve predicted from RGB-PD spectral data. A spectrophotometer coupled in parallel with the RGB-PD would have provided a means of assessing this effect. Although

spectrophotometer measurements were made in parallel with the RGB-PD in the pH work described in Chapter 3, poor light throughput prevented the method being repeated. Adding additional components in the fibre optic line such as an extra bifurcated fibre reduced the photodiode reference signal to below acceptable levels, even with the LED light sources at maximum output. This could be improved with brighter LEDs, shorter optical fibre runs, improved coupling, and a shorter flow cell path length.

5.2.5 Analysis of real seawater samples

Artificial alkalinity standards were useful for characterising the system and improving performance, but do not represent the true complexity of the seawater matrix. Analysis of certified reference materials (CRMs, e.g. the certified alkalinity seawater samples supplied by A. Dickson, Scripps Institution of Oceanography), and true seawater samples is important therefore in further examination of system performance. Using the Technology Readiness Levels (TRLs) outlined in Table 2-1, the TA analysis system described here is at level 3 – 4. Further work should aim to increase readiness to level 5 - 6 (demonstration of a prototype in a relevant environment). Comparison with an established total alkalinity measurement instrument such as Apollo or VINDTA is a practical way to determine the TA system's performance. [49, 50] Removal of the water bath and working at *in situ* or ambient temperature is possible with better temperature characterisation of the indicator and accurate temperature measurement. Temperature and salinity dependent constants for seawater acid/base species are well reported, though accuracy is debated [15, 24, 146, 147].

5.2.6 Sample consumption and analysis time

The required sample volume per analysis was comparable to existing systems at about 30 ml, largely due to flushing requirements of the particular microfluidic design. The current analysis time per sample is significant however, at 2.5 hours with the microfluidic system described, compared to ≈ 15 minutes for commercial alkalinity systems. For the purpose of demonstrating the use of the RGB-PD, sample processing time was not important, and for infrequent measurement in an *in situ* instrument the time achieved is not unreasonable [84]. This is fast enough to resolve tidal effects, which have a frequency of 12 hours. Laboratory based systems would likely require faster processing. The simplest approach is multiplexing, where several systems are run in parallel. This would require multiple sets of optical components, which adds little cost but increases complexity. Microfluidics are perfect candidates for this type of instrument

as they lend themselves to mass production, or could be engineered to accommodate multiple flow cell systems on a single chip. Pumping would more of an issue, as the syringe pumps are by far the most expensive part of the system (>£1000 per unit). By moving the sample syringe to the waste end and drawing sample through the system, two syringe pumps can drive a large number of flow cells. By this method the sample syringe need not be flushed when sample is changed.

5.2.7 Improvement to titration routine

The titration routine was designed so that the same series of flow rate ratios would be suitable for measurement of samples between 2000 and 2500 μmol kg^{-1}. Consequently some of the titration points recorded are outside the working range of the indicator. Active analysis of data collected as the titration progresses could guide the choice of subsequent flow rates. The titration is then terminated once sufficient data has been recorded. This requires modification of the LabVIEW routine for continual evaluation of collected data, but allows for faster analysis. Section 4.6.2 suggests that an increased number of titration points may improve results. This is particularly true in instances where the least squares regression rejected the majority of data points. Performing analysis at the time of titration, the system could determine whether the titration was successful and whether repeats of individual titration points are necessary.

5.2.8 Titrant and indicator characterisation

Characterisation of bromocresol green in this instance was limited to molar extinction coefficients (ϵ) and estimation of pKa_2. Impurities in BCG were suggested as a possible cause of offsets in pH measurement (Section 3.4.8), and could affect TA determination. Obtaining high purity bromocresol green indicator for future analyses would be advantageous. Currently the highest purity offered in the online catalogue of Sigma Aldrich is ≥ 95%. Further purification by high performance liquid chromatography (HPLC) could be performed or outsourced. Methods exist to purify other indicators by this method[104, 148], and flash chromatography [149]. Verification of the titrant acidity would also be useful in improving the uncertainty associated with measurements.

5.2.9 Single step titrations

Single step titrations using the excess acid method were ruled out at an early stage due to the requirement of purging with an inert gas, or the inclusion of a membrane (Section 2.3.1). This was deemed unsuitable for future deployment in situ (inert gas) or would

result in too complex a design for the microfluidics (membrane). Strategies exist to incorporate membranes into microfluidic devices [150, 151]. This would require fewer titration steps which would improve analysis time, and would reduce the issue of sample carry over in dead volumes as multiple titration steps need not be performed. This is ideal for the microfluidic approach and it is recommended that this method is considered for future microfluidic TA analysers.

5.2.10 Final remarks

It is clear that significant opportunity exists for further examination of total alkalinity measurement with RGB-PDs. In the event that RGB-PDs are deemed unsuitable in this role, substantial improvements in the cost and size of instrumentation may still be achieved with other optical systems. Microfluidic technologies have great potential in facilitating further improvements in terms of cost and size. In the near term, continuation of this work is planned to improve instrument design and make quality total alkalinity measurements at sea.

References

1. Solomon, S., D. Qin, M. Manning, Z. Chen, M. Marquis, K.B. Averyt, M. Tignor, and H.L. Miller, *Climate Change 2007: The Physical Science Basis: Contribution of Working Group I to the Fourth Assessment Report of the Intergovernmental Panel on Climate Change.* New York: Cambridge Univ. Press, 2007.
2. Tans, P. and R. Keeling, *Mauna Loa monthly mean CO2 data*, N.E.S.I.o. Oceanography, Editor 2013.
3. Schmittner, A., A. Oschlies, H.D. Matthews, and E.D. Galbraith, *Future changes in climate, ocean circulation, ecosystems, and biogeochemical cycling simulated for a business-as-usual CO2 emission scenario until year 4000 AD.* GLOBAL BIOGEOCHEMICAL CYCLES,, 2008. **22**(GB1013, doi:10.1029/2007GB002953.).
4. Solomon, S., G.-K. Plattner, R. Knutti, and P. Friedlingstein, *Irreversible climate change due to carbon dioxide emissions.* PNAS, 2009. **106**(6): p. 1704-1709.
5. Sabine, C.L., R.A. Feely, N. Gruber, R.M. Key, K. Lee, J.L. Bullister, R. Wanninkhof, C.S. Wong, D.W.R. Wallace, B. Tilbrook, F.J. Millero, T.-H. Peng, A. Kozyr, T. Ono, and A.F. Rios, *The Oceanic Sink for Anthropogenic CO2*, 2004. p. 367-371.
6. Doney, S.C., V.J. Fabry, R.A. Feely, and J.A. Kleypas, *Ocean Acidification: The Other CO2 Problem.* Annual Review of Marine Science, 2009. **1**: p. 169-192.
7. Hofmann, M. and H.J. Schellnhuber, *Ocean acidification: a millennial challenge.* Energy & Environmental Science, 2010. **3**(12): p. 1883-1896.
8. Tyrrell, T., B. Schneider, and A. Charalampopoulou, *Coccolithophores and calcite saturation state in the Baltic and Black Seas.* Biogeosciences, 2008. **5**(2): p. 485-494.
9. Iglesias-Rodriguez, M.D., P.R. Halloran, R.E.M. Rickaby, I.R. Hall, E. Colmenero-Hidalgo, J.R. Gittins, D.R.H. Green, T. Tyrrell, S.J. Gibbs, P. von Dassow, E. Rehm, E.V. Armbrust, and K.P. Boessenkool, *Phytoplankton Calcification in a High-CO2 World*, 2008. p. 336-340.
10. Wood, H.L., J.I. Spicer, and S. Widdicombe, *Ocean acidification may increase calcification rates, but at a cost.* Proc. R. Soc. B, 2008. **275**: p. 1767-1733.
11. Ridgwell, A., D.N. Schmidt, C. Turley, C. Brownlee, M.T. Maldonado, P. Tortell, and J.R. Young, *From laboratory manipulations to Earth system models: scaling calcification impacts of ocean acidification.* Biogeosciences, 2009. **6**: p. 2611–2623.
12. Byrne, R.H., M.D. DeGrandpre, R.T. Short, T.R. Martz, L. Merliva, C. McNeil, F.L. Sayles, R. Bell, and P. Fietzek, *Sensors and systems for in situ observations of marine carbon dioxide system variables.* OceanObs '09, 2009.
13. Ellison, S.L.R. and A. Williams (Eds), *Eurachem/CITAC guide: Quantifying Uncertainty in Analytical Measurement*. Third ed2012.
14. Tebbutt, P., *Basic Mathematics for Chemists*. Second ed1998: John Wiley and Sons.
15. Zeebe, R.E. and D. Wolf-Gladrow, *CO2 in seawater: Equilibrium, kinetics, isotopes.* Elsevier Oceanography Series, 2001: p. 1-346.

16. Weiss, R.F., *Carbon dioxide in water and seawater: the solubility of a non-ideal gas.* Marine Chemistry, 1974. **2**(3): p. 203-215.
17. Mehrbach, C., C.H. Culberson, J.E. Hawley, and R.M. Pytkowicz, *Measurement of the Apparent Dissociation Constants of Carbonic Acid in Seawater at Atmospheric Pressure.* Limnology and Oceanography, 1973. **18**(6): p. 897-907.
18. Stumm, W. and J.J. Morgan, *Aquatic chemistry : an introduction emphasizing chemical equilibria in natural waters.* New York, NY : Wiley-Interscience, 1970.
19. Dickson, A.G., J.D. Afghan, and G.C. Anderson, *Reference materials for oceanic CO_2 analysis: a method for the certification of total alkalinity.* Marine Chemistry, 2003. **80**(2-3): p. 185-197.
20. Millero, F.J., R.H. Byrne, R. Wanninkhof, R. Feely, T. Clayton, P. Murphy, and M.F. Lamb, *The internal consistency of CO2 measurements in the equatorial Pacific.* Marine Chemistry, 1993. **44**(2-4): p. 269-280.
21. Millero, F.J., *Thermodynamics of the carbon dioxide system in the oceans.* Geochimica et Cosmochimica Acta, 1995. **59**(4): p. 661-677.
22. Wang, Z.A., X. Liu, R.H. Byrne, R. Wanninkhof, R.E. Bernstein, E.A. Kaltenbacher, and J. Patten, *Simultaneous spectrophotometric flow-through measurements of pH, carbon dioxide fugacity, and total inorganic carbon in seawater.* Analytica Chimica Acta, 2007. **596**(1): p. 23-36.
23. Sayles, F.L. and C. Eck, *An autonomous instrument for time series analysis of TCO2 from oceanographic moorings.* Deep Sea Research Part I: Oceanographic Research Papers, 2009. **56**(9): p. 1590-1603.
24. Rérolle, V.M.C., C.F.A. Floquet, M.C. Mowlem, D.P. Connelly, E.P. Achterberg, and R.R.G.J. Bellerby, *Seawater-pH measurements for ocean-acidification observations.* TrAC Trends in Analytical Chemistry, 2012. **40**(0): p. 146-157.
25. Dickson, A.G. and J.P. Riley, *The effect of analytical error on the evaluation of the components of the aquatic carbon-dioxide system.* Marine Chemistry, 1978. **6**(1): p. 77-85.
26. Martz, T.R., *A tracer monitored titration for seawater total alkalinity*, 2005, University of Montana, USA.
27. SCOR Working Group 75, W.H., U.S.A., *Methodology for oceanic CO, measurements.* UNESCO technical papers in marine science 65, 1992.
28. Yao, W. and R.H. Byrne, *Simplified seawater alkalinity analysis: Use of linear array spectrometers.* Deep Sea Research Part I: Oceanographic Research Papers, 1998. **45**(8): p. 1383-1392.
29. Martz, T.R., A.G. Dickson, and M.D. DeGrandpre, *Tracer monitored titrations: measurement of total alkalinity.* Analytical Chemistry, 2006. **78**(6): p. 1817-1826.
30. KIMOTO, H., H. KAYANNE, S. KUDO, K. NOZAKI, A. NEGISHI, and K. KATO, *A High Time-Resolution Analyzer for Total Alkalinity of Seawater, Based on Continuous Potentiometric Measurement.* Anal. Sci.(suppl.), 2001. **17**.
31. Taberham, A., *A deep sea lab on a chip chemical sensor*, in *School of Electronics and Computer Science*2010, University of Southampton.
32. Bates, N.R., A.F. Michaels, and A.H. Knap, *Seasonal and interannual variability of oceanic carbon dioxide species at the U.S. JGOFS Bermuda Atlantic Time-series Study (BATS) site.* Deep Sea Research Part II: Topical Studies in Oceanography, 1996. **43**(2-3): p. 347-383.
33. Libes, S., *Introduction to marine biogeochemistry*2009: Elsevier.
34. Gattuso, J.P., M. Frankignoulle, I. Bourge, S. Romaine, and R.W. Buddemeier, *Effect of calcium carbonate saturation of seawater on coral calcification.* Global and Planetary Change, 1998. **18**(1-2): p. 37-46.

35. Riebesell, U., V.J. Fabry, L. Hansson, and J.P.G. (Eds.), *Guide to best practices for ocean acidification research and data reporting.* Luxembourg: Publications Office of the European Union, 2010: p. 260 p.
36. Nondal, G., R.G.J. Bellerby, A. Olsen, T. Johannessen, and J. Olafsson, *Optimal evaluation of the surface ocean CO2 system in the northern North Atlantic using data from voluntary observing ships.* Limnol. Oceanogr.: Methods, 2009. **7**: p. 109–118.
37. Muller, F.L.L. and B. Bleie, *Estimating the organic acid contribution to coastal seawater alkalinity by potentiometric titrations in a closed cell.* Analytica Chimica Acta, 2008. **619**(2): p. 183-191.
38. Bradshaw, A.L. and P.G. Brewer, *High precision measurements of alkalinity and total carbon dioxide in seawater by potentiometric titration -- 1. Presence of unknown protolyte(s)?* Marine Chemistry, 1988. **23**(1-2): p. 69-86.
39. Dickson, A.G., *pH scales and proton-transfer reactions in saline media such as sea water.* Geochimica et Cosmochimica Acta, 1984. **48**(11): p. 2299-2308.
40. Dickson, A.G., *The measurement of sea water pH.* Marine Chemistry, 1993. **44**(2–4): p. 131-142.
41. Hansson, I., *A new set of pH-scales and standard buffers for sea water.* Deep Sea Research and Oceanographic Abstracts, 1973. **20**(5): p. 479-491.
42. Bates, R.G. and C.H. Culberson, *Hydrogen ions and the thermodynamic state of marine systems. In: N.R. Anderson and A. Malahoff, Editors.* The fate of fossil fuel CO2 in the oceans, Plenum Press, 1977: p. 45–61.
43. Dickson, A.G., *pH buffers for sea water media based on the total hydrogen ion concentration scale.* Deep Sea Research Part I: Oceanographic Research Papers, 1993. **40**(1): p. 107-118.
44. Gran, G., *Determination of the Equivalence Point in Potentiometric Titrations. Part II.* Analyst, 1952. **77**: p. 661-671.
45. Dyrssen, D., *A Gran Titration of Sea Water on Board Sagitta.* Acta Chem. Scand., 1965. **19**(5): p. 1265.
46. Hansson, I. and D. Jagner, *Evaluation of the accuracy of gran plots by means of computer calculations : Application to the potentiometric titration of the total alkalinity and carbonate content in sea water.* Analytica Chimica Acta, 1973. **65**(2): p. 363-373.
47. Culberson, C., R.M. Pytkowics, and J.E. Hawley, *Seawater Alkalinity Determination by the pH Method.* J. Mar. Res., 1970. **28**: p. 15-21.
48. Dickson, A.G., C.L. Sabine, and J.R. Christian, *Guide to best practices for ocean CO2 measurements.* PICES Special Publication, 2007. **3**: p. 176pp.
49. *Marianda marina analytics and data VINDTA system.* http://www.marianda.com.
50. *Apollo SciTech Inc.* http://www.apolloscitech.com/titrator1.htm.
51. Watson, A.J., C. Robinson, J.E. Robinson, P.J. le B. Williams, and M.J.R. Fasham, *Spatial variability in the sink for atmospheric carbon dioxide in the North Atlantic.* Nature, 1991. **350**(6313): p. 50-53.
52. Key, R.M., A. Kozyr, C.L. Sabine, K. Lee, R. Wanninkhof, J.L. Bullister, R.A. Feely, F.J. Millero, C. Mordy, and T.H. Peng, *A global ocean carbon climatology: Results from Global Data Analysis Project (GLODAP).* Global Biogeochem. Cycles, 2004. **18**(4): p. GB4031.
53. Watanabe, A., H. Kayanne, K. Nozaki, K. Kato, A. Negishi, S. Kudo, H. Kimoto, M. Tsuda, and A.G. Dickson, *A rapid, precise potentiometric determination of total alkalinity in seawater by a newly developed flow-through analyzer designed for coastal regions.* Marine Chemistry, 2004. **85**(1-2): p. 75-87.

54. Roche, M.P. and F.J. Millero, *Measurement of total alkalinity of surface waters using a continuous flowing spectrophotometric technique.* Marine Chemistry, 1998. **60**(1-2): p. 85-94.
55. Cullison Gray, S.E., M.D. DeGrandpre, T.S. Moore, T.R. Martz, G.E. Friederich, and K.S. Johnson, *Applications of in situ pH measurements for inorganic carbon calculations.* Marine Chemistry, 2011. **125**(1–4): p. 82-90.
56. Pavlova, G., P. Tishchenko, T. Volkova, A. Dickson, and K. Wallmann, *Intercalibration of Bruevich's method to determine the total alkalinity in seawater.* Oceanology, 2008. **48**(3): p. 438-443.
57. *Metrohm AG.* http://www.metrohm.com/.
58. *SI Analytics titration systems.* http://www.si-analytics.com/.
59. Sarazin, G., G. Michard, and F. Prevot, *A rapid and accurate spectroscopic method for alkalinity measurements in sea water samples.* Water Research, 1999. **33**(1): p. 290-294.
60. Mesquita, R.B.R., A. Rangel, oacute, and O.S.S. nio, *A Sequential Injection System for the Spectrophotometric Determination of Calcium, Magnesium and Alkalinity in Water Samples.* Analytical Sciences, 2004. **20**(8): p. 1205-1210.
61. Fletcher, P.J. and J.F. van Staden, *Determination of carbonate and hydrogencarbonate by titration using sequential injection analysis.* Analytica Chimica Acta, 2003. **485**(2): p. 187-194.
62. Seiter, J.C. and M.D. DeGrandpre, *Redundant chemical sensors for calibration-impossible applications.* Talanta, 2001. **54**(1): p. 99-106.
63. Robert-Baldo, G.L., M.J. Morris, and R.H. Byrne, *Spectrophotometric determination of seawater pH using phenol red.* Analytical Chemistry, 1985. **57**(13): p. 2564-2567.
64. King, D.W. and D.R. Kester, *Determination of seawater pH from 1.5 to 8.5 using colorimetric indicators.* Marine Chemistry, 1989. **26**(1): p. 5-20.
65. Clayton, T.D. and R.H. Byrne, *Spectrophotometric seawater pH measurements: total hydrogen ion concentration scale calibration of m-cresol purple and at-sea results.* Deep Sea Research Part I: Oceanographic Research Papers, 1993. **40**(10): p. 2115-2129.
66. Bellerby, R.G.J., A. Olsen, T. Johannessen, and P. Croot, *A high precision spectrophotometric method for on-line shipboard seawater pH measurements: the automated marine pH sensor (AMpS).* Talanta, 2002. **56**(1): p. 61-69.
67. Bellerby, R.G.J., D.R. Turner, G.E. Millward, and P.J. Worsfold, *Shipboard flow injection determination of sea water pH with spectrophotometric detection.* Analytica Chimica Acta, 1995. **309**(1–3): p. 259-270.
68. Mosley, L.M., S.L.G. Husheer, and K.A. Hunter, *Spectrophotometric pH measurement in estuaries using thymol blue and m-cresol purple.* Marine Chemistry, 2004. **91**(1–4): p. 175-186.
69. Ohline, S.M., M.R. Reid, S.L.G. Husheer, K.I. Currie, and K.A. Hunter, *Spectrophotometric determination of pH in seawater off Taiaroa Head, Otago, New Zealand: Full-spectrum modelling and prediction of pCO_2 levels.* Marine Chemistry, 2007. **107**(2): p. 143-155.
70. Tapp, M., K. Hunter, K. Currie, and B. Mackaskill, *Apparatus for continuous-flow underway spectrophotometric measurement of surface water pH.* Marine Chemistry, 2000. **72**(2-4): p. 193-202.
71. Rérolle, V.M.C., C.F.A. Floquet, A.J.K. Harris, M.C. Mowlem, R.R.G.J. Bellerby, and E.P. Achterberg, *Development of a colorimetric microfluidic pH sensor for autonomous seawater measurements.* Analytica Chimica Acta, 2013. **786**(0): p. 124-131.

72. Byrne, R.H. and J.A. Breland, *High precision multiwavelength pH determinations in seawater using cresol red.* Deep Sea Research Part A. Oceanographic Research Papers, 1989. **36**(5): p. 803-810.
73. Okamura, K., H. Kimoto, and T. Kimoto, *Open-cell Titration of Seawater for Alkalinity Measurements by Colorimetry Using Bromophenol Blue Combined with a Non-linear Least-squares Method.* Analytical Sciences. **26**(6): p. 709-713.
74. Liu, X., R.H. Byrne, M. Lindemuth, R.A. Easley, and M.C. Patsavas, *A rapid automated procedure for laboratory and shipboard spectrophotometric measurements of seawater alkalinity: continuously monitored single-step acid additions*, in *Fall Meeting, AGU* 2012: San Francisco, Calif., 3-7 Dec.
75. Breland, J.A. and R.H. Byrne, *Spectrophotometric Procedures for Determination of Sea-Water Alkalinity Using Bromocresol Green.* Deep-Sea Research Part I-Oceanographic Research Papers, 1993. **40**(3): p. 629-641.
76. Byrne, R.H., G. Robert-Baldo, S.W. Thompson, and C.T.A. Chen, *Seawater pH measurements: an at-sea comparison of spectrophotometric and potentiometric methods.* Deep Sea Research Part A. Oceanographic Research Papers, 1988. **35**(8): p. 1405-1410.
77. Anderson, L. and M. Wedborg, *Comparison of potentiometric and photometric titration methods for determination of alkalinity and total carbonate in seawater.* . OCEANOL. ACTA., 1985. **8**(4): p. 479-483.
78. Cullison Gray, S.E., M.D. DeGrandpre, T.S. Moore, T.R. Martz, G.E. Friederich, and K.S. Johnson, *Applications of in situ pH measurements for inorganic carbon calculations.* Marine Chemistry. **In Press, Corrected Proof**.
79. Friis, K., A. Körtzinger, and D.W.R. Wallace, *Spectrophotometric pH measurement in the ocean: Requirements, design, and testing of an autonomous charge-coupled device detector system.* Limnol. Oceanogr.: Methods, 2004. **2**: p. 126–136.
80. Prien, R.D., *The future of chemical in situ sensors.* Marine Chemistry, 2007. **107**(3): p. 422-432.
81. Boulart, C., D.P. Connelly, and M.C. Mowlem, *Sensors and technologies for in situ dissolved methane measurements and their evaluation using Technology Readiness Levels.* TrAC Trends in Analytical Chemistry. **29**(2): p. 186-195.
82. *Technology Readiness Levels (TRLs).* http://www.aof.mod.uk/aofcontent/tactical/techman/content/trl_applying.htm
83. Liu, X., Z.A. Wang, R.H. Byrne, E.A. Kaltenbacher, and R.E. Bernstein, *Spectrophotometric Measurements of pH in-Situ: Laboratory and Field Evaluations of Instrumental Performance.* Environmental Science & Technology, 2006. **40**(16): p. 5036-5044.
84. Spaulding, R.S. and M.D. DeGrandpre, *SAMI-alk, an autonomous in-situ sensor for total alkalinity measurements*, in *ASLO aquatic sciences meeting* 2013, Association for the Sciences of Limnology and Oceanography: New Orleans, USA.
85. Gray, S.M., P.S. Ellis, M.R. Grace, and I.D. McKelvie, *Underway determination of alkalinity in estuarine waters by reagent-injection gas-diffusion flow analysis.* Talanta, 2008. **77**(2): p. 533-540.
86. Dumousseaud, C., E.P. Achterberg, T. Tyrrell, A. Charalampopoulou, U. Schuster, M. Hartman, and D.J. Hydes, *Contrasting effects of temperature and winter mixing on the seasonal and inter-annual variability of the carbonate system in the Northeast Atlantic Ocean.* Biogeosciences, 2010. **7**(5): p. 1481-1492.
87. Millero, F.J., J.-Z. Zhang, K. Lee, and D.M. Campbell, *Titration alkalinity of seawater.* Marine Chemistry, 1993. **44**(2-4): p. 153-165.

88. *Carbon Dioxide Information Analysis Center.* http://cdiac.ornl.gov/ - Metadata for CLIVAR A16S cruise, R/V Ronald H. Brown.
89. Bradshaw, A.L., P.G. Brewer, D.K. Shafer, and R.T. Williams, *Measurements of total carbon dioxide and alkalinity by potentiometric titration in the GEOSECS program.* Earth and Planetary Science Letters, 1981. **55**(1): p. 99-115.
90. Dickson, A.G., *An exact definition of total alkalinity and a procedure for the estimation of alkalinity and total inorganic carbon from titration data.* Deep Sea Research Part A. Oceanographic Research Papers, 1981. **28**(6): p. 609-623.
91. Breland, J.A. and R.H. Byrne, *Determination of Sea-Water Alkalinity by Direct Equilibration with Carbon-Dioxide.* Analytical Chemistry, 1992. **64**(19): p. 2306-2309.
92. Bruevich, S.V., *Determination of Alkalinity in Small Volumes of Seawater Using Direct Filtration.* Manual on Chemical Studies of Seawater, 1944. **(Glavsevmorput', Moscow, 1944) [in Russian]**.
93. Ruzicka, J. and E.H. Hansen, *Flow injection analysis, 2nd Ed.* Wiley, New York, 1988.
94. Martz, T., Y. Takeshita, R. Rolph, and P. Bresnahan, *Tracer Monitored Titrations: Measurement of Dissolved Oxygen.* Analytical Chemistry, 2011. **84**(1): p. 290-296.
95. DeGrandpre, M.D., T.R. Martz, R.D. Hart, D.M. Elison, A. Zhang, and A.G. Bahnson, *Universal Tracer Monitored Titrations.* Analytical Chemistry, 2011. **83**(24): p. 9217-9220.
96. Granéli, A. and T. Anfält, *A simple automatic phototitrator for the determination of total carbonate and total alkalinity of sea water.* Analytica Chimica Acta, 1977. **91**(2): p. 175-180.
97. Hart, R.D., *The Development of An in-Situ Instrument for Measurement of Seawater Alkalinity.* American Chemical Society 64th Northwest Regional Meeting, 2009. **Abstracts**: p. 34.
98. Byrne, R.H. and W. Yao, *Procedures for measurement of carbonate ion concentrations in seawater by direct spectrophotometric observations of Pb(II) complexation.* Marine Chemistry, 2008. **112**(1-2): p. 128-135.
99. Martz, T.R., H.W. Jannasch, and K.S. Johnson, *Determination of carbonate ion concentration and inner sphere carbonate ion pairs in seawater by ultraviolet spectrophotometric titration.* Marine Chemistry, 2009. **115**(3-4): p. 145-154.
100. Freeman, B.D. and I. Pinnau, *Gas and Liquid Separations Using Membranes: An Overview*, in *Advanced Materials for Membrane Separations*2004, American Chemical Society. p. 1-23.
101. Perez, F.F. and F. Fraga, *A precise and rapid analytical procedure for alkalinity determination.* Marine Chemistry, 1987. **21**(2): p. 169-182.
102. Byrne, R.H., E. Kaltenbacher, and X. Liu, *System and method for spectrophotometric measurement of total alkalinity using a liquid core qaveguide.* United States Patent, 2010. **US 7,727,770 B2**.
103. Hopkins, A.E., K.S. Sell, A.L. Soli, and R.H. Byrne, *In-situ spectrophotometric pH measurements: the effect of pressure on thymol blue protonation and absorbance characteristics.* Marine Chemistry, 2000. **71**(1-2): p. 103-109.
104. Yao, W., X. Liu, and R.H. Byrne, *Impurities in indicators used for spectrophotometric seawater pH measurements: Assessment and remedies.* Marine Chemistry, 2007. **107**(2): p. 167-172.
105. Husheer, S.L.G., *On Spectrophotometric pH Measurement in Seawater Media.* MSc Thesis 2001.
106. Chatwal, G.R., *Spectroscopy : (atomic and molecular) Rev. ed.* Ebook, 2009.

107. Mantle, T.J. and D.A. Harris, *"Spectrophotometric assays" in.* Spectrophotometry and Spectrofluorimetry A Practical Approach 2000 (- Edited by Michael G. Gore, Oxford University Press).
108. Floquet, C.F.A., V.J. Sieben, A. Milani, E.P. Joly, I.R.G. Ogilvie, H. Morgan, and M.C. Mowlem, *Nanomolar detection with high sensitivity microfluidic absorption cells manufactured in tinted PMMA for chemical analysis - **Appendix A - Supplementary data***. Talanta, 2011. **84**(1): p. 235-239.
109. Chan, G.C.Y. and W. Chan, *Beer's Law Measurements Using Non-monochromatic Light Sources—A Computer Simulation.* Journal of Chemical Education, 2001. **78**(9): p. 1285.
110. Floquet, C.F.A., V.J. Sieben, A. Milani, E.P. Joly, I.R.G. Ogilvie, H. Morgan, and M.C. Mowlem, *Nanomolar detection with high sensitivity microfluidic absorption cells manufactured in tinted PMMA for chemical analysis.* Talanta. **84**(1): p. 235-239.
111. Poole, R.K. and U. Kalnenieks, *"Introduction to light absorption; visible and ultraviolet spectra" in.* Spectrophotometry and Spectrofluorimetry A Practical Approach 2000(Edited by Michael G. Gore (Oxford University Press, 2000)).
112. O'Toole, M. and D. Diamond, *Absorbance Based Light Emitting Diode Optical Sensors and Sensing Devices.* Sensors, 2008. **8**(4): p. 2453-2479.
113. Dasgupta, P.K., I.-Y. Eom, K.J. Morris, and J. Li, *Light emitting diode-based detectors: Absorbance, fluorescence and spectroelectrochemical measurements in a planar flow-through cell.* Analytica Chimica Acta, 2003. **500**(1-2): p. 337-364.
114. Brennan, D., J. Justice, B. Corbett, T. McCarthy, and P. Galvin, *Emerging optofluidic technologies for point-of-care genetic analysis systems: a review.* Analytical and Bioanalytical Chemistry, 2009. **395**(3): p. 621-636.
115. Lau, K.-T., S. Baldwin, M. O'Toole, R. Shepherd, W.J. Yerazunis, S. Izuo, S. Ueyama, and D. Diamond, *A low-cost optical sensing device based on paired emitter–detector light emitting diodes.* Analytica Chimica Acta, 2006. **557**(1-2): p. 111-116.
116. Koronkiewicz, S. and S. Kalinowski, *A novel direct-injection photometric detector integrated with solenoid pulse-pump flow system.* Talanta, 2011. **86**(0): p. 436-441.
117. Cocovi-Solberg, D.J., M. Miró, V. Cerdà, M. Pokrzywnicka, Ł. Tymecki, and R. Koncki, *Towards the development of a miniaturized fiberless optofluidic biosensor for glucose.* Talanta, 2012. **96**(0): p. 113-120.
118. Orpen, D., S. Beirne, C. Fay, K.T. Lau, B. Corcoran, and D. Diamond, *The optimisation of a paired emitter–detector diode optical pH sensing device.* Sensors and Actuators B: Chemical, 2011. **153**(1): p. 182-187.
119. Tymecki, L., M. Pokrzywnicka, and R. Koncki, *Fluorometric paired emitter detector diode (FPEDD).* Analyst, 2011. **136**(1): p. 73-76.
120. O'Toole, M.O., L. Barron, R. Shepherd, B. Paull, P. Nesterenko, and D. Diamond, *Paired emitter-detector diode detection with dual wavelength monitoring for enhanced sensitivity to transition metals in ion chromatography with post-column reaction.* Analyst, 2009. **134**(1): p. 124-130.
121. Koronkiewicz, S. and S. Kalinowski, *Application of direct-injection detector integrated with the multi-pumping flow system to photometric stop-flow determination of total iron.* Talanta, 2012. **96**: p. 68-74.
122. Tan, A.M., J.L. Huang, J.D. Geng, J.H. Xu, and X.N. Zhao, *A multichannel photometric detector for multicomponent analysis in flow-injection analysis.* Journal of Automatic Chemistry, 1994. **16**(2): p. 71-73.

123. Tan, A. and C. Xiao, *Direct determination of caustic hydroxide by a micro-titration method with dual-wavelength photometric end-point detection.* Analytica Chimica Acta, 1997. **341**(2–3): p. 297-301.
124. Shimazaki, Y., F. Fujioka, and M. Iwatsuki, *A portable colorimeter using light-emitting diodes and photodiodes with fast-Fourier-transformation signal processing.* Field Analytical Chemistry & Technology, 1998. **2**(3): p. 173-178.
125. Nazarenko, A.Y., *Optical Sensors for Manual and Automatic Titration in Undergraduate Laboratory.* Spectroscopy Letters, 2010. **43**(7-8): p. 555-560.
126. da Rocha, Z.M., C.S. Martinez-Cisneros, A.C. Seabra, F. Valdes, M.R. Gongora-Rubio, and J. Alonso-Chamarro, *Compact and autonomous multiwavelength microanalyzer for in-line and in situ colorimetric determinations.* Lab on a Chip, 2012. **12**(1): p. 109-117.
127. Bembnowicz, P. and K. Malecha, *The LTCC based continuous flow optical sensor for absorbance measurements.* 2011 34th International Spring Seminar on Electronics Technology. "New Trends in Micro/Nanotechnology", 2011: p. 587-91.
128. Ghorude, T.N., A.L. Chaudhari, and A.D. Shaligram, *Quantitative color measurement of pH indicator paper using trichromatic LEDs and TCS230 color sensor.* 2008.
129. Yao, L. and Z. Lei. *An automatic determination method based on color sensor at the end point of the titration*. in *Mechanic Automation and Control Engineering (MACE), 2011 Second International Conference on*. 2011.
130. Kragten, J., *Tutorial review. Calculating standard deviations and confidence intervals with a universally applicable spreadsheet technique.* Analyst, 1994. **119**(10): p. 2161-2165.
131. Taylor, J.R., *An Introduction to Error Analysis: The Study of Uncertainties in Physical Measurements*. Second ed1997: University Science Books.
132. Mathworks_Inc., *fzero.* MATLAB product documentation, r2010b.
133. Beaton, A.D., V.J. Sieben, C.F.A. Floquet, E.M. Waugh, S. Abi Kaed Bey, I.R.G. Ogilvie, M.C. Mowlem, and H. Morgan, *An automated microfluidic colourimetric sensor applied in situ to determine nitrite concentration.* Sensors and Actuators B: Chemical, 2011. **156**(2): p. 1009-1014.
134. Kuswandi, B., Nuriman, J. Huskens, and W. Verboom, *Optical sensing systems for microfluidic devices: A review.* Analytica Chimica Acta, 2007. **601**(2): p. 141-155.
135. Ogilvie, I.R.G., V.J. Sieben, C.F.A. Floquet, M.C. Mowlem, and H. Morgan, *Solvent processing of PMMA and COC chips for bonding devices with optical quality surfaces*, in *14th International Conference on Miniaturized Systems for Chemistry and Life Sciences*, S. Verpoorte, et al., Editors. 2010, The Printing House for Chemical and Biological Microsystems Society. p. 1244-1246.
136. Patel, V.M., C.K. Patel, K.C. Patel, and R.D. Patel, *Diffusion of gases in poly(methyl methacrylate).* Die Makromolekulare Chemie, 1972. **158**(1): p. 65-79.
137. Squires, T.M. and S.R. Quake, *Microfluidics: Fluid physics at the nanoliter scale.* Reviews of Modern Physics, 2005. **77**(3): p. 977.
138. Gravesen, P., J. Branebjerg, and O.S. Jensen, *Microfluidics-a review.* Journal of Micromechanics and Microengineering, 1993. **3**(4): p. 168.
139. Ottino, J.M. and S. Wiggins, *Introduction: mixing in microfluidics.* Philosophical Transactions of the Royal Society of London. Series A: Mathematical, Physical and Engineering Sciences, 2004. **362**(1818): p. 923-935.
140. Valko, E., *Measurements of the diffusion of dyestuffs.* Transactions of the Faraday Society, 1935. **31**(0): p. 230-245.
141. Dawson, *Data for Biochemical Research* 1986: Oxford : Clarendon Press.

142. Ogilvie, I.R.G., V.J. Sieben, B. Cortese, M.C. Mowlem, and H. Morgan, *Chemically resistant microfluidic valves from Viton membranes bonded to COC and PMMA.* Lab on a Chip, 2011. **11**(14): p. 2455-2459.
143. Grover, W.H., A.M. Skelley, C.N. Liu, E.T. Lagally, and R.A. Mathies, *Monolithic membrane valves and diaphragm pumps for practical large-scale integration into glass microfluidic devices.* Sensors and Actuators B: Chemical, 2003. **89**(3): p. 315-323.
144. Zhang, C., D. Xing, and Y. Li, *Micropumps, microvalves, and micromixers within PCR microfluidic chips: Advances and trends.* Biotechnology Advances, 2007. **25**(5): p. 483-514.
145. Tsaloglou, M.-N., M.M. Bahi, E.M. Waugh, H. Morgan, and M. Mowlem, *On-chip real-time nucleic acid sequence-based amplification for RNA detection and amplification.* Analytical Methods, 2011. **3**(9): p. 2127-2133.
146. Roy, R.N., L.N. Roy, K.M. Vogel, C. Porter-Moore, T. Pearson, C.E. Good, F.J. Millero, and D.M. Campbell, *The dissociation constants of carbonic acid in seawater at salinities 5 to 45 and temperatures 0 to 45°C.* Marine Chemistry, 1993. **44**(2–4): p. 249-267.
147. Millero, F.J., T.B. Graham, F. Huang, H. Bustos-Serrano, and D. Pierrot, *Dissociation constants of carbonic acid in seawater as a function of salinity and temperature.* Marine Chemistry, 2006. **100**(1–2): p. 80-94.
148. Liu, X., M.C. Patsavas, and R.H. Byrne, *Purification and Characterization of meta-Cresol Purple for Spectrophotometric Seawater pH Measurements.* Environmental Science & Technology, 2011. **45**(11): p. 4862-4868.
149. Patsavas, M.C., R.H. Byrne, and X. Liu, *Purification of meta-cresol purple and cresol red by flash chromatography: Procedures for ensuring accurate spectrophotometric seawater pH measurements.* Marine Chemistry, 2013. **150**(0): p. 19-24.
150. de Jong, J., R.G.H. Lammertink, and M. Wessling, *Membranes and microfluidics: a review.* Lab on a Chip, 2006. **6**(9): p. 1125-1139.
151. Ohira, S.-I. and K. Toda, *Micro gas analyzers for environmental and medical applications.* Analytica Chimica Acta, 2008. **619**(2): p. 143-156.

Appendix 1

MATLAB models

A 1.1 Model to compare pH measurement with an RGB-PD and spectrophotometer

This model predicts pH measurement using the RGB-PD and LEDs based on their spectral properties.

TAOS TCS3414 Optical Model for pH measurement

```
% load all spectra required for the calculation. This includes molar
% extinction coefficients (MECs), the RGB-PD red and blue channels, and the
% combined LED light source. Each is formatted to be an nx1 (or 1xn)
% array. Wavelength scales are separate from data.
clear all
load('spectra_for_pH_simulation.mat');
```

Interpolation

```
% Each spectrum might have a different wavelength scale. Interpolate to
% create a common wavelength dimension for all data. Interp_ prefix
% denotes interpolated data

Interp_wl = 300:0.2:1100; % set up interpolation size
Interp_wl = Interp_wl(:);

% interpolate all spectra
Interp_pd_red = interp1(RGB_PD_wl, RGB_PD_Red, Interp_wl);
Interp_pd_blue = interp1(RGB_PD_wl, RGB_PD_Blue, Interp_wl);
Interp_Combined_LEDs = interp1(LED_wl, Combined_LEDs, Interp_wl);
Interp_MEC_I2 = interp1(MEC_wl, MEC_I2, Interp_wl);
Interp_MEC_HI = interp1(MEC_wl, MEC_HI, Interp_wl);

% convert NaNs to 0 (where interpolation has exceeded data size)
Interp_pd_red(isnan(Interp_pd_red)) = 0;
Interp_pd_blue(isnan(Interp_pd_blue)) = 0;
Interp_Combined_LEDs(isnan(Interp_Combined_LEDs)) = 0;
Interp_MEC_I2(isnan(Interp_MEC_I2)) = 0;
Interp_MEC_HI(isnan(Interp_MEC_HI)) = 0;
```

RGB-PD Molar extinction coefficient experiment simulation

```
% set maximum concentrations for photodiode MEC determination.
% Too large and you will get non-linearity at the higher end.

MaxConcI2 = 2e-5;
MaxConcHI = 5.0e-5;

% assumes pathlength is 1cm. CalibAbs is absorbance for concentrations of
% BCG used in MEC determination. simulation size is number of
% concentrations used

simulation_size=100;

% Multiply MECs by concentrations to obtain absorbance spectra for each
% concentration of HI and I2. Beer Lambert rearrangement.
for j = 1:simulation_size;
PD_MEC_det_AbsI2(:,j)=Interp_MEC_I2.*(MaxConcI2/simulation_size).*(j-1);
PD_MEC_det_AbsHI(:,j)=Interp_MEC_HI.*(MaxConcHI/simulation_size).*(j-1);
end

% we also need arrays of the concentrations themselves.
PD_MEC_det_Conc_I2 = ((1:simulation_size).*(MaxConcI2/simulation_size));
PD_MEC_det_Conc_HI=((1:simulation_size).*(MaxConcHI/simulation_size));

% Determine the spectrum of reference light when LEDs pass through
% RGB-PD filters for red and blue channel. Photodiode will integrate all this light.
% Rearrangement of abs=-log10(I/I0).
PD_MEC_det_I0 = Interp_Combined_LEDs;
PD_MEC_det_PDRed_I0 = PD_MEC_det_I0.*Interp_pd_red;
PD_MEC_det_PDBlue_I0 = PD_MEC_det_I0.*Interp_pd_blue;

% Based on I0, concentrations and beer lambert law,
for k=1:simulation_size,
%calculate incident light for each RGB-PD channel and each concentration.
    PD_MEC_det_I_I2 = PD_MEC_det_I0.*(10.^((PD_MEC_det_AbsI2(:,k))./-1));
    PD_MEC_det_I_HI = PD_MEC_det_I0.*(10.^((PD_MEC_det_AbsHI(:,k))./-1));
%apply filter for RGB-PD channels.
    PD_MEC_det_PDRed_II2 = (PD_MEC_det_I_I2).*Interp_pd_red;
    PD_MEC_det_PDBlue_II2 = (PD_MEC_det_I_I2).*Interp_pd_blue;

    PD_MEC_det_PDRed_IHI = (PD_MEC_det_I_HI).*Interp_pd_red;
    PD_MEC_det_PDBlue_IHI = (PD_MEC_det_I_HI).*Interp_pd_blue;
%calculate absorbance, as interpreted by RGB-PD (integration)
    PD_MEC_det_PDRed_I2Abs(k,1) = -
1.*log10((trapz(PD_MEC_det_PDRed_II2))./(trapz(PD_MEC_det_PDRed_I0)));
    PD_MEC_det_PDBlue_I2Abs(k,1) = -
1.*log10((trapz(PD_MEC_det_PDBlue_II2))./(trapz(PD_MEC_det_PDBlue_I0)));

    PD_MEC_det_PDRed_HIAbs(k,1) = -
1.*log10((trapz(PD_MEC_det_PDRed_IHI))./(trapz(PD_MEC_det_PDRed_I0)));
    PD_MEC_det_PDBlue_HIAbs(k,1) = -
1.*log10((trapz(PD_MEC_det_PDBlue_IHI))./(trapz(PD_MEC_det_PDBlue_I0)));

end

% the data used needed
PD_MEC_det_Conc_I2 = PD_MEC_det_Conc_I2(:);
PD_MEC_det_Conc_HI = PD_MEC_det_Conc_HI(:);
```

Perform linear best fit of the RGB-PD absorbance

```
% Have calculated how the RGB-PD will interpret the absorbance of the
% indicator at various pHs. Now fit straight lines to these absorbances.

% option to limit the upper bounds of linear MEC fit. set to simulation_size
% to consider all data, or choose based on examination of the RGB-PD MEC
% absorbance data
i2rc=60;
hirc=19;
```

```
i2bc=49;
hibc=100;


%perform linear fits using epsilon_FIT function (linear fitting). Output is
%an array of the MECs to be used in pH calculation
   [cf_] = epsilon_FIT(PD_MEC_det_Conc_I2(1:i2rc),PD_MEC_det_PDRed_I2Abs(1:i2rc));
     epsilon_temp = coeffvalues(cf_);
     epsilon(1,:) = epsilon_temp;

   [cf_] = epsilon_FIT(PD_MEC_det_Conc_HI(1:hirc),PD_MEC_det_PDRed_HIAbs(1:hirc));
     epsilon_temp = coeffvalues(cf_);
     epsilon(2,:) = epsilon_temp;

   [cf_] = epsilon_FIT(PD_MEC_det_Conc_I2(1:i2bc),PD_MEC_det_PDBlue_I2Abs(1:i2bc));
     epsilon_temp = coeffvalues(cf_);
     epsilon(3,:) = epsilon_temp;

   [cf_] = epsilon_FIT(PD_MEC_det_Conc_HI(1:hibc),PD_MEC_det_PDBlue_HIAbs(1:hibc));
     epsilon_temp = coeffvalues(cf_);
     epsilon(4,:) = epsilon_temp;
```

RGB-PD pH measurement setup

```
% Specify indicator and pH exerimental parameters

indicator_pKa = 4.479;
Conc_BCG_stock = 1e-6;

%specify pH range and array size
simulation_pH = 3:0.1:5.5;
simulation_pH=simulation_pH';
simulation_size = length(simulation_pH);%simulation size now used for pH array length
simulation_pKi(1:length(simulation_pH),1)=indicator_pKa;
```

Create pH Absorption data for pHs, interpret with RGB-PD

```
% calc BCG species concentrations at each pH
    Conc_HI = Conc_BCG_stock./((10.^(simulation_pH-simulation_pKi))+1);
    Conc_I = Conc_BCG_stock-Conc_HI;

% convert concs to combined absorbance spectra
     for i = 1:(length(Conc_HI)),
        Abs_HI(i,:) = Interp_MEC_HI.*Conc_HI(i,1);
        Abs_I2(i,:) = Interp_MEC_I2.*Conc_I(i,1);
     end
        Abs_Comb = Abs_HI+Abs_I2;
        % assume this is also what a spectrophotometer will measure
        SPECAbs_Comb = Abs_Comb;

    % RGB-PD I0 calculated from LEDs and RGB-PD channel response.
    PDRed_I0 = Interp_Combined_LEDs.*Interp_pd_red;
    PDBlue_I0 = Interp_Combined_LEDs.*Interp_pd_blue;

    % As before, interpret absorbance with the RGB-PD. trapz simulates
    % light integration.
for j = 1:length(Abs_Comb(:,1)),
    temp = Abs_Comb(j,:);
    temp=temp(:);
    Phot_I = Interp_Combined_LEDs.*(10.^((temp)./-1));

    Phot_PDRed_I = (Phot_I).*Interp_pd_red;
    Phot_PDBlue_I = (Phot_I).*Interp_pd_blue;

    % do not need noise added data here
    Phot_PDRed(j,1) = -1.*log10 ( (trapz(Phot_PDRed_I)) ./ (trapz(PDRed_I0)) );
    Phot_PDBlue(j,1) = -1.*log10 ( (trapz(Phot_PDBlue_I)) ./ (trapz(PDBlue_I0)) );
```

```
end

% At this point analogue/digital conversion can be inputted for photodiode
% interpretation.
```

Analyse RGB-PD absorbances

```
% For clarity, extract individual MECs from the array.
E1i = epsilon(1,1);
E2i = epsilon(2,1);
E3i = epsilon(3,1);
E4i = epsilon(4,1);

% Calculate the concentration of I2-
ConcentrationI2 = (( Phot_PDRed - (Phot_PDBlue .* (E2i/E4i) )) / ( E1i - (E3i *
(E2i/E4i) ) ) );

% Calculate the concentration of HI-
ConcentrationHI = (( Phot_PDBlue - (Phot_PDRed .* (E3i/E1i) )) / ( E4i - (E3i *
(E2i/E1i) ) ) );

% Total concentration of I2- and HI
ConcentrationI2andHI = ConcentrationI2 + ConcentrationHI;

indicatorKa=10.^-indicator_pKa;
% Concentration of H+ ions
ConcentrationH = indicatorKa * (ConcentrationHI ./ ConcentrationI2);
% ConcentrationH(isnan(ConcentrationH)) = 1e-8;

PD_Determined_pH = -log10(ConcentrationH);
```

Analyse the absorbances as if with a spectrophotometer

```
% Assume this measurement is perfect - essentially reverse the operation.

% Use the experimental MECs, index of 1576 and 721 correspond to 615nm and
% 444nm, absorbance maxima for indicator.

E1i=Interp_MEC_I2(1576,1);
 E2i=Interp_MEC_HI(1576,1);
 E3i=Interp_MEC_I2(721,1);
 E4i=Interp_MEC_HI(721,1);

 %Extract absorbances at a single wavelength
 Absorbance444nm = SPECAbs_Comb(:,721);
 Absorbance615nm = SPECAbs_Comb(:,1576);

% Calculate the concentration of I2-
ConcentrationI2 = (( Absorbance615nm - (Absorbance444nm .* (E2i/E4i) )) / ( E1i - (E3i *
(E2i/E4i) ) ) );

% Calculate the concentration of HI-
ConcentrationHI = (( Absorbance444nm - (Absorbance615nm .* (E3i/E1i) )) / ( E4i - (E3i *
(E2i/E1i) ) ) );

% Total concentration of I2- and HI
ConcentrationI2andHI = ConcentrationI2 + ConcentrationHI;

% Concentration of H+ ions
ConcentrationH = indicatorKa * (ConcentrationHI ./ ConcentrationI2);

SPEC_Determined_pH = -log10(ConcentrationH);
```

A 1.2 Epsilon_fit function

This performs linear fits for molar extinction determination.

```
function [cf_] = epsilon_FIT(conc,output_temp)

% --- Create fit "fit 1"
ok_ = isfinite(conc) & isfinite(output_temp);
if ~all( ok_ )
    warning( 'GenerateMFile:IgnoringNansAndInfs', ...
        'Ignoring NaNs and Infs in data' );
end
ft_ = fittype('poly1');

% Fit this model using new data
cf_ = fit(conc(ok_),output_temp(ok_),ft_);

end
```

A 1.3 Generic titration model

This model predicts pH change of an artificial alkalinity standard with known TA as acid is added. The experiment used syringe pumps, so flow rates are used in the calculation.

Inputs

```
clear  all;

Acidity = 7e-3; %acidity of titrant

DIC = 2e-3; % estimate of DIC, if unsure set to TA
TA = 2250e-6; % total alkalinity of sample

% non-temperature dependent constants for carbonate, and water ionic product
K1 = 1.4548e-6; K2 = 1.1082e-9; Kw = 6.0632e-014;
pK1 = -log10(K1); pK2 = -log10(K2); pKw = -log10(Kw);
```

simulation

```
flowrate_sample = 50; % flowrate of sample during titration. units not important
flowrate_indicator_LUT = 10:0.1:25; % indicator flowrates (LUT = lookup table)
simulation_size = length(flowrate_indicator_LUT);

% simulate titration
% fzero finds the values of H between set bounds where H_det_fun = 0
% (hydrogen determination function,
for i = 1:simulation_size,
   flowrate_indicator = flowrate_indicator_LUT(i);
    hydrogen = fzero(@(H) H_det_fun(Acidity, flowrate_indicator, flowrate_sample, TA,
DIC, K1, K2, Kw, H), [1e-9, 1e-2]);

    simulation_pH(i,1) = -1 .* log10(hydrogen);
    simulation_HCO3(i,1) = ((DIC.*K1.*hydrogen.*(1-
(flowrate_indicator./(flowrate_indicator+flowrate_sample)))./((hydrogen.^2)+(K1.*hydrog
en)+(K1.*K2)));
    simulation_CO3(i,1) = ((DIC.*K1.*K2.*(1-
(flowrate_indicator./(flowrate_indicator+flowrate_sample)))./((hydrogen.^2)+(K1.*hydrog
en)+(K1.*K2)));
    simulation_D(i,1) = (flowrate_indicator./(flowrate_indicator+flowrate_sample));
    simulation_H(i,1) = hydrogen;
```

```
    simulation_sample_flowrate(i,1) = flowrate_sample;
end
```

A 1.4 H_det_fun Function

The function called by fzero in the titration model, based on equations (3.4) to (3.6).

```
function y = H_det_fun(Acidity, flowrate_indicator, flowrate_sample, TA, CT, K1, K2, Kw,
H)

y = (Acidity.*(flowrate_indicator./(flowrate_indicator+flowrate_sample))) - (TA.*(1-
(flowrate_indicator./(flowrate_indicator+flowrate_sample)))) - H + (Kw./H) +
((CT.*K1.*H.*(1-
(flowrate_indicator./(flowrate_indicator+flowrate_sample)))./((H.^2)+(K1.*H)+(K1.*K2)))
+ ((2.*CT.*K1.*K2.*(1-
(flowrate_indicator./(flowrate_indicator+flowrate_sample)))./((H.^2)+(K1.*H)+(K1.*K2)))
;
end
```

A 1.5 Non-linear least squares (NLLS)

The non-linear least squares function was adapted for MATLAB from the Microsoft Excel and .vba script described in the appendices of Martz's 2005 dissertation [26]. As previously described, Dr Edward Waugh performed the initial translation, and developed the TASearchError function described later. I then adapted this for all future use of the NLLS routine. Photodiode intensities recorded during titration are converted to pH measurements with associated dilution factors. A model is then fitted to these to obtain a first estimate of TA. Outlying points are then rejected, and the fit repeated to determine TA.

```
%% NLLS method for analysis of titration data using tracer monitored titration (TMT)
% Load titration results - I and I0 measurements for red and blue RGB-PD
% channels, and temperature data if recorded using thermistor probe. This
% method is for performing a single titration, but can be easily expanded
% to repeat for several replicates
clear all
load('titration_result_2500.mat')
% Titrant data
Acidity=0.007981;
OriginalDyeConcentration = 80e-6;

% BCG pKi and molar extinction coefficients
pKi=4.5;
E1i = 3.8992e+04;
E2i = 7.79e+02;
E3i = 3.557e+03;
E4i = 1.4531e+04;
```

Setup physical and chemical constants

```
% enter average temperature if not recorded for every point
TC=27;
T=273.15+TC;

S=40; %salinity

%for Temperature dependent pKi
Ki=10.^-pKi;
```

```
KiT = Ki * exp(((3.*1000)./8.3145)*((1./295.14) - (1./T))); %taken from martz 2005
thesis
pKiT = -log10(KiT);

% Temperature dependent carbonate constants K1 and K2, and ionic product of
% water Kw. Taken from Zeebe & Wolf Gladrow.
K1 = exp( 2.83655  - (2307.1266./T) - (1.5529413.*log(T))...
    - ((0.207608410 +  4.0484./T).*(S.^0.5)) + (0.0846834.*S)...
    - (0.00654208.* S.^(3/2)) + log(1 - 0.001005.*S));
K2 = exp(-9.226508 - (3351.6106./T) - (0.2005743.*log(T))...
    - ((0.106901773 + 23.9722./T).*(S.^0.5)) + (0.1130822.*S)...
    - (0.00846934.* S.^(3/2)) + log(1 - 0.001005.*S));
Kw = exp(148.96502 - (13847.26./T) - (23.6521.*(log(T)))...
    + (((118.67./T) - 5.977 + ((1.0495.*log(T)))).*(S.^0.5))...
    - (0.01615.*S));
```

Setup inputs and constraints for NLLS

```
% set DIC (to within 10% of sample)
DIC = 2500e-6;
TA = 2250e-6; %an estimate of TA for preliminary calculations
% set constraints for NLLS. Based on working range of indicator,
% absorbances which can be resolved. Vary R-threshold depending on desired
% precision, experimental quality may limit this.
pHMinimum = 3;
pHMaximum = 5.5;
AbsorbanceMinimum = 0.01;
AbsorbanceMaximum = 0.8;
R_Threshold = 1e-8;


% IsGoodFlag rejects bad datapoints
% If the value is 1 the data is good for use in the Total Alkalinity
% calculation, if it is zero it has been rejected, all data is assumed good
% to start with
IsGoodFlag = ones(length(I_blue), 1);

% Calculate red and blue absorbance. If an absorbance is outside the range,
% it is rejected by modifying isgoodflag
AbsorbanceBlue = -(log10( I_blue / I0_blue));
    for index = 1:length(I_blue)
        if( (AbsorbanceBlue(index) < AbsorbanceMinimum) || (AbsorbanceBlue(index) >
AbsorbanceMaximum) )
            IsGoodFlag(index) = 0;
        end
    end

AbsorbanceRed = -(log10( I_red / I0_red));
    for index = 1:length(I_red)
        if( (AbsorbanceRed(index) < AbsorbanceMinimum) || (AbsorbanceRed(index) >
AbsorbanceMaximum) )
            IsGoodFlag(index) = 0;
        end
    end

    AbsorbanceRatio = AbsorbanceRed ./ AbsorbanceBlue;
```

Perform NLLS on data

```
e2e = E1i ./ E4i;
e3e = E3i ./ E4i;

% Calculate the concentration of I2-
ConcentrationHI = (( AbsorbanceBlue - (AbsorbanceRed .* (E3i/E1i) )) / ( E4i - (E3i *
(E2i/E1i) ) ) );
ConcentrationI2 = (( AbsorbanceRed - (AbsorbanceBlue .* (E2i/E4i) )) / ( E1i - (E3i *
(E2i/E4i) ) ) );

% Total concentration of I2- and HI
ConcentrationI2andHI = ConcentrationI2 + ConcentrationHI;
```

```
% Concentration of Hydrogen ions in moles/kg
ConcentrationH = Ki * (ConcentrationHI ./ ConcentrationI2);

% Concentration of Hydroxide ions in moles/kg
ConcentrationOH = Kw ./ ConcentrationH;

% Dilution factor of dye
DilutionFactorOfDye = ConcentrationI2andHI ./ OriginalDyeConcentration;

% Calculate HCO3 Concentration
ConcentrationHCO3 = DIC .* (1 - DilutionFactorOfDye) .* K1 .* ConcentrationH
./((ConcentrationH .^2) + (K1 .* ConcentrationH) + (K1 .* K2));
% Calculate CO3 Concentration
ConcentrationCO3 = DIC .* (1 - DilutionFactorOfDye) .* K1 .* K2 ./((ConcentrationH .^2)
+ (K1 .* ConcentrationH) + (K1 .* K2));

% Calculate Denominator
Denominator = e2e - (AbsorbanceRatio .* e3e);
% Calculate pH
pH = -log10(ConcentrationH);
    for index = 1:length(pH)
        if( (pH(index) < pHMinimum) || (pH(index) > pHMaximum) )
            IsGoodFlag(index) = 0;
        end
    end

Error = ( (Acidity .* DilutionFactorOfDye) - (TA .* (1 - DilutionFactorOfDye)) -
ConcentrationH ...
        - ConcentrationHI + ConcentrationOH + ConcentrationHCO3 + (2 .*
ConcentrationCO3));
R_Square = Error.^2;

% Calculate sum of squares
SumOfSquares=0;
for index = 1 : length(Error)
   if IsGoodFlag(index) == 1
       SumOfSquares = SumOfSquares + (Error(index))^2;
   end
end

% specify starting value for TA
StartingValForTA = 0.0025;

% we also need to input a value of TA, just use the same.
TA=StartingValForTA;

% Perform first minimisation.
% TolFun is the tolerance on the result, our result is a small value so
% this needs to be very small
OptOptions = optimset('TolFun', 1E-30);

[TA, fval] = fminsearch(@(TA) TASearchError(Acidity, DilutionFactorOfDye,...
    TA, ConcentrationH,  ConcentrationHI, ConcentrationOH, ConcentrationHCO3,...
    ConcentrationCO3, IsGoodFlag), StartingValForTA, OptOptions);


for index = 1 : length(Error)
   if IsGoodFlag(index) == 1
       SumOfSquares = SumOfSquares + (Error(index))^2;
   end
end

% Perform the second minimisation

[TA, fval] = fminsearch(@(TA) TASearchError(Acidity, DilutionFactorOfDye,...
    TA, ConcentrationH,  ConcentrationHI, ConcentrationOH, ConcentrationHCO3,...
    ConcentrationCO3, IsGoodFlag), StartingValForTA, OptOptions);

Determined_TA = TA;
Number_titration_points_used=sum(IsGoodFlag);
```

A 1.6 TASearchError Function

```
function SumOfSquares = TASearchError(Acidity, DilutionFactorOfDye, TA, ConcentrationH,
ConcentrationHI, ConcentrationOH, ConcentrationHCO3, ConcentrationCO3, IsGoodFlag);

Error = ( (Acidity .* DilutionFactorOfDye) - (TA .* (1 - DilutionFactorOfDye)) -
ConcentrationH ...
        - ConcentrationHI + ConcentrationOH + ConcentrationHCO3 + (2 .*
ConcentrationCO3));

SumOfSquares=0;
for index = 1 : length(Error)
   if IsGoodFlag(index) == 1
       SumOfSquares = SumOfSquares + (Error(index))^2;
   end
end
```

A 1.7 Random error model for total alkalinity titration using the RGB-PD

```
%% Simulating a seawater titration with RGB-PD detection and random errors
% Combines titration simulation with RGB-PD used for spectrophotometric
% detection.
% simulates each titration point to generate the values for
% variables which will be required by the calculation.
% Then apply random errors in temperature and photometric intensity to each
% titration point.
% TA evaluated with NLLS as if it were experimental data. This requires
% photodiode intensities for each titration point. NLLS performed 100
% times, mean and std of determined TA gives result and precision.

clear all
% Create 100 repeats, gives each titration point 100 variations due to
% error
for run=1:1:100;
```

Setup temperature error.

```
% Set temperature
TC=25;
TK=273.15+TC;
S=40;

% choose acidity of titrant, set TA and DIC of sample (in unsure, set DIC
% to = TA)
Acidity=0.008;
TA = 2500e-6;
DIC = 2500e-6;

% choose syringe pump flowrate range. This uses 30 different ratios, too
% many will cause calculations to be very slow.
flowrate_sample = 55;
flowrate_titrant_initial = 25;

% set simulation size. I set this up so that titration is finished when
% flowrates are equal
simulation_size = flowrate_sample-flowrate_titrant_initial;

% preallocate arrays for speed - more important for larger simulations
simulation_preallocation = 1:simulation_size;
simulation_preallocation = simulation_preallocation(:);
simulation_pH = simulation_preallocation;
simulation_HCO3 = simulation_preallocation;
simulation_CO3 = simulation_preallocation;
```

```
simulation_D = simulation_preallocation;
simulation_H = simulation_preallocation;

% Temperature fluctuations will affect the actual composition of pH etc.
% Salinity will not. Temperature fluctuation needs to be brought in as an
% error here rather than later in the measurement.

% create unstable temperature for titration
T_err = 0.1; % this is the +/- of waterbath, or ability to measure T
% Randn gives normally distributed random numbers. here mean = TK, std =
% T_err
T = TK + T_err.*randn(1,simulation_size);

% T dependent carbonate K1 K2 and water Kw from Zeebe + Wolf-Gladrow
K1star = exp( 2.83655  - (2307.1266./T) - (1.5529413.*log(T))...
    - ((0.207608410 +  4.0484./T).*(S.^0.5)) + (0.0846834.*S)...
    - (0.00654208.* S.^(3/2)) + log(1 - 0.001005.*S));
K2star = exp(-9.226508 - (3351.6106./T) - (0.2005743.*log(T))...
    - ((0.106901773 + 23.9722./T).*(S.^0.5)) + (0.1130822.*S)...
    - (0.00846934.* S.^(3/2)) + log(1 - 0.001005.*S));
KWstar = exp(148.96502 - (13847.26./T) - (23.6521.*(log(T)))...
    + (((118.67./T) - 5.977 + ((1.0495.*log(T)))).*(S.^0.5))...
    - (0.01615.*S));
```

Simulate titration

```
% modified titration simulation

    for i = 1:simulation_size,
        % increase flowrate with every iteration. /2 only relevant to the
        % way I programmed (1/2 size titrant syringe, but kept same
        % flowrates from full size)
        flowrate_indicator=(flowrate_titrant_initial-1+i)/2;

        % extract Ks from lookup table
        K1=K1star(1,i); K2=K2star(1,i); Kw=KWstar(1,i);

        % perform fzero on H_det_fun
        hydrogen = fzero(@(H) H_det_fun(Acidity, flowrate_indicator, flowrate_sample,
TA, DIC, K1, K2, Kw, H), [1e-20, 1e-1]);%[1e-9, 1e-2]);

        % Output simulation data
        simulation_pH(i,1) = -1 .* log10(hydrogen);
        simulation_HCO3(i,1) = ((DIC.*K1.*hydrogen.*(1-
(flowrate_indicator./(flowrate_indicator+flowrate_sample)))./((hydrogen.^2)+(K1.*hydrog
en)+(K1.*K2)));
        simulation_CO3(i,1) = ((DIC.*K1.*K2.*(1-
(flowrate_indicator./(flowrate_indicator+flowrate_sample)))./((hydrogen.^2)+(K1.*hydrog
en)+(K1.*K2)));
        % D is silution factor of acid in sample
        simulation_D(i,1) = (flowrate_indicator./(flowrate_indicator+flowrate_sample));
        simulation_H(i,1) = hydrogen;

    end
```

Optics

```
% uses same optical system as pH simulation, so load interpolated values
% for RGB-PD, LED, and MEC with wavelength scale.
load('Interp_optics.mat')
```

T errors for BCG, and BCG concs used

```
% Apply T error to pKa of indicator (pKiT)
pKi=4.479;
Ki=10.^-pKi;
% from Martz 2005 thesis
KiT = Ki * exp(((3.*1000)./8.3145)*((1./295.14) - (1./T)));
pKiT = -log10(KiT);
```

```
concIStock = 100e-6; %Conc BCG in titrant
conc_BCG=concIStock.*simulation_D; % dilute BCG for each titration point

simulation_pKi(1:length(simulation_pH),1)=pKiT; %true pKi for dataset will have the
undetectable T error
```

Create absorption spectra for each titration point

```
% calculate concs of individual BCG species
Conc_HI = conc_BCG./((10.^(simulation_pH-simulation_pKi))+1);
Conc_I2 = conc_BCG-Conc_HI;


% from Concs and MECs calculate absorbance spectra
     for i = 1:(length(Conc_HI)),
        OOAbs_HI(i,:) = Interp_MEC_HI.*Conc_HI(i,1);
        OOAbs_I2(i,:) = Interp_MEC_I2.*Conc_I2(i,1);
     end
        OOAbs_Comb = OOAbs_HI+OOAbs_I2;
    OOAbs_Comb(isnan(OOAbs_Comb))=0;
```

Interpret absorption spectra with LEDs and RGB-PD

```
% Calculate I0 for RGB-PD measurement. Trapz integrates light.
comb_blue = Interp_pd_blue.*Interp_Combined_LEDs;
comb_red = Interp_pd_red.*Interp_Combined_LEDs;
Intensity_Blue_I0 = trapz(Interp_wl,(comb_blue));
Intensity_Red_I0 = trapz(Interp_wl,(comb_red));

% Calculate I for RGB-PD
    for i = 1:simulation_size,
        temp_Abs=OOAbs_Comb(i,:);
        temp_I_fullspec = Interp_Combined_LEDs.'.*10.^(-temp_Abs);

        Intensity_Blue_I(i,1) = trapz(Interp_wl,(Interp_pd_blue.'.*temp_I_fullspec));
        Intensity_Red_I(i,1)= trapz(Interp_wl,(Interp_pd_red.'.*temp_I_fullspec));
        clear temp_*
    end
```

Add RGB-PD noise

```
% blue noise is 1.4765 on 16 bit scale, red is 2.6898, so use this number
% (highest, therefore worst)

% Convert RGB-PD data to 16 bit digital signal scale (not quantized here)
max_int = max([Intensity_Blue_I0, Intensity_Red_I0]);
conv_444 = 65536./max_int;
conv_615 = 65536./max_int;
Intensity_Blue_I0=Intensity_Blue_I0.*conv_444;
Intensity_Red_I0=Intensity_Red_I0.*conv_615;

Intensity_Blue_I=Intensity_Blue_I.*conv_444;
Intensity_Red_I=Intensity_Red_I.*conv_615;
clearvars -except Intensity* run

% apply photodiode error, same method as for T
Phot_err = 2.6898;
    for i = 1:length(Intensity_Blue_I),
        Intensity_Blue_I_errored(i,run)=Intensity_Blue_I(i,1)+Phot_err*randn;
        Intensity_Red_Ierrored(i,run)=Intensity_Red_I(i,1)+Phot_err*randn;
        Intensity_Blue_I0errored(run,1)=Intensity_Blue_I0+Phot_err*randn;
        Intensity_Red_I0errored(run,1)=Intensity_Red_I0+Phot_err*randn;
    end


end % from here send data to NLLS.
```

A 1.8 Calculation of uncertainty in molar extinction coefficients to produce lookup tables.

```
clear all

% Input PD

Load('photodiode_data')

% load 'light source (LEDs)
scan1 = dlmread(light_source.txt', '\t', [17, 0, 2059, 1]);
scan_wl=scan1(:,1);
scan1=scan1(:,2);
scan1=scan1-min(scan1);
scan1=scan1./max(scan1);

Light = scan1;
LED_wl = scan_wl;

Interp_wl = 300:0.2:1100;
Interp_wl = Interp_wl(:);

Interp_pd_red = interp1(Channel_wl, Channel_Red, Interp_wl);
Interp_pd_blue = interp1(Channel_wl, Channel_Blue, Interp_wl);

Interp_Light = interp1(LED_wl, Light, Interp_wl);

Interp_pd_red(isnan(Interp_pd_red)) = 0;
Interp_pd_blue(isnan(Interp_pd_blue)) = 0;
Interp_Light(isnan(Interp_Light)) = 0;
```

Perform MEC calculation for PD

```
load('MECs.mat')

clear wl;

Interp_MEC_I2 = interp1(MEC_wl, MEC_I2, Interp_wl);
Interp_MEC_HI = interp1(MEC_wl, MEC_HI, Interp_wl);
Interp_MEC_I2(isnan(Interp_MEC_I2)) = 0;
Interp_MEC_HI(isnan(Interp_MEC_HI)) = 0;

MaxConcI2 = 5e-5;
MaxConcHI = 5.0e-5;
% MaxConcI2 = 2.5e-5;
% MaxConcHI = 5.75e-5;

for j = 1:1000;
CalibAbsI2(:,j)=Interp_MEC_I2.*(MaxConcI2/1000).*(j-1);
CalibAbsHI(:,j)=Interp_MEC_HI.*(MaxConcHI/1000).*(j-1);
end

Calib_Conc_I2 = ((1:1000).*(MaxConcI2/1000));
Calib_Conc_HI=((1:1000).*(MaxConcHI/1000));

Calib_I0 = Interp_Light;
Calib_PDRed_I0 = Calib_I0.*Interp_pd_red;
Calib_PDBlue_I0 = Calib_I0.*Interp_pd_blue;

for k=1:1000,
    % I=I0 x 10^(A/-1)
    Calib_I_I2 = Calib_I0.*(10.^((CalibAbsI2(:,k))./-1));
    Calib_I_HI = Calib_I0.*(10.^((CalibAbsHI(:,k))./-1));

    Calib_PDRed_II2 = (Calib_I_I2).*Interp_pd_red;
    Calib_PDBlue_II2 = (Calib_I_I2).*Interp_pd_blue;

    Calib_PDRed_IHI = (Calib_I_HI).*Interp_pd_red;
    Calib_PDBlue_IHI = (Calib_I_HI).*Interp_pd_blue;

    Calib_PDRed_I2(k,1) = -1.*log10((trapz(Calib_PDRed_II2))./(trapz(Calib_PDRed_I0)));
```

```
    Calib_PDBlue_I2(k,1)                                =                                -
1.*log10((trapz(Calib_PDBlue_II2))./(trapz(Calib_PDBlue_I0)));

    Calib_PDRed_HI(k,1) = -1.*log10((trapz(Calib_PDRed_IHI))./(trapz(Calib_PDRed_I0)));
    Calib_PDBlue_HI(k,1)                                =                                -
1.*log10((trapz(Calib_PDBlue_IHI))./(trapz(Calib_PDBlue_I0)));

end

Calib_Conc_I2 = Calib_Conc_I2(:);
Calib_Conc_HI = Calib_Conc_HI(:);
```

produce Uc_Abs

```
% can either generate Uc_Eps by linear fitting 3, then 4, then 5 etc, or
% linear fit up to the desired amount, then calculate residual, or base the
% calculation on the linear portion of the graph, and calculate the
% difference between this an the concentration.


i2rc=300;
hirc=300;
i2bc=300;
hibc=300;

%perform linear fits
   [cf_] = epsilon_FIT(Calib_Conc_I2(1:i2rc),Calib_PDRed_I2(1:i2rc));
     epsilon_temp = coeffvalues(cf_);
     epsilon(1,:) = epsilon_temp;

   [cf_] = epsilon_FIT(Calib_Conc_HI(1:hirc),Calib_PDRed_HI(1:hirc));
     epsilon_temp = coeffvalues(cf_);
     epsilon(2,:) = epsilon_temp;

   [cf_] = epsilon_FIT(Calib_Conc_I2(1:i2bc),Calib_PDBlue_I2(1:i2bc));
     epsilon_temp = coeffvalues(cf_);
     epsilon(3,:) = epsilon_temp;

   [cf_] = epsilon_FIT(Calib_Conc_HI(1:hibc),Calib_PDBlue_HI(1:hibc));
     epsilon_temp = coeffvalues(cf_);
     epsilon(4,:) = epsilon_temp;

Sim_E615I2=epsilon(1,1);
Sim_E615HI=epsilon(2,1);
Sim_E444I2=epsilon(3,1);
Sim_E444HI=epsilon(4,1);

% see what this looks like.
E615I2 = Calib_Conc_I2.*Sim_E615I2;
E615HI = Calib_Conc_HI.*Sim_E615HI;
E444I2 = Calib_Conc_I2.*Sim_E444I2;
E444HI = Calib_Conc_HI.*Sim_E444HI;

% check plots... bigest nonlinearity is in 615HI. seems biggest ~UC
figure;
plot(Calib_Conc_I2,Calib_PDRed_I2);hold all;plot(Calib_Conc_I2,E615I2);hold off;
figure;plot(Calib_Conc_I2,Calib_PDBlue_I2);hold all;plot(Calib_Conc_I2,E444I2);hold off;
figure;plot(Calib_Conc_HI,Calib_PDRed_HI);hold all;plot(Calib_Conc_HI,E615HI);hold off;
figure;plot(Calib_Conc_HI,Calib_PDBlue_HI);hold all;plot(Calib_Conc_HI,E444HI);hold off;

UC_E615I2 = E615I2-Calib_PDRed_I2;
UC_E615HI = E615HI-Calib_PDRed_HI;
UC_E444I2 = E444I2-Calib_PDBlue_I2;
UC_E444HI = E444HI-Calib_PDBlue_HI;


clearvars -except UC* Calib_Conc*
save('THE_3_UCEps.mat');
M=cat(2,Calib_Conc_HI,Calib_Conc_I2,UC_E444HI,UC_E444I2,UC_E615HI,UC_E615I2);
dlmwrite('THE_3_UCeps_Out.txt', M, '\t');
```

A 1.9 A comparison of calculation of uncertainty by Kragtens method and the algebraic method

```
%% algebraic method


% define symbolic variables for each of the parameters used

% e_ prefix signified error

syms grams_BCG rmm_BCG grams_H20_dissolve grams_BCG_mother grams_Titrant

syms e_grams_BCG e_rmm_BCG e_grams_H20_dissolve e_grams_BCG_mother e_grams_Titrant


% define the equations for

number_of_mols = grams_BCG ./ rmm_BCG; %number of moles BCG used

concentration_mother = (number_of_mols.*1000)./grams_H20_dissolve; % molality of the
mother solution

concentration_BCG=(concentration_mother.*grams_BCG_mother)./grams_Titrant;


% Define the expression for uncertainty

Uc_concentration_BCG = (sqrt((((diff(m_titrant, grams_BCG))^2)*((e_grams_BCG)^2))...

    + (((diff(m_titrant,  rmm_BCG))^2)*((e_rmm_BCG)^2))...

    + (((diff(m_titrant,  grams_H20_dissolve))^2)*((e_grams_H20_dissolve)^2))...

    + (((diff(m_titrant,  grams_BCG_mother))^2)*((e_grams_BCG_mother)^2))...

    + (((diff(m_titrant,  grams_Titrant))^2)*((e_grams_Titrant)^2))));


% substitute values for symbolic parameters and their errors

grams_BCG = 0.4; rmm_BCG = 689; grams_H20_dissolve = 500;

grams_BCG_mother = 70; grams_Titrant = 1000;


e_grams_BCG = 0.00005; e_rmm_BCG = 0.005;

e_grams_H20_dissolve = 0.005;  e_grams_BCG_mother = 0.00005;

e_grams_Titrant = 0.005;


%substitute these values into the uncertainty equation

Algebraic_Uc = subs(Uc_concentration_BCG);
```

```
%% Kragtens method

% substitute values to determine the absolute value of [BCG]
concentration_BCG_Absolute = subs(concentration_BCG);
save('temp.mat'); %save the workspace so we can recall absolute [BCG] value

% for each parameter...
% Load absolute [BCG] value
load('temp.mat')
% change 1 parameter by its error
grams_BCG=grams_BCG+e_grams_BCG;
%substitute the now errored parameter along with others in [BCG] expression
UC_grams_BCG = (subs(concentration_BCG) - concentration_BCG_Absolute)^2;

% Repeat for each parameter
load('concentration_BCG.mat')
rmm_BCG=rmm_BCG+e_rmm_BCG;
UC_rmm_BCG = (subs(concentration_BCG) - concentration_BCG_Absolute)^2;

load('temp.mat')
grams_H20_dissolve=grams_H20_dissolve+e_grams_H20_dissolve;
UC_grams_H20_dissolve = (subs(concentration_BCG) - concentration_BCG_Absolute)^2;

load('temp.mat')
grams_BCG_mother=grams_BCG_mother+e_grams_BCG_mother;
UC_grams_BCG_mother = (subs(concentration_BCG) - concentration_BCG_Absolute)^2;

load('temp.mat')
grams_Titrant=grams_Titrant+e_grams_Titrant;
UC_grams_Titrant = (subs(concentration_BCG) - concentration_BCG_Absolute)^2;

% Uc [BCG] is the root of individual uncertaintied squared
Kragtens_Uc = (UC_grams_BCG + UC_rmm_BCG ...
    +UC_grams_H20_dissolve + UC_grams_BCG_mother + UC_grams_Titrant).^0.5;
```

A 1.10 Kragtens uncertainty calculation for total alkalinity titration using the RGB-PD

```
%% Uncertainty analysis of systematic errors in titration by Kragtens method
% This is based on analysis performed by Martz 2005 to determine
% uncertainty in TMT measurements. It is adapted for MATLAB using symbolic
% math, though plots are best produced in Excel.
clear all
```

Simulate a titration to obtain pH vs D

```
% Want a linear pH scale in plot, so;
% 1) simulate the titration as with other analyses
% 2) choose the linear pH range
% 3) Interpolate to obtain the required values of dilution D (sometimes
% called simulation_D here) that give these linear pHs
% 4) Perform Kragtens on these points
% Variables carried over are DilutionFactors pH_Scale TC TK S Acidity DIC
load('pH_data_setup');
```

Load interpolated optics data for the RGB-PD system, and MECs

```
load('Interp_optics.mat');
```

Setup symbolic variables and expressions for calculation

```
% The labels 444 and 615 refer to the red and blue channels
syms concIStock E444I2 E444HI E615I2 E615HI I_444 I0_444
syms I_615 I0_615 Ki T S DIC Acidity
syms e_concIStock e_E444I2 e_E444HI e_E615I2 e_E615HI e_I_444 e_I0_444
syms e_I_615 e_I0_615 e_Ki e_T e_S e_DIC e_Acidity

% indicator pKi
TK=T+273.15;
KiT = Ki * exp(((3*1000)/8.3145)*(1/295.14-1/TK));

pKi = -log10(KiT);
pKi=pKi+0.002578*(35-S);
KiT=10.^(-pKi);

% Expressions for absorbance and concentrations
A615=-log10(I_615./I0_615);
A444=-log10(I_444./I0_444);
ConcI2 = (( A615 - (A444 .* (E615HI./E444HI) )) ./ ( E615I2 - (E444I2 .*
(E615HI./E444HI) ) ) );
ConcHI = (( A444 - (A615 .* (E444I2./E615I2) )) ./ ( E444HI - (E444I2 .*
(E615HI./E615I2) ) ) );

Itotal = ConcI2 + ConcHI;
H = (KiT.*ConcHI)./ConcI2;
pH=-log10(H);

D = Itotal./concIStock;

% carbonate and water constants

K1 = exp( 2.83655  - (2307.1266./TK) - (1.5529413.*log(TK))...
    - ((0.207608410 +  4.0484./TK).*(S.^0.5)) + (0.0846834.*S)...
    - (0.00654208.* S.^(3/2)) + log(1 - 0.001005.*S));
K2 = exp(-9.226508 - (3351.6106./TK) - (0.2005743.*log(TK))...
    - ((0.106901773 + 23.9722./TK).*(S.^0.5)) + (0.1130822.*S)...
```

```
    - (0.00846934.* S.^(3/2)) + log(1 - 0.001005.*S));
Kw = exp(148.96502 - (13847.26./TK) - (23.6521.*(log(TK)))...
    + (((118.67./TK) - 5.977 + ((1.0495.*log(TK)))).*(S.^0.5))...
    - (0.01615.*S));

% expressions for carbonate and oh concentrations
HCO3 = ((DIC.*K1.*H.*(1-(D)))./((H.^2)+(K1.*H)+(K1.*K2));
CO3 = ((DIC.*K1.*K2.*(1-(D)))./((H.^2)+(K1.*H)+(K1.*K2));
OH = Kw ./ H;

% exression for TA
TA=(HCO3 + 2.*(CO3) + OH - H - Acidity.*(D)) ./ (1-D);
```

Substitutions into symbolic expressions

```
% those which are constant for every titration point, or represented in
% arrays
load('pH_data_setup');

S=40;
Ki=10.^-4.479;
T=25;
Ki=subs(KiT);

pKi = -log10(Ki);

% Titrant concentration.
concIStock = 100e-6;

simulation_pH=pH_Scale;
simulation_pH=simulation_pH';
simulation_size = length(simulation_pH);
simulation_pKi(1:simulation_size,1)=pKi;


Itotal = concIStock.*DilutionFactors;
Itotal=Itotal';

% expressions for concentration

Conc_HI = Itotal./((10.^(simulation_pH-simulation_pKi))+1);
Conc_I2 = Itotal-Conc_HI;


% Absorbance simulation for photodiode
     for i = 1:(length(Conc_HI)),
        OOAbs_HI(i,:) = Interp_MEC_HI.*Conc_HI(i,1);
        OOAbs_I2(i,:) = Interp_MEC_I2.*Conc_I2(i,1);
     end
        OOAbs_Comb = OOAbs_HI+OOAbs_I2;
OOAbs_Comb(isnan(OOAbs_Comb))=0;


comb_blue = Interp_pd_blue.*Interp_Combined_LEDs;
comb_red = Interp_pd_red.*Interp_Combined_LEDs;
Intensity_444_I0 = trapz(Interp_wl,(comb_blue));
Intensity_615_I0 = trapz(Interp_wl,(comb_red));


for i = 1:simulation_size,
    temp_Abs=OOAbs_Comb(i,:);
    temp_I_fullspec = Interp_Combined_LEDs.'.*10.^(-temp_Abs);

Intensity_444_I(i,1) = trapz(Interp_wl,(Interp_pd_blue.'.*temp_I_fullspec));
Intensity_615_I(i,1)= trapz(Interp_wl,(Interp_pd_red.'.*temp_I_fullspec));
clear temp_*
end
```

Load lookup table for MEC uncertainties

```
% these were calculated separately, see text.
load('THE_3_UCEps.mat');

LookupUC_E444HI=interp1(Calib_Conc_HI,UC_E444HI, Conc_HI);
LookupUC_E615HI=interp1(Calib_Conc_HI,UC_E615HI, Conc_HI);
LookupUC_E444I2=interp1(Calib_Conc_I2,UC_E444I2, Conc_I2);
LookupUC_E615I2=interp1(Calib_Conc_I2,UC_E615I2, Conc_I2);

clear calib* Uc*
```

Calculate intenities for each pH

```
Ki = 10.^(-pKi);
E615I2 = 3.8992e+04;
E615HI = 7.79e+02;
E444I2 = 3.557e+03;
E444HI = 1.4531e+04;

I0_444 = Intensity_444_I0;
I0_615 = Intensity_615_I0;
```

convert to 16 bit size.

```
% no quantisation
conv_444 = 65536./max([I0_444, I0_615]);
conv_615 = 65536./max([I0_444, I0_615]);
I0_444=I0_444.*conv_444;
I0_615=I0_615.*conv_615;

Intensity_444_I=Intensity_444_I.*conv_444;
Intensity_615_I=Intensity_615_I.*conv_615;

I_444 = Intensity_444_I;
I_615 = Intensity_615_I;
```

Substitute values for errors

```
e_concIStock = 1.021e-08;
e_S=0.00108;
e_DIC=DIC.*0.01;% 10% is fine
e_Acidity = 7.981e-06;
e_I_444 = 1; % assumes intensities are close to true value
e_I_615 = 1;
e_I0_444 = 1;
e_I0_615 = 1;
e_Ki=0.01*Ki;
T = 25;
e_T = 0.01;

% reset.mat allows the original values to be reloaded after manipulation
save('reset.mat')
```

calculate uncertainties for every pH

```
% kk cycles through the pHs used
for kk = 1:length(simulation_pH),
    load('reset.mat');
    I_444 = Intensity_444_I(kk);
    I_615 = Intensity_615_I(kk);
    e_E444I2 = LookupUC_E444I2(kk);
    e_E444HI  = LookupUC_E444HI(kk);
    e_E615I2 = LookupUC_E615I2(kk);
    e_E615HI = LookupUC_E615HI(kk);
```

```
 %Perform Kragtens calculations

    TA_Absolute = subs(TA); %create absolute pH
    save('temp.mat'); %save everything
    clearvars -except TA_Absolute concIStock E444I2 E444HI E615I2 E615HI ...
        I_444 I0_444 I_615 I0_615 Ki T S DIC Acidity K1; %clear everything except
unchanging UC variables
    save('TA.mat'); %save unchanging UC variables
    load('temp.mat');

load('TA.mat')
concIStock=concIStock+e_concIStock;
UC_concIStock(kk) = (subs(TA) - TA_Absolute)^2;

load('TA.mat')
E444I2 = E444I2+e_E444I2;
UC_xE444I2(kk) = (subs(TA) - TA_Absolute)^2;

load('TA.mat')
E444HI = E444HI + e_E444HI;
UC_xE444HI(kk) = (subs(TA) - TA_Absolute)^2;

load('TA.mat')
E615I2 = E615I2+e_E615I2;
UC_xE615I2(kk) = (subs(TA) - TA_Absolute)^2;

load('TA.mat')
E615HI = E615HI + e_E615HI;
UC_xE615HI(kk) = (subs(TA) - TA_Absolute)^2;

load('TA.mat')
I_444 = I_444+e_I_444;
UC_I_444(kk) = (subs(TA) - TA_Absolute)^2;

load('TA.mat')
I0_444 = I0_444+e_I0_444;
UC_I0_444(kk) = (subs(TA) - TA_Absolute)^2;

load('TA.mat')
I_615 = I_615+e_I_615;
UC_I_615(kk) = (subs(TA) - TA_Absolute)^2;
test(kk)=(I_615);

load('TA.mat')
I0_615 = I0_615 + e_I0_615;
UC_I0_615(kk) = (subs(TA) - TA_Absolute)^2;

load('TA.mat')
Ki = Ki+e_Ki;
UC_Ki(kk) = (subs(TA) - TA_Absolute)^2;

load('TA.mat')
T = T+e_T;
UC_T(kk) = (subs(TA) - TA_Absolute)^2;

load('TA.mat')
S = S+e_S;
UC_S(kk) = (subs(TA) - TA_Absolute)^2;

load('TA.mat')
DIC = DIC+e_DIC;
UC_DIC(kk) = (subs(TA) - TA_Absolute)^2;

load('TA.mat')
Acidity = Acidity+e_Acidity;
UC_Acidity(kk) = (subs(TA) - TA_Absolute)^2;


end
UC_TA = ( UC_concIStock + UC_xE444I2 + UC_xE444HI + UC_xE615I2 + UC_xE615HI +
UC_I_444...
     +  UC_I0_444 + UC_I_615 + UC_I0_615 + UC_Ki+UC_T+UC_S+UC_DIC+UC_Acidity).^0.5;
```

Appendix 2

Temperature calibration data

A thermistor measurement system designed by Mr Andy Harris was intended for measurement of temperature during TA determination. Unfortunately water ingress into the epoxy resin potted thermistors prevented its use. Temperature measurements with the system were satisfactory in calibration, and if the water ingress issue could be overcome would be suitable for monitoring temperature in a future total alkalinity analysis system. The thermistor measurement system was calibrated in a water bath fitted with a chiller and thermo-regulator for temperatures between 5 and 35 ℃ in 1 ℃ increments. The water bath was controlled with software supplied by Dr Xi Huang, dwelling at each temperature for 1 hour while measurements were made, and recording temperature using a calibrated temperature probe (F250 MkII, Automatic Systems Laboratories). The voltage output of the thermistor measurement system was monitored using a data acquisition card (NI PCI-6289, National Instruments) and LabVIEW software. The resulting signals were averaged for each dwell temperature and standard deviations calculated. The results are shown in figure A2-1 and Table A2-1 below, and included on the attached CD-ROM.

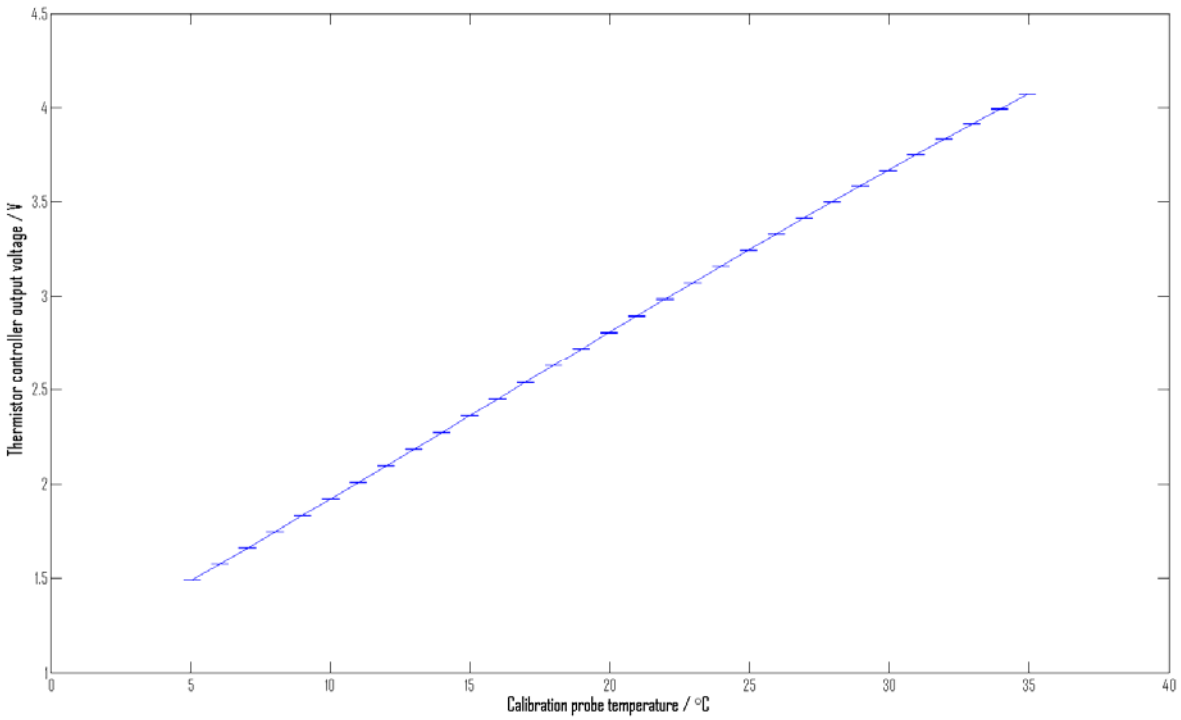

Figure A2-1 – Thermistor 1 calibration results. Only thermistor 1 data is shown for the sake of clarity. Error bars are included for ± 1σ of thermistor controller voltage. Because these are very small compared to the voltage scale (y axis) error bars appear to be single lines.

Calibration probe		Thermistor voltage / V			Thermistor Std / V		
Temperature / °C	Standard Deviation / °C	1	2	3	1	2	3
5.062	0.016	1.4918	1.4793	1.4948	0.0006	0.0006	0.0005

6.048	0.009	1.5762	1.5634	1.5791	0.0008	0.0008	0.0007
7.041	0.007	1.6614	1.6484	1.6644	0.0006	0.0007	0.0006
8.033	0.006	1.7473	1.7340	1.7503	0.0007	0.0008	0.0006
9.023	0.008	1.8332	1.8197	1.8363	0.0007	0.0008	0.0007
10.020	0.007	1.9205	1.9067	1.9235	0.0010	0.0010	0.0008
11.009	0.011	2.0077	1.9934	2.0108	0.0011	0.0012	0.0010
12.001	0.013	2.0955	2.0810	2.0985	0.0014	0.0016	0.0012
12.990	0.009	2.1835	2.1688	2.1867	0.0010	0.0011	0.0009
13.980	0.016	2.2715	2.2567	2.2746	0.0015	0.0018	0.0015
14.987	0.018	2.3616	2.3468	2.3647	0.0018	0.0019	0.0017
15.984	0.015	2.4502	2.4355	2.4534	0.0016	0.0017	0.0014
16.982	0.018	2.5394	2.5249	2.5426	0.0018	0.0018	0.0018
17.982	0.015	2.6285	2.6140	2.6316	0.0017	0.0017	0.0015
18.981	0.016	2.7178	2.7033	2.7209	0.0014	0.0014	0.0013
19.978	0.013	2.8064	2.7917	2.8094	0.0014	0.0015	0.0013
20.973	0.011	2.8943	2.8795	2.8972	0.0014	0.0015	0.0012
21.973	0.019	2.9832	2.9684	2.9859	0.0021	0.0020	0.0021
22.970	0.013	3.0707	3.0556	3.0733	0.0013	0.0013	0.0013
23.973	0.013	3.1582	3.1433	3.1609	0.0014	0.0014	0.0013
24.966	0.020	3.2449	3.2296	3.2475	0.0018	0.0017	0.0018
25.963	0.012	3.3309	3.3158	3.3334	0.0011	0.0011	0.0011
26.961	0.011	3.4164	3.4011	3.4190	0.0010	0.0009	0.0010
27.955	0.015	3.5007	3.4857	3.5034	0.0013	0.0013	0.0012
28.957	0.012	3.5850	3.5701	3.5875	0.0010	0.0011	0.0011

29.956	0.018	3.6684	3.6535	3.6709	0.0019	0.0019	0.0020
30.948	0.016	3.7506	3.7357	3.7530	0.0014	0.0014	0.0014
31.949	0.020	3.8326	3.8179	3.8348	0.0019	0.0018	0.0019
32.947	0.021	3.9133	3.8983	3.9155	0.0016	0.0017	0.0017
33.945	0.020	3.9931	3.9784	3.9953	0.0019	0.0019	0.0019
34.938	0.016	4.0715	4.0569	4.0736	0.0015	0.0015	0.0015

Table A2-1 – Results from thermistor calibration